LA REPUBLIQUE ALGERIANNE DEMOCRATIQUE ET POPULAIRE

MINISTRE DE L'ENSIEGNEMENT SUPERIEUR ET DE LA RECHERCHE SCIENTIFIQUE

Université de DJILALI LIABES – Sidi Bel Abbas

Faculté de Technologie

Département D'électronique

Thèse en vue de l'obtention du diplôme de

Docteur en Science

Ecole Doctorale : Matériaux et Composants

Option: Matériaux Et Composants Optoélectroniques

Présenter par

M^r^. Hamza HEBAL

Thème

Crystal orientation effects on electronic and optical properties of wurtzite CdZnO/ZnO quantum well lasers

Soutenue le 26/11/2015 devant le jury

Pr. SOUDINI bel abbes	(UDL- Sidi Bel Abbes)	Président
Pr. ABID Hamza	(UDL-Sidi Bel Abbes)	Encadreur
Pr. DJELLOULI Bouaza	(UMT-Saida)	Examinateur
Dr. ARBOUCHE Omar	(UMT-Saida)	Examinateur
Pr. BENSAAD Zouaoui	(UDL-Sidi Bel Abbes)	Invité

Année Universitaire 2015-2016

All Praise is due to Allah, and peace and blessings be upon Prophet Muhammad and upon his family and his Companions. This work is dedicated to my mother and father who raised me up to the good values of hardworking with full devotion. I would like to dedicate this work also to my Brothers and Sisters especially my sister Shames and my nephew Heythem.

Abstract

The object of this work is to investigate crystal orientation‘s effects on electronic properties of wurtzite CdZnO/ZnO quantum wells (QWs) with piezoelectric (PZ) and spontaneous (SP) polarization using the multiband effective-mass theory and the non-Markovian gain model with many-body effects. In this research, we address the electronic and the optical properties of wurtzite CdZnO grown on ZnO substrate, the valence-band structures for the QW structure are calculated based on the k.p method .The results will be confronted with those of WZ GaN/InGaN QW structures and also similar studies. The effect of internal field in the c-plane oriented ZnO/CdZnO QW structure is relatively small compared to that of GaN/ InGaN QW structure and thus, a larger optical gain is shown while it disappears in the a- and m-planes for both QW structures where the optical gain as a result is match larger. Energy dispersion, transition strength and the average hole effective masses are anisotropic in non-polar structures. The bandgap transition wavelength of the QW structure with a-plane orientation is smaller than that of m-plane orientation by 2 nm in ZnO/CdZnO QW while it is 10 nm in the case of GaN/InGaN QW structure.

Acknowledgments

I would like to thank my advisor, Professor ABID Hamza, for his patient guidance and constant encouragement during the course of my research.

I would like to thank all members of our Doctoral School and all our teachers.

I would like to thank all members of Aestimo group and especially Dr. Sefer Bora Lisesivdin for giving me the opportunity to enjoy programing in this group.

I would like to thank all faculty members, staff persons, and fellow students at SBA University.

I would like to thank my family and especially, my parents for their patience and support during my years of graduate studies.

I would like to thank all my relatives and friends especially my friend Abd Razzak Kadri, who has kept asking me for progress report during many days of typing and programming.

Contents

Chapter II

Chapter III

Chapter IV

List of figures

Chapter I

Chapter II

Chapter III

Chapter IV

Chapter V

List of tables

General Introduction

1. Problem Statement:

Theoretically, ZnO and GaN based quantum structures are studied extensively by several groups also the same for the use of quantum structures with non-polar crystal orientation , but there was a focusing on (Al and In)-GaN and (Mg)-ZnO based quantum structures and there were no sufficient investigation on (Cd)-ZnO based quantum structures with crystal orientation. Also the methods used in the integration considered in calculating the optical gain which is in one dimension rather than two dimensions and the same for the value of the momentum matrix elements. we consider the theoretical electronic and optical properties of ZnO/CdZnO QW structures as object of studying using a Gaussian line shape function in the gain model including many-body effects .To obtain the band structures and the wave functions, we solve the Schrodinger equation for electrons and the Hamiltonian for holes for c-, a- and m-plane considering the electric field due to build in polarization. These results are compared with those for GaN/InGaN QW structures.

2. Device Perspectives:

Semiconductor lasers are unique when compared to other types of lasers. They are very small, they operate with relatively low power input, and they are very efficient. The first semiconductor lasers were homostructure devices where each laser was fabricated with only one semiconductor material. These lasers had high threshold current densities, In addition to not working at room temperature; these lasers also could not operate cw. The quantum well laser has much lower threshold current and high output power unlike homostructure lasers; they work in at room temperature and also could operate CW.

3. Materials Perspective:

Quantum wells (QWs) based on zinc oxide (ZnO) and related alloys have gained an important amount of interest as an active region in short wavelength light-emitting diodes and laser diodes competing with GaN-based QW structures in the same field with many distinctive properties. Due to the large exciton binding energy (60 meV) of ZnO which allows excitonic recombination even above room

temperature ZnO system renewed the interest in its usage in blue and ultraviolet wavelengths.

4. Summary:

In chapter (I), we will introduce the elementary k·p theory in this chapter and focus on the derivation of the corresponding Hamiltonian for Wurtzite materials such as ZnO and GaN, also because of two other important considerations. One is that the strain effects in the k.p framework are very straight forwardly treated, whether on band structure or band energy edges, the other is investigating the strain effects on the effective masse.

In chapter II, we will be studying the basic formalism of EFA and applying it directly to our ZnO based quantum well structure and present the comparison of the ZnO's results with its counterpart GaN based structure, using numerical means such as finite difference method.

In chapter (III), we will be discussing the basic optical gain formalism starting from the definition of optical transition and their transition strength or as called momentum matrix elements to broadening effect, where a different type from the conventional Lorentzian function is presented and thus the Gaussian or non-Markovian line shape function .Numerous effects on optical gain are will be discussed in this chapter for instance built in electric field due to piezoelectric and spontaneous polarization , many body effects , strain effect and carrier concentration effect.

Finally in chapter (IV) and (V), we consider the theoretical electronic and optical properties of ZnO/CdZnO QW structures as object of studying .To obtain the band structures and the wave functions ,we solve (a finite difference method was used in numerical calculations, un example for zincblende is implemented in the open source code called Aestimo 0.9 and for wurtzite in version 1.0) the Schrodinger equation for electrons and the 6×6 Hamiltonian for holes for arbitrary crystal orientation in chapter (IV) and focus on a- and m-planes oriented structures in chapter (V) with considering the electric field due to build in polarization . These results are compared with those for GaN/InGaN QW structures.

Chapter I

Theory of Electronic Band Structure in Semiconductors

(The k.p Method)

I.1 Introduction:

The k.p method was first introduced by Bardeen [1] and Seitz [2] and soon after that it was used in many semiconductor researches [3] before its development by Luttinger [4] and Kane [5, 6], where bands and spin-orbit interaction degenerate are taken into account, respectively. It is based on the perturbation theory, and usually referred to as the effective mass theory. Many of the k.p parameters are accurately determined by magneto-optical experiments such as the band gap, Eg, split-off energy, Δ, the conduction-valence band coupling element, Ep, and the electron and hole effective masses, etc. Thus the high precision treatment found in band structure calculations. One important feature of the k.p method is the very small basis set, and the possibility of diagonalization of its Hamiltonian with an easy way to analyze and apply to semiconductor optics, magnetism, and transport.

We will introduce the elementary k·p theory in this chapter and focus on the derivation of the corresponding Hamiltonian for Wurtzite materials such as ZnO and GaN, also because of two other important considerations. One is that the strain effects in the k.p framework are very straight forwardly treated, whether on band structure or band energy edges, the other is investigating the strain effects on the effective masse.

I.2 Elementary k.p Theory:

When only a weak interaction is considered with all remaining states, the simplest form of k.p theory is obtained and thus the one-electron Schrodinger equation is written:

$$H\psi_{n,k}(r) = E\psi_{n,k}(r) \tag{I.1}$$

with the Hamiltonian

$$H = \frac{p^2}{2m_0} + V(r) + \frac{\hbar}{4m_0^2c^2}(\sigma \times \nabla V)\cdot \mathrm{p} \tag{I.2}$$

The last term in the Hamiltonian *H* represent spin-orbit interaction, and σ is the vector of the Pauli spin matrices $\sigma = (\sigma_1, \sigma_2, \sigma_3)^T$, which are defined as

$$\sigma_1 = \begin{pmatrix} 0 & 1 \\ 1 & 0 \end{pmatrix}, \sigma_2 = \begin{pmatrix} 0 & -i \\ i & 0 \end{pmatrix}, \sigma_3 = \begin{pmatrix} 1 & 0 \\ 0 & -1 \end{pmatrix} \tag{I.3}$$

and the Bloch wave-function

$$\psi_{n,k}(r) = e^{i\cdot k\cdot r}u_{n,k}(r) \tag{I.4}$$

Which is the product of a plane wave $e^{i\cdot k\cdot r}$ and the periodic Bloch factors $u_{n,k}(r)$, *n* is the band index and *k* is a wave vector in the first Brillouin zone which corresponds to the periodicity of the potential energy $V(r)$.

The plan wave part of the wave-function is cancelled after its insertion in Equation (I.1) and the Schrodinger equation changes to:

$$\left(\frac{p^2}{2m_0} + V(r) + \frac{\hbar^2k^2}{2m_0} + \frac{\hbar}{m_0}k\cdot p + \frac{\hbar^2}{4m_0^2c^2}(\sigma\times\nabla V)\cdot(\hbar k + \mathrm{p})\right)u_{n,k}(r) = E_{n,k}\cdot u_{n,k}(r) \tag{I.5}$$

reducing equation (I.5) with

$$\pi = p + \frac{\hbar}{4m_0c^2}(\sigma\times\nabla V)$$

to become

$$\left(\frac{p^2}{2m_0}+V(r)+\frac{\hbar^2k^2}{2m_0}+\frac{\hbar}{m_0}k\cdot p+\frac{\hbar^2}{4m_0^2c^2}(\sigma\times\nabla V)\cdot \mathrm{p}\right)u_{n,k}(r)=E_{n,k}\cdot u_{n,k}(r) \qquad \text{(I.6)}$$

Using second order non-degenerate perturbation theory to solve Equation (I.6).Where the perturbation is represented by the k dependent part of the Hamiltonian and the solution is:

$$E_{n,k}=E_{n,0}+\frac{\hbar^2k^2}{2m_0}+\frac{\hbar k}{m_0}\cdot\langle n,0|\pi|n,0\rangle+\frac{\hbar^2}{m_0^2}\sum_{n\neq m}\frac{\left|k\langle n,0|\pi|m,0\rangle\right|^2}{E_{n,0}-E_{m,0}} \qquad \text{(I.7)}$$

The energy band has a minimum at $k = 0$, thus the term linear in k is zero. We use same Cartesian indices introduced by Ref. [7], where $\alpha,\beta = x, y, z$ and Einstein's summation convention for these indices.to have

$$E_{n,k}=E_{n,0}+\frac{\hbar^2k^2}{2m_0}+\frac{\hbar^2}{m_0^2}k_\alpha k_\beta\sum_{n\neq m}\frac{\langle n,0|\pi_\alpha|m,0\rangle\langle m,0|\pi_\beta|n,0\rangle}{E_{n,0}-E_{m,0}} \qquad \text{(I.8)}$$

$$E_{n,k}=E_{n,0}+\frac{\hbar^2k^2}{2m_0}+\frac{\hbar^2}{2}k_\alpha k_\beta\left(\frac{1}{m_n^*}\right)_{\alpha,\beta} \qquad \text{(I.9)}$$

where the tensor of the effective mass is

$$\left(\frac{1}{m_n^*}\right)_{\alpha,\beta}=\left(\frac{1}{m_0}\right)\delta_{\varepsilon,\beta}+\frac{2}{m_0^2}\sum_{n\neq m}\frac{\langle n,0|\pi_\alpha|m,0\rangle\langle m,0|\pi_\beta|n,0\rangle}{E_{n,0}-E_{m,0}} \qquad \text{(I.10)}$$

Equation (I.9) represents the basic form of single band model.

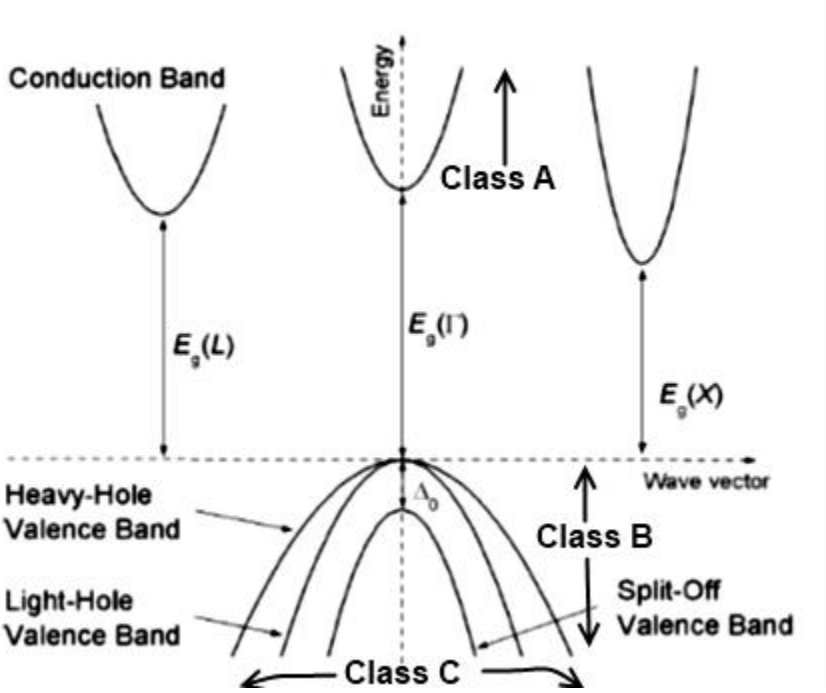

Figure 1: Band classification where the conduction is called class A, while the heavy-hole, light-hole, and spin-split-off bands in double degeneracy are of interest and are called class B. All other bands are denoted as class C.

I.3 Wurtzite Hamiltonian

Pikus studied the band structure and optical properties of Wurtzite materials in the late 1950s and beginning of 1960s using the invariants method introducing a six-band model [8]. In 1990s the interest in Wurtzite materials was renewed due to the growth of high-quality epitaxial GaN and AlN [9]. Thus Chuang *et al* used Kane model to construct an 8-band model for Wurtzite materials and starting from Luttinger-kohn model a 6-band model was introduced using the perturbation theory and then was compared with the one obtained by invariant method [10].

Our work is based on using Wurtzite semiconductors i.e. ZnO material system, where they are generally large-band-gap materials (except for InN with a band gap of ~ 0.7 eV [11, 12]) with a direct gap at the Γ point. Due to both a crystal-field splitting (compared to a cubic structure) and spin-orbit interaction the complex valence-band structure consist of three doubly-degenerate bands at the Γ point, they are grouped into three classes as A, B, and C as shown in Figure (1) . The Wurtzite structure, Figure (2),

consists of two interpenetrating hexagonal closely packed sublattices, offset along the c axis (z axis by 5/8 of the cell height c. The sixfold rotation symmetry is used in deriving some of the fundamental physical parameters [10]

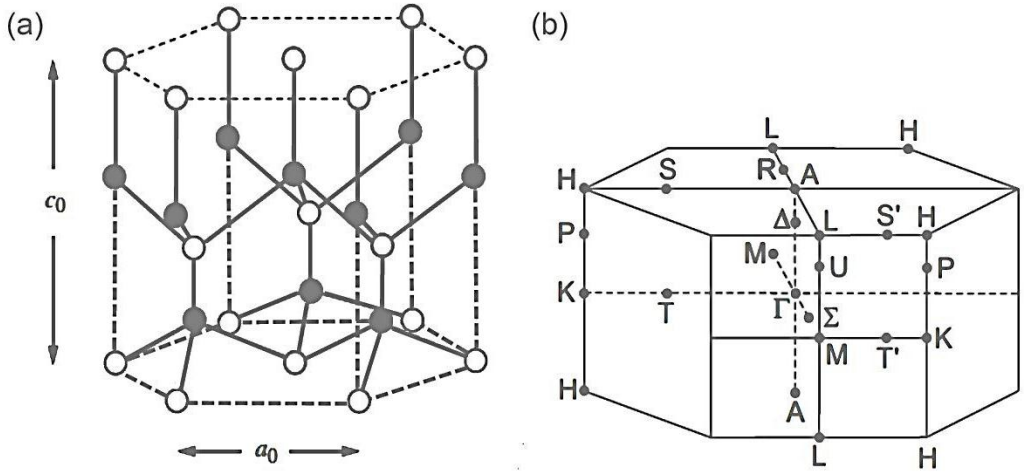

Figure 2: a) Wurtzite crystal with lattice constants c_0 and a_0. The structure is formed by two intertwined hexagonal sublattices of, e.g., Ga and N atoms or Zn and O, b) Brillouin zones and special k points for the hcp lattice.

I.3.1 Six band model for strained Wurtzite Hamiltonian (Luttinger-kohn Model):

Chuang *et al* used Löwdin's perturbation method [13, 3] (see Appendixes (I.7) and (I.8)), which provides the Hamiltonian to the second order in the k.p contributions in the case of class A bands[10], see Figure (1).

I.3.1.1 Hamiltonian and Basis Functions

The total Hamiltonian is written as [3]

$$Hu_k(r) = E(k)u_k(r).$$

$$H = H_0 + \frac{\hbar^2 k^2}{2m_0} + H_{SO} + H', \tag{I.11}$$

$$H' = \frac{\hbar}{m_0} \mathrm{k}.\prod,$$

$$\prod = p + \frac{\hbar}{4m_0c^2}\sigma \times \nabla V \cdot$$

The last term in *p* is usually neglected for simplicity [14, 3]. The band-edge wave function can be written as

$$u_k(r) = \sum_{j'}^{A} a_{j'}(k) u_{j'0}(r) + \sum_{\gamma}^{B} a_{\gamma}(k) u_{\gamma 0}(r) \tag{I.12}$$

The six valence-band wave functions, $\{u_1, u_2, ..., u_6\}$ defined in the following are assigned as the bases for the states of interest (called class B), and all other states of no interest are called class (A and C) see figure (1).

$$\begin{aligned}
|U_1\rangle &= -\frac{1}{\sqrt{2}}\left|(X + iY)\uparrow\right\rangle \\
|U_2\rangle &= \frac{1}{\sqrt{2}}\left|(X - iY)\uparrow\right\rangle \\
|U_3\rangle &= \left|Z\uparrow\right\rangle \\
|U_4\rangle &= \frac{1}{\sqrt{2}}\left|(X - iY)\downarrow\right\rangle \\
|U_5\rangle &= -\frac{1}{\sqrt{2}}\left|(X + iY)\downarrow\right\rangle \\
|U_6\rangle &= \left|Z\downarrow\right\rangle
\end{aligned} \tag{I.13}$$

Löwdin's perturbation theory (Appendixes (I.7) and (I.8)) requires finding the solution of the following system:

$$\sum_{j'}^{A}\left(U^{A}_{jj'} - E\delta_{jj'}\right)a_{j'}(k) = 0 \tag{I.14}$$

Using Löwdin's method, [13], the 6x6 Hamiltonian matrix for the valence bands can be written as the sum of a band-edge contribution and a k-dependent contribution.

$$H_{6\times 6\,jj'}(k) = H_{6\times 6\,jj'}(k=0) + D_{jj'} \tag{I.15}$$

and the k-dependent matrix is

$$D_{jj'} = \sum_{\alpha\beta} D^{\alpha\beta}_{jj'} k_\alpha k_\beta$$

$$D_{jj'}^{\alpha\beta} = \frac{\hbar^2}{2m_0}\left(\delta_{jj'}\delta_{\alpha\beta} + \sum_{\gamma}^{B}\frac{p_{j\gamma}^{\alpha}p_{\gamma j'}^{\beta} + p_{j\gamma}^{\beta}p_{\gamma j'}^{\alpha}}{m_0\left(E_0 - E_\gamma\right)}\right) \tag{I.16}$$

where the indices j,j'=1,2, . . . , $6\in \mathrm{A}$, $\gamma\in \mathrm{B}$, and α,β=x,y,z.

Using Kane's model [6], the band-edge Hamiltonian matrix is given by

$$H_{6\times6}(k=0)=\begin{pmatrix} E_v+\Delta_1+\Delta_2 & 0 & 0 & 0 & 0 & 0 \\ 0 & E_v+\Delta_1-\Delta_2 & 0 & 0 & 0 & \sqrt{2}\Delta_3 \\ 0 & 0 & E_v & 0 & \sqrt{2}\Delta_3 & 0 \\ 0 & 0 & 0 & E_v+\Delta_1+\Delta_2 & 0 & 0 \\ 0 & 0 & \sqrt{2}\Delta_3 & 0 & E_v+\Delta_1-\Delta_2 & 0 \\ 0 & \sqrt{2}\Delta_3 & 0 & 0 & 0 & E_v \end{pmatrix} \tag{I.17}$$

I.3.1.2 The D matrix in the $|\mathrm{X}\rangle$, $|\mathrm{Y}\rangle$, and $|\mathrm{Z}\rangle$ bases

The method used by Chaung *et al* is similar to that of the Luttinger-Kohn paper [4] in defining the fundamental band-structure parameters, L_1, L_2, M_1, M_2, M_3, N_1, and N_2. The 3×3 matrix with components, $D_{i\,j}$, *i*, *j*=X, Y, Z, can be written in the following form:

$$D_{3\times3}=\begin{pmatrix} L_1k_x^2+M_1k_y^2+M_2k_z^2 & N_1k_xk_y & N_2k_xk_z \\ N_1k_xk_y & M_1k_x^2+L_1k_y^2+M_2k_z^2 & N_2k_yk_z \\ N_2k_xk_z & N_2k_yk_z & M_3\left(k_x^2+k_y^2\right)+L_2k_z^2 \end{pmatrix}\begin{matrix}|X\rangle \\ |Y\rangle \\ |Z\rangle\end{matrix} \tag{I.18}$$

Similarly to the band-structure parameters of Luttinger-Kohn Y_1, Y_2, and Y_3 for zinc-blende structures, Chaung's band-structure parameters are defined as

$$L_1=\frac{\hbar^2}{2m_0}\left(1+\sum_{\gamma}^{B}\frac{2p_{X\gamma}^{x}p_{\gamma X}^{x}}{m_0\left(E_0-E_\gamma\right)}\right)$$
$$=\frac{\hbar^2}{2m_0}\left(1+\sum_{\gamma}^{B}\frac{2p_{Y\gamma}^{y}p_{\gamma Y}^{y}}{m_0\left(E_0-E_\gamma\right)}\right)$$

$$L_2=\frac{\hbar^2}{2m_0}\left(1+\sum_{\gamma}^{B}\frac{2p_{Z\gamma}^{z}p_{\gamma Z}^{z}}{m_0\left(E_0-E_\gamma\right)}\right)$$

$$M_1 = \frac{\hbar^2}{2m_0}\left(1+\sum_\gamma^B \frac{2p_{X\gamma}^y p_{\gamma X}^y}{m_0\left(E_0-E_\gamma\right)}\right) = \frac{\hbar^2}{2m_0}\left(1+\sum_\gamma^B \frac{2p_{Y\gamma}^x p_{\gamma Y}^x}{m_0\left(E_0-E_\gamma\right)}\right)$$

$$M_2 = \frac{\hbar^2}{2m_0}\left(1+\sum_\gamma^B \frac{2p_{X\gamma}^z p_{\gamma X}^z}{m_0\left(E_0-E_\gamma\right)}\right) = \frac{\hbar^2}{2m_0}\left(1+\sum_\gamma^B \frac{2p_{Y\gamma}^z p_{\gamma Y}^z}{m_0\left(E_0-E_\gamma\right)}\right)$$

$$M_3 = \frac{\hbar^2}{2m_0}\left(1+\sum_\gamma^B \frac{2p_{Z\gamma}^x p_{\gamma Z}^x}{m_0\left(E_0-E_\gamma\right)}\right) = \frac{\hbar^2}{2m_0}\left(1+\sum_\gamma^B \frac{2p_{Z\gamma}^y p_{\gamma Z}^y}{m_0\left(E_0-E_\gamma\right)}\right)$$

$$N_1 = \frac{\hbar^2}{m_0^2}\sum_\gamma^B \frac{p_{X\gamma}^x p_{\gamma Y}^y + p_{X\gamma}^y p_{\gamma Y}^x}{\left(E_0-E_\gamma\right)}$$

$$N_2 = \frac{\hbar^2}{m_0^2}\sum_\gamma^B \frac{p_{X\gamma}^x p_{\gamma Z}^z + p_{X\gamma}^z p_{\gamma Z}^x}{\left(E_0-E_\gamma\right)} = \frac{\hbar^2}{m_0^2}\sum_\gamma^B \frac{p_{Y\gamma}^y p_{\gamma Z}^z + p_{Z\gamma}^z p_{\gamma Z}^y}{\left(E_0-E_\gamma\right)} \qquad \text{(I.19)}$$

where $p_{X\gamma}^y = \langle X | p^y | \gamma \rangle$, etc., and $p^y = (\hbar/i)(\partial/\partial y)$ is the y component of the momentum operator.

I.3.1.3 The 6x6 Hamiltonian matrix in the bases $\{u_1, u_2, ..., u_6\}$

The derivation of $D_{6\times6}$ matrix in the bases $\{u_1, u_2, ..., u_6\}$ becomes easy with using the previous results of the matrix elements, D_{XX}, D_{XY}, D_{XZ}, etc. in Equation (I.18),

$$D_{6\times6} = \begin{pmatrix} D_{11} & D_{21}^* & -D_{23}^* & 0 & 0 & 0 \\ D_{21} & D_{11} & D_{23} & 0 & 0 & 0 \\ -D_{23} & D_{23}^* & D_{ZZ} & 0 & 0 & 0 \\ 0 & 0 & 0 & D_{11} & D_{21} & D_{23} \\ 0 & 0 & 0 & D_{21}^* & D_{11} & -D_{23}^* \\ 0 & 0 & 0 & D_{11} & -D_{23} & D_{ZZ} \end{pmatrix} \qquad \text{(I.20)}$$

where the whole matrix can be expressed by using only four distinctive matrix elements,

$$D_{11} = \left(\frac{L_1+M_1}{2}\right)\left(k_x^2+k_y^2\right)+M_2k_z^2$$

$$D_{ZZ} = M_3\left(k_x^2 + k_y^2\right) + L_2 k_z^2$$

$$D_{21} = -\frac{1}{2}\left(L_1 - M_1\right)\left(k_x^2 - k_y^2\right) + 2ik_x k_y$$
$$= -\frac{1}{2}N_1\left(k_x + ik_y\right)^2$$

$$\mathrm{D}_{23} = -\frac{1}{\sqrt{2}}N_2\left(k_x + ik_y\right)k_x \qquad \text{(I.21)}$$

and it can be shown from symmetry consideration that

$$L_1 - M_1 = N_1$$

The full Hamiltonian, $H = H_{6\times6}(k=0) + D_{6\times6}$, can be written as

$$H = \begin{pmatrix} F & -K^* & -H^* & 0 & 0 & 0 \\ -K & G & H & 0 & 0 & \Delta \\ -H & H^* & \lambda & 0 & \Delta & 0 \\ 0 & 0 & 0 & F & -K & H \\ 0 & 0 & \Delta & -K^* & G & -H^* \\ 0 & \Delta & 0 & H^* & -H & \lambda \end{pmatrix} \begin{matrix} |U_1\rangle \\ |U_2\rangle \\ |U_3\rangle \\ |U_4\rangle \\ |U_5\rangle \\ |U_6\rangle \end{matrix} \qquad \text{(I.22)}$$

$$F = \Delta_1 + \Delta_2 + \lambda + \theta$$

$$G = \Delta_1 - \Delta_2 + \lambda + \theta$$

$$\lambda = \frac{\hbar^2}{2m_0}\left[A_1 k_z^2 + A_2\left(k_x^2 + k_y^2\right)\right]$$

$$\theta = \frac{\hbar^2}{2m_0}\left[A_3 k_z^2 + A_4\left(k_x^2 + k_y^2\right)\right] \qquad \text{(I.23)}$$

$$K = \frac{\hbar^2}{2m_0}A_5(k_x + ik_y)^2$$

$$H = \frac{\hbar^2}{2m_0}A_6(k_x + ik_y)k_z$$

$$\Delta = \sqrt{2}\Delta_3$$

Chuang *et al* obtained the relations between the band-structure parameters derived using the k.p method and the more commonly used A_i parameters in the Pikus-Bir model [10],

$$\frac{\hbar^2}{2m_0}A_1 = L_2, \frac{\hbar^2}{2m_0}A_2 = M_3, \frac{\hbar^2}{2m_0}A_3 = M_2 - L_2,$$

$$\frac{\hbar^2}{2m_0}A_4 = \frac{L_1 + M_1}{2} - M_3, \frac{\hbar^2}{2m_0}A_5 = \frac{N_1}{2}, \frac{\hbar^2}{2m_0}A_6 = \frac{N_2}{\sqrt{2}} \qquad \text{(I.24)}$$

It was noted that there is a minus sign in front of all the *K* terms in Equation (I.22) and the absence of a factor of *i* in the definition of the *H* terms compared with those used in Refs. [8] and [15]. But the latter differences do not affect the band-structure dispersion relation. The results derived by Chaung *et al* are consistent with the results derived by Pikus *el al* in Ref. [8], using the invariant method

The strain effects can be easily included by the same symmetry consideration and a straightforward addition of corresponding terms:

$$k_\alpha k_\beta \to \varepsilon_{\alpha\beta},$$

with the deformation potentials, D_1 , D_2 , . . . , D_6 , at the corresponding positions of A_1 , A_2 , . . . , A_6 .

$$F = \Delta_1 + \Delta_2 + \lambda + \theta$$

$$G = \Delta_1 - \Delta_2 + \lambda + \theta$$

$$\lambda = \frac{\hbar^2}{2m_0}\left[A_1 k_z^2 + A_2\left(k_x^2 + k_y^2\right)\right] + \lambda_\varepsilon$$

$$\lambda_\varepsilon = D_1\varepsilon_{zz}^{(0)} + D_2(\varepsilon_{xx}^{(0)} + \varepsilon_{yy}^{(0)})$$

$$\theta = \frac{\hbar^2}{2m_0}\left[A_3 k_z^2 + A_4\left(k_x^2 + k_y^2\right)\right] + \theta_\varepsilon \qquad \text{(I.25)}$$

$$\theta_\varepsilon = D_3\varepsilon_{zz}^{(0)} + D_4(\varepsilon_{xx}^{(0)} + \varepsilon_{yy}^{(0)})$$

$$K = \frac{\hbar^2}{2m_0}A_5(k_x + ik_y)^2 + D_5\varepsilon_{\pm}$$

$$H = \frac{\hbar^2}{2m_0} A_6 (k_x + ik_y) k_z + D_6 \varepsilon_{z\pm}$$

$$\Delta = \sqrt{2}\Delta_3$$

where

$$\varepsilon_{\pm} = \varepsilon_{xx} \pm 2i\varepsilon_{xx} - \varepsilon_{yy} \qquad \text{(I.26)}$$

$$\varepsilon_{z\pm} = \varepsilon_{zx} \pm i\varepsilon_{yz}$$

Under the cubic approximation, [14, 15] the following relations hold for the parameters A_i's and D_i's:

$$A_1 - A_2 = -A_3 = 2A_4, A_3 - 4A_5 = \sqrt{2}A_6, \Delta_2 = \Delta_3$$

$$D_1 - D_2 = -D_3 = 2D_4, D_3 - 4D_5 = \sqrt{2}D_6 \qquad \text{(I.27)}$$

Consequently, only A_1, A_2, A_5, Δ_1, and Δ_2, and three deformation potentials are needed for the calculation of the valence-band structures. The cubic approximation idea is based on the resemblance of the Wurtzite structure to the cubic crystal. It has also been found [14] that a seventh coefficient A_7 for the linear k terms vanishes; therefore, only the quadratic terms of k, in addition to the band-edge energy terms must be kept. For a strained-layer Wurtzite crystal pseudomorphically grown along the (0001) (z axis) direction, the strain tensor $\varepsilon_{\alpha\beta}$ has only the following non-vanishing diagonal elements:

$$\varepsilon_{xx}^{(0)} = \varepsilon_{yy}^{(0)} = \frac{(a_s - a_e)}{a_e}$$

$$\varepsilon_{zz}^{(0)} = \frac{2C_{13}}{C_{33}} \varepsilon_{xx}^{(0)} \qquad \text{(I.28)}$$

where a_0 and a are the lattice constants of the substrate and the layer material, and C_{13} and C_{33} are the stiffness constants .The general strain-stress relation (Hooke's Law) for the hexagonal crystal can be found in Ref. [17].

I.3.2 Block Diagonalization of Wurtzite Hamiltonians:

We rewrite equation (I.22) to a more convenient notation, to become:

$$H=\begin{pmatrix} H_{11} & -H_{12}^{*} & -H_{23}^{*} & 0 & 0 & 0 \\ -H_{21} & H_{22} & H_{23} & 0 & 0 & \Delta \\ -H_{23} & H_{23}^{*} & H_{33} & 0 & \Delta & 0 \\ 0 & 0 & 0 & H_{11} & -H_{21} & H_{23} \\ 0 & 0 & \Delta & -H_{12}^{*} & H_{22} & -H_{23}^{*} \\ 0 & \Delta & 0 & H_{23}^{*} & -H_{23} & H_{33} \end{pmatrix}\begin{matrix} |U_1\rangle \\ |U_2\rangle \\ |U_3\rangle \\ |U_4\rangle \\ |U_5\rangle \\ |U_6\rangle \end{matrix} \tag{I.29}$$

The full 6×6 Hamiltonian matrix can be block diagonalized using the basis transformation. The off - diagonal terms such as H_{21} and H_{23} contain the ϕ dependence, and we can write

$$H_{21}=K_{21}e^{i2\phi}$$

$$H_{23}=K_{23}e^{i\phi} \tag{I.30}$$

where $k_x+ik_y=k_te^{i\phi}$. Here, the K_{21} and K_{23} matrix elements for two Hamiltonians are given by

$$K_{21}=\frac{\hbar^2}{2m_0}A_5k_t^{\,2}$$

$$K_{23}=\frac{\hbar^2}{2m_0}A_6k_tk_z \tag{I.31}$$

for the Hamiltonian $H^{(0001)}$. We define the transformation matrix T as

$$T=\begin{pmatrix} \alpha^{*} & 0 & 0 & \alpha & 0 & 0 \\ 0 & \beta & 0 & 0 & \beta^{*} & 0 \\ 0 & 0 & \beta^{*} & 0 & 0 & \beta \\ \alpha^{*} & 0 & 0 & \alpha & 0 & 0 \\ 0 & \beta & 0 & 0 & -\beta^{*} & 0 \\ 0 & 0 & -\beta^{*} & 0 & 0 & \beta^{*} \end{pmatrix} \tag{I.32}$$

where

$$\alpha = \frac{1}{\sqrt{2}} e^{i\left(\frac{3\pi}{4}+\frac{3\phi}{2}\right)}, \quad \beta = \frac{1}{\sqrt{2}} e^{i\left(\frac{\pi}{4}+\frac{\phi}{2}\right)}$$

The block-diagonalized Hamiltonian, $H_{Block-diagonalized} = T^* H T^t$, is given by

$$H_{Block-diagonalized} = \begin{pmatrix} H^U & 0 \\ 0 & H^L \end{pmatrix} \tag{I.33}$$

where the upper 3×3 Hamiltonian is

$$H^U = \begin{pmatrix} H_{11} & K_{12} & -iK_{13} \\ K_{21} & H_{22} & \Delta - iK_{23} \\ iK_{31} & \Delta + iK_{32} & H_{33} \end{pmatrix} \tag{I.34}$$

where the lower 3×3 Hamiltonian is

$$H^L = \begin{pmatrix} H_{11} & K_{12} & iK_{13} \\ K_{21} & H_{22} & \Delta + iK_{23} \\ -iK_{31} & \Delta - iK_{32} & H_{33} \end{pmatrix} \tag{I.35}$$

The lower Hamiltonian is the complex conjugate of the upper Hamiltonian. Therefore, they have exactly the same eigenvalues, since the eigenenergies are real. The wave functions of the lower Hamiltonian are the complex conjugates of the corresponding wave functions of the upper Hamiltonian.

I.4 Analytical Solutions for Valence Band Energies and Wave Functions in Bulk Semiconductors

The eigenequation for the valence band energy *E* at the band edge is given by

$$\begin{pmatrix} H_{11}-E & K_{12} & -iK_{13} \\ K_{21} & H_{22}-E & \Delta - iK_{23} \\ iK_{31} & \Delta + iK_{32} & H_{33}-E \end{pmatrix} \begin{pmatrix} g_1 \\ g_2 \\ g_3 \end{pmatrix} = 0 \tag{I.36}$$

The eigenequation is a third - order polynomial equation that can always be solved analytically. The complete Bloch wave functions for the valence bands are given by

$$|\Psi_m\rangle = \frac{1}{\sqrt{V}} e^{ik\cdot r} \sum_{u=1}^{3} \left[g_m^{(u)}(k) |v\rangle \right] \tag{I.37}$$

where

$$\begin{aligned} |1\rangle &= \alpha^* |U_1\rangle + \alpha |U_4\rangle \\ |2\rangle &= \beta |U_2\rangle + \beta^* |U_5\rangle \\ |3\rangle &= \beta^* |U_3\rangle + \beta |U_6\rangle \end{aligned} \tag{I.38}$$

Similar expressions hold for the lower Hamiltonian (Equation (I.34)) with bases $|4\rangle, |5\rangle$ and $|6\rangle$.The analytical solutions can be derived for the valence band dispersion [18]

$$\begin{aligned} E_{hh}(k_t, k_z) &= S_1 + S_2 - \frac{C_2}{3} \\ E_{lh}(k_t, k_z) &= -\frac{S_1 + S_2}{2} - \frac{C_2}{3} - i\frac{\sqrt{3}}{2}(S_1 - S_2) \\ E_{ch}(k_t, k_z) &= -\frac{S_1 + S_2}{2} - \frac{C_2}{3} + i\frac{\sqrt{3}}{2}(S_1 - S_2) \end{aligned} \tag{I.39}$$

Where

$$\begin{aligned} S_1 &= \left(R + \sqrt{Q^3 + R^2} \right)^{1/3} \\ S_2 &= \left(R - \sqrt{Q^3 + R^2} \right)^{1/3} \\ R &= \frac{1}{3}(C_1 C_2 - 3C_0) - \frac{1}{27} C_2^3 \\ Q &= \frac{1}{3} C_1 - \frac{1}{9} C_2^2 \end{aligned} \tag{I.40}$$

and

$$\begin{aligned} C_0 &= -\det\left[H^U \right] \\ C_1 &= H_{11}H_{22} + H_{22}H_{33} + H_{11}H_{33} - \Delta^2 - K_{12}^2 - 2K_{13}^2 \\ C_2 &= -(H_{11} + H_{22} + H_{33}) \end{aligned} \tag{I.41}$$

The envelope functions corresponding to the three eigenvalues are determined by

$$\begin{pmatrix} g_1 \\ g_2 \\ g_3 \end{pmatrix} = \frac{1}{D}\begin{pmatrix} D_1 \\ D_2 \\ D_3 \end{pmatrix} \tag{I.42}$$

where

$$\begin{aligned} D_1 &= iK_{13}(H_{22}-E)+(\Delta-K_{13})K_{12} \\ D_2 &= iK_{13}K_{12}(H_{11}-E)(\Delta-K_{13})K_{12} \\ D_3 &= (H_{11}-E)+(H_{22}-E)-K_{12}^2 \end{aligned} \tag{I.43}$$

And

$$D = \sqrt{|D_1|^2+|D_2|^2+|D_3|^2} \tag{I.44}$$

The conduction bands can be characterized by a parabolic band model, and the effective mass Hamiltonians is given by [19]

$$H_c(k,\varepsilon) = \frac{\hbar^2}{2}\left(\frac{k_x^2+k_y^2}{m_e^t}+\frac{k_z^2}{m_e^z}\right)+E_c^0 \tag{I.45}$$

where the band edge energy is given by

$$E_c^0 = \Delta_1+\Delta_2+E_g+P_{c\varepsilon} \tag{I.46}$$

which is shifted by a hydrostatic energy

$$P_{c\varepsilon} = a_{cz}\varepsilon_{zz}+a_{ct}(\varepsilon_{xx}+\varepsilon_{yy}) \tag{I.47}$$

The factors a_{cz} and a_{ct} are the conduction band hydrostatic deformation potentials along the c-axis and perpendicular to the c-axis and E_g is the band gap energy. We set a_{cz} = a_{ct} for simplicity. The conduction band wave function is of the form

$$|\Psi_{c\eta}\rangle = \frac{1}{\sqrt{V}}e^{ik\cdot r}|S\eta\rangle \tag{I.48}$$

where $\eta = \uparrow or \downarrow$ and S is a spherically symmetric wave function.

The conduction band dispersion for bulk is given by

$$E_c(k,\varepsilon)=\frac{\hbar^2}{2}\left(\frac{k_x^2+k_y^2}{m_e^t}+\frac{k_z^2}{m_e^z}\right)+E_c^0 \tag{I.49}$$

Figures (4) and (5) shows the valence band structure of ZnO and GaN as calculated from the above equations for different strain conditions. At the Γ point, the hole effective masses can be approximated as [10]

$$\begin{aligned}
m_{hh}^z &= -m_0\left(A_1+A_3\right)^{-1}\\
m_{hh}^t &= -m_0\left(A_2+A_4\right)^{-1}\\
m_{lh}^z &= -m_0\left(A_1+\left(\frac{E_{lh}^0-\lambda_\varepsilon}{E_{lh}^0-E_{ch}^0}\right)A_3\right)^{-1}\\
m_{lh}^t &= -m_0\left(A_2+\left(\frac{E_{lh}^0-\lambda_\varepsilon}{E_{lh}^0-E_{ch}^0}\right)A_4\right)^{-1}\\
m_{ch}^z &= -m_0\left(A_1+\left(\frac{E_{lh}^0-\lambda_\varepsilon}{E_{lh}^0-E_{ch}^0}\right)A_3\right)^{-1}\\
m_{ch}^t &= -m_0\left(A_2+\left(\frac{E_{ch}^0-\lambda_\varepsilon}{E_{ch}^0-E_{ch}^0}\right)A_4\right)^{-1}
\end{aligned} \tag{I.50}$$

The resulting parabolas are plotted as dashed lines in Figure (4) and (5), indicating that some of these effective masses are not valid at larger k values, where the following approximations are more reasonable [10]

$$\begin{aligned}
m_{hh}^z &= -m_0\left(A_1+A_3\right)^{-1}\\
m_{hh}^t &= -m_0\left(A_2+A_4-A_5\right)^{-1}\\
m_{lh}^z &= -m_0\left(A_1+A_3\right)^{-1}\\
m_{lh}^t &= -m_0\left(A_2+A_4-A_5\right)^{-1}\\
m_{ch}^z &= -m_0A_1^{-1}\\
m_{ch}^t &= -m_0A_2^{-1}
\end{aligned} \tag{I.51}$$

I.5 Strain Effects on Bulk Semiconductors:

A layer of ZnO (GaN) considered under either a compressive or tensile strain as in Figure (3), depending on the barrier materials, with the convention that the in-plane strain ε_{xx}, is negative for compression and positive for tension. The conduction band edge energy in the ZnO (GaN) bulk layer is

$$E_c(k,\varepsilon) = \Delta_1 + \Delta_2 + E_g + P_{c\varepsilon} \tag{I.52}$$

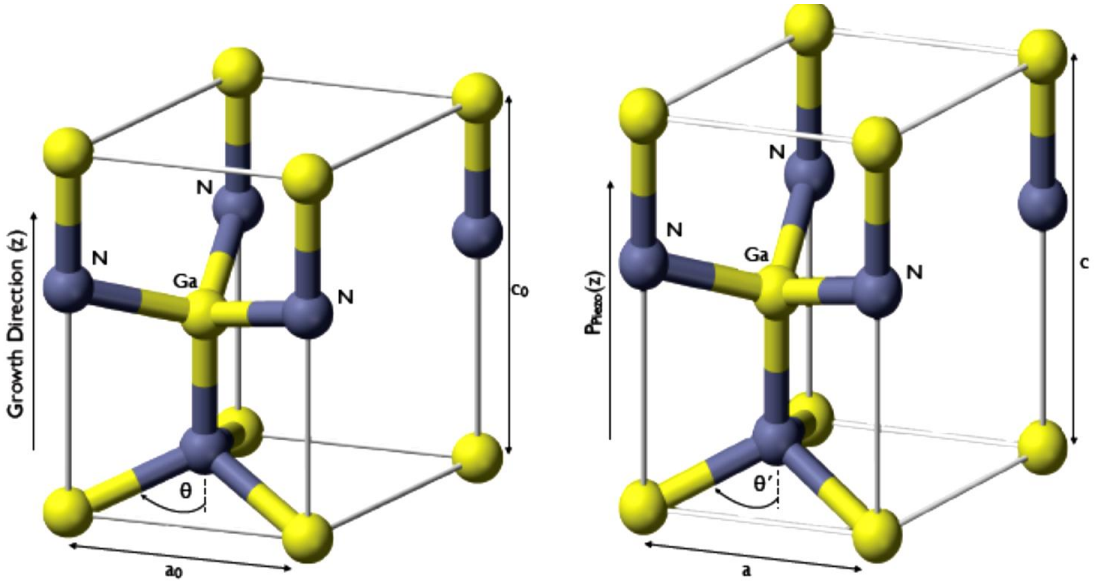

(a) Unstrained (b) Under bi-axial compressive strain

Figure 3: The unit cell of the Wurtzite crystal structure [20]. The change in bond lengths/angles when placed under bi-axial strain is demonstrated in (b).

The valence band-edge energies can be obtained by finding the eigenvalues of the three-by-three Hamiltonians, (I.33), evaluated at the zone center (k = 0)

$$\begin{aligned} E_{hh} &= \Delta_1 + \Delta_2 + \lambda + \theta \\ E_{lh} &= \frac{\Delta_1 - \Delta_2 + \lambda}{2} + \theta + \sqrt{\left(\frac{\Delta_1 - \Delta_2 + \lambda}{2}\right)^2 + 2\Delta_3^2} \\ E_{ch} &= \frac{\Delta_1 - \Delta_2 + \lambda}{2} + \theta - \sqrt{\left(\frac{\Delta_1 - \Delta_2 + \lambda}{2}\right)^2 + 2\Delta_3^2} \end{aligned} \tag{I.53}$$

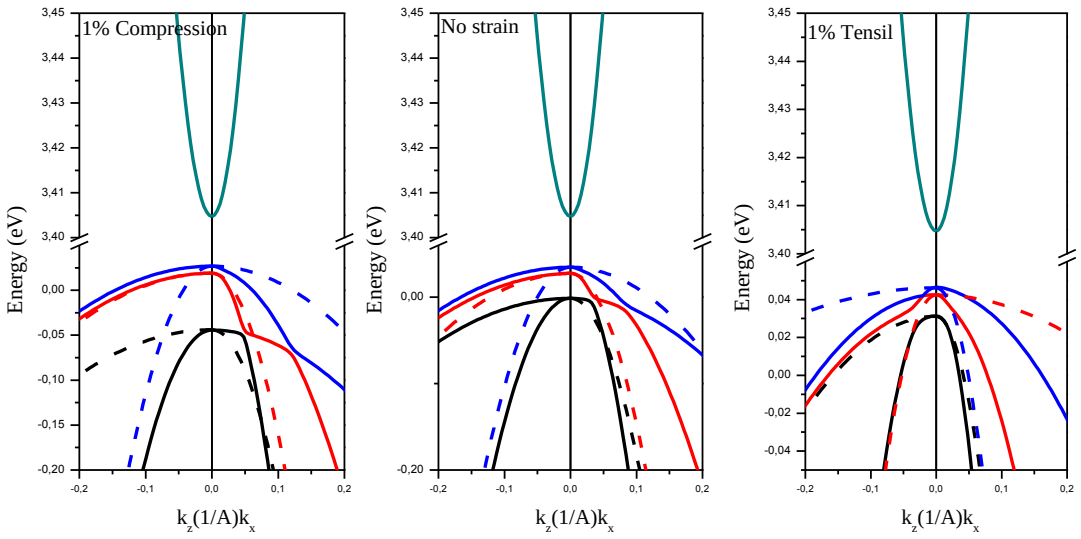

Figure 4: ZnO energy bands for different strain conditions as calculated from Equations (I.52) and (I.53) (C, conduction band; HH, heavy hole band; LH, light hole band; CH, Crystal-field split-hole band)[21].

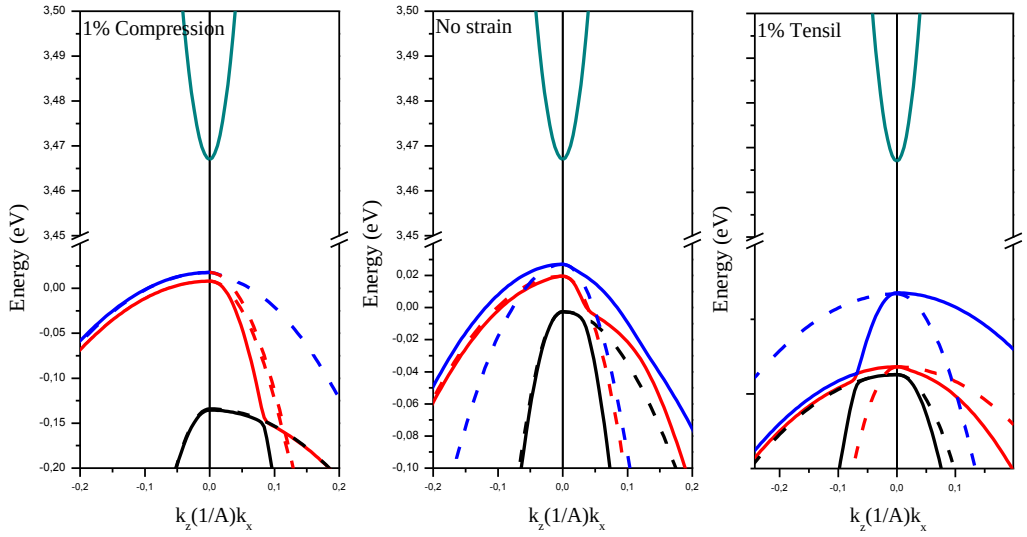

Figure 5 : GaN energy bands for different strain conditions as calculated from Equations (I.52) and (I.53) (C, conduction band; HH, heavy hole band; LH, light hole band; CH, Crystal-field split-hole band) [21].

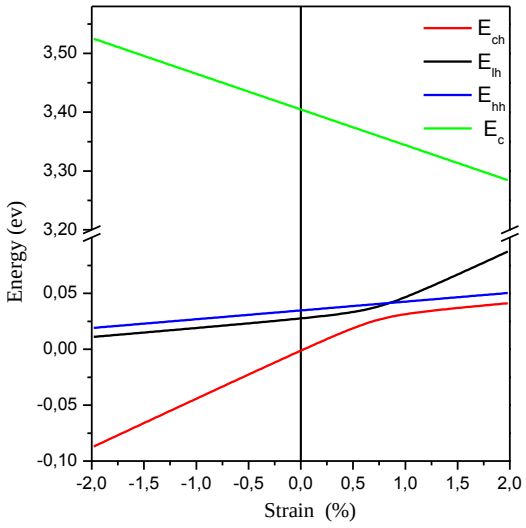

Figure 6: ZnO band edge shift vs biaxial strain for conduction band and valence bands [21].

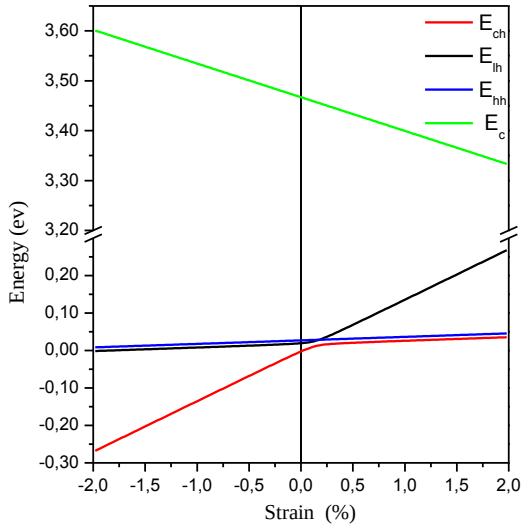

Figure 7: GaN band edge shift vs biaxial strain for conduction band and valence bands [21].

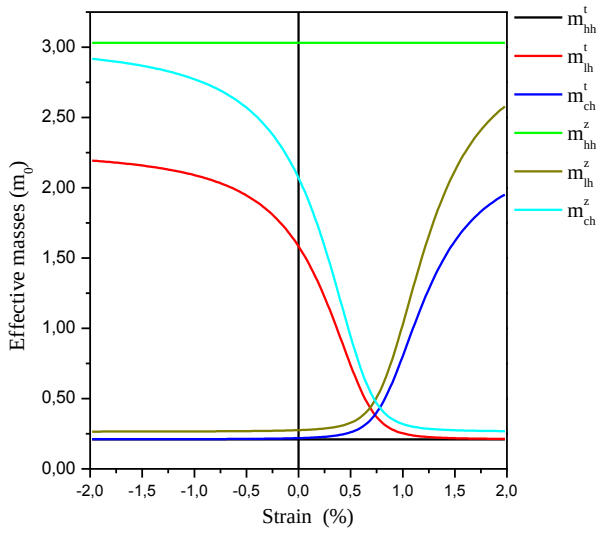

Figure 8: The ZnO bulk's effective masses (m_z/m_0 and m_t/m_0) near the band edges calculated using the analytical expressions in Equations (I.44) as a function of the in-plane compressive strain are plotted for the HH, LH, and CH bands [21].

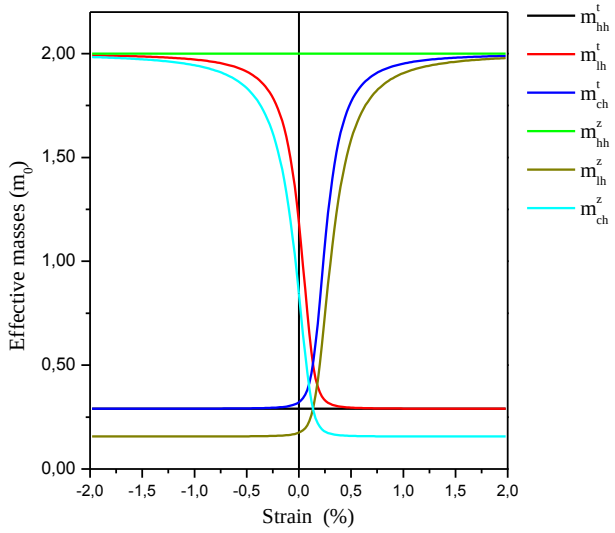

Figure 9: The GaN bulk's effective masses (m_z/m_0 and m_t/m_0) near the band edges calculated using the analytical expressions in Equations (I.44) as a function of the in-plane compressive strain are plotted for the HH, LH, and CH bands [21].

Figure (4) and (5) show ZnO and GaN energy bands for different strain conditions as calculated from Equations (I.33) and (I.43) (C, conduction band; HH, heavy hole band; LH, light hole band; CH, Crystal-field split-hole band) [21].The materials data used in all calculations are listed in Tables (3) and (4) in Appendix (A) for ZnO and GaN respectively. In all calculations a compressive strain of -1% is similar to a layer of ZnO (GaN) sandwiched between two layers of MgZnO (AlGaN) with Mg (Al) ratio of 63.5% (40%), respectively. Parabolic band are plotted for each subband and with its corresponding effective mass where it is obvious that the calculated effective masses do not agree with the real band structure .

Figure (6) and (7) show ZnO and GaN band edge shifts versus biaxial strain for conduction band and valence bands [21]. The results in the bulk of GaN (Figure (5) and (7)) are consistent with those found in Ref. [22]. With increasing tensile strain, both conduction and valence bands edges tend to close up, which in turn shrinks the band gap compared to the unstrained case. However, we note an increase in the band gap with compressive strain with smaller change compared to the tensile strained case.

Figure (8) and (9) show the ZnO and GaN bulk's effective masses ($m_z/m0$ and $m_t/m0$) near the band edges calculated using the analytical expressions in Equations (I.44) as a function of the in-plane compressive strain are plotted for the HH, LH, and CH bands [21].Both effective masses exhibit similar behavior toward strain whether it is compression or tensile strain but the only difference is in the upper and lower values for the magnitude of effective masses, where it is three times the mass of free electron in ZnO and only twice that value in GaN. The main raison for these differences is the deformation potential for each material see Tables (3) and (4) in Appendix (A). Note that the sign of D_i is opposite to that of [23] because D_i in [23] is defined as a deformation potential for the band gap.

I.6 Summary

In this chapter, we presented the elementary k.p theory to be an introduction to Chuang *et al*'s derivation of the Wurtzite Hamiltonian using Luttinger-Kohn model and showed the its similarity with the one obtained by Bir and Pikus using invariant method. Also we outlined the method to bloc diagonalize the 6x6 Wurtzite Hamiltonian to become a 3x3 matrix which is easy to solve analytically. Band structure for both conduction and valence were calculated taking into account strain effects whether it is tensile or compressive and in the same way conduction band edges, valence band edges and effective masses calculated with their parabolic bands that insufficient to predict a correct band structure.

Chapter II

Theory of electronic states in semiconductor nanostructures

II.1 Introduction:

In previous chapter we introduced the bulk Hamiltonian of Wurtzite semiconductors using k.p theory, and by using this Hamiltonian we were able to calculate the band structure of bulk Wurtzite materials such as ZnO and GaN and discuss the corresponding strain effects. Due to new technological achievements in hetero-structures fabrication using advanced epitaxial techniques for example molecular beam epitaxy MBE or metal-organic chemical vapor deposition MOCVD where the scale range from microstructures to nanostructures, the study of resulted structures become very important and while the traditional k.p theory for bulk semiconductor is no longer applicable in this situation, there for a new technique was introduced which is called Envelope Function Approximation (EFA) or Effective Mass Approximation (EMA) in some text books, the basic idea behind this method is the treatment of shallow impurities where the Bloch function is slowly varying . The application of the theory has been to many different types of nanostructures; in particular, to quantum wells (QW's), superlattices, quantum wires and nanowires, and quantum dots.

In this chapter we will be studying the basic formalism of EFA and applying it directly to our ZnO based quantum well structure and present the comparison of the ZnO's results with its counterpart GaN based structure, using numerical means such as finite difference method.

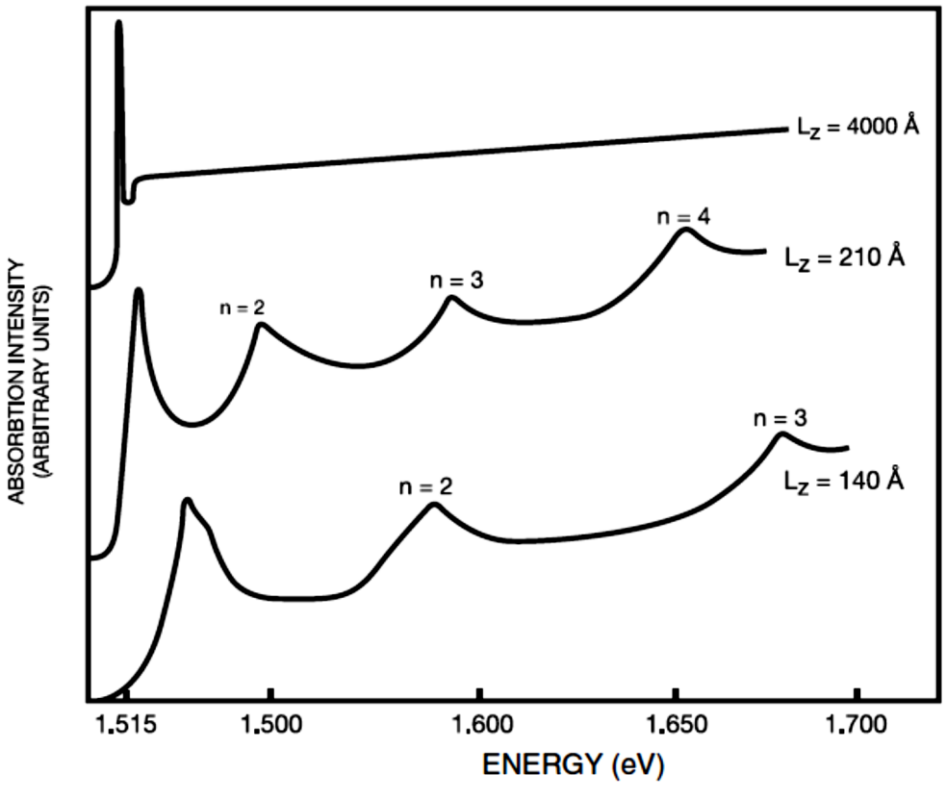

Figure 10: Absorption spectra at 2K for GaAs quantum wells [24].

II.2 The envelope function Approximation (EFA):

To fully understand the theory of electronic states in semiconductor nanostructures we must first know how to explain the origin of the discrete energy states, such as is evident in an optical spectrum for GaAs quantum wells obtained by Dingle *et al* [24] see figure (10) and to do so the effective mass approximation was introduced first by Wannier and Luttinger–Kohn theory [25,4] and subsequently applied to graded semiconductors [26] and to semiconductor inversion layers [27], with new technological growth technique such as molecular beam epitaxy MBE or metal-organic chemical vapor deposition MOCVD, where nanostructures with sharp band edges become possible, Luttinger–Kohn theory was applied also to those structures [28]. Another approaches existed after Luttinger–Kohn theory for instance the envelope-function theory of Bastard [28-30] and the most recent first principle theory by of Burt and Foreman [31- 33]. The latter differs primarily from the previous two in

attempting to derive the effective Hamiltonian from first principles. We are using the symmetrized Luttinger–Kohn Hamiltonian for the envelope function approximation for two raisons:

1-Because we are treating wide band gap materials such as ZnO and GaN, where the coupling between conduction and valence bands is not taken in consideration, thus the use of Chaung *et al* Hamiltonian [10].

2-The difference between symmetrized Luttinger–Kohn Hamiltonian for band structure (which we are using) and the other approaches are insignificant in the valence band calculations [7, 9].

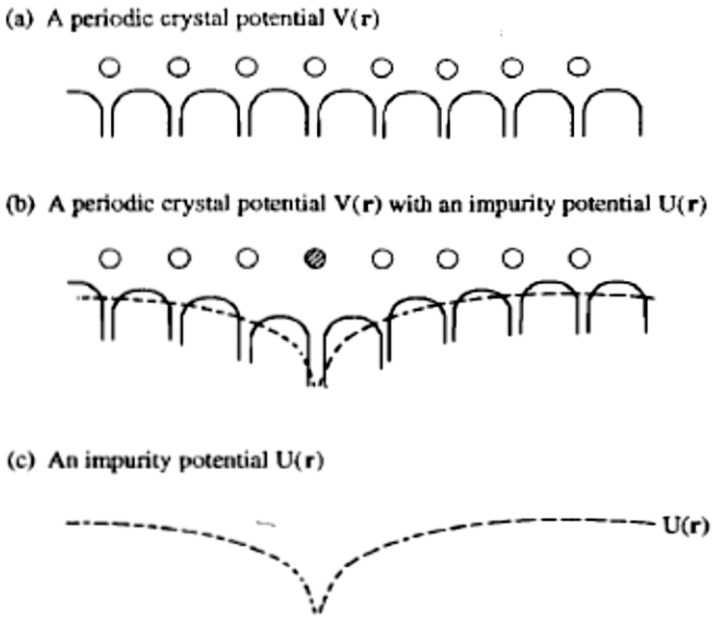

Figure 11 Illustrations of (a) the periodic potential *V(r)* and (b) the sum of the periodic potential *V(r)* and the impurity potential *U(r)*, and (c) only the impurity potential *U(r)* for the effective mass theory [3].

We can summarize the important outline of the effective mass theory (EMT) for a single band is as follows: The energy dispersion relation for a single band near k=0**,** is given by [3]

$$E_n(k) = E_n(0) + \sum_{\alpha,\beta} \frac{\hbar^2}{2}\left(\frac{1}{m^*}\right)_{\alpha,\beta} k_\alpha k_\beta \qquad \text{(II.1)}$$

for the Hamiltonian H_0, with a periodic potential $V(r)$, where

$$H_0\psi_{n,k}(r) = E_n\psi_{n,k}(r) \tag{II.2}$$

$$H_0 = \frac{p^2}{2m_0} + V(r) \tag{II.3}$$

then the solution for the Schrodinger equation with a perturbation $U(r)$ such as an impurity potential or a quantum-well potential

$$[H_0 + U(r)]\psi(r) = E\psi(r) \tag{II.4}$$

is obtainable by solving

$$\left[\sum_{\alpha,\beta}\frac{\hbar^2}{2}\left(\frac{1}{m^*}\right)_{\alpha,\beta}\left(-i\frac{\partial}{\partial x_\alpha}\right)\left(-i\frac{\partial}{\partial y_\beta}\right) + U(r)\right]F(r) = EF(r) \tag{II.5}$$

for the envelope function $F(r)$ and the energy E. The wave function is approximated by

$$\psi(r) = F(r)u_{nk_0}(r) \tag{II.6}$$

The most important result is that the periodic potential V(r) determines the energy bands and the effective masses, $\left(1/m^*\right)_{\alpha\beta}$, and the effective mass equation (II.5) contains only the extra perturbation potential $U(r)$, since the effective masses already take into account the periodic potential (Figure 11). The perturbation potential can also be a quantum-well potential, as in a semiconductor hetero-structure such as ZnO/CdZNO or GaN/InGaN quantum wells.

And with a similar way for degenerate bands to obtain:

$$\sum_{j=1}^{6}\left[E_j(0)\delta_{jj'} + \sum_{\alpha,\beta}D_{jj'}^{\alpha,\beta}\left(-i\frac{\partial}{\partial x_\alpha}\right)\left(-i\frac{\partial}{\partial y_\beta}\right) + U(r)\delta_{jj'}\right]F_j(r) = EF_j(r) \tag{II.7}$$

for the envelope function $F(r)$ and the energy E. The wave function is approximated by

$$\psi(r) = \sum_{j=1}^{6}F_j(r)u_{j0}(r) \tag{II.8}$$

To prove the effective mass theory for single band or degenerate bands, we refer you to these references [3, 34, and 35].

II.3 Numerical calculation of conduction and valence bands dispersions in quantum wells

The energy bands $E_c(k)$, $E_v(k)$ and wave functions φ_n^{η} and Ψ_m of conduction and valence states respectively, are obtained from a numerical solution of the Schrödinger equations for electrons with the electron wave function is given by

$$\left|\phi_n^{\eta}\right\rangle = e^{ik_x x' + ik_y y}\phi_n(z)\left|S\eta\right\rangle \tag{II.9}$$

where $\eta = \uparrow or \downarrow$ and S is a spherically symmetric wave function and $\phi_n(z)$ is the envelope function that satisfies

$$\left[\tilde{H}_c(k_x, k_y, -i\partial/\partial z) + (v_c(z) + eF_z z)\delta_{vu}\right]\phi_n(k_x, k_y, z) = E_c(k_x, k_y)\phi_n(k_x, k_y, z) \tag{II.10}$$

and for holes with the hole wave function is given by

$$\left|\Psi_m\right\rangle = \sum_{u=1}^{6}\left[e^{ik_x x + ik_y y} g_m^{(u)}(z)\left|v\right\rangle\right] \tag{II.11}$$

where $g_m^{(u)}(z)$ is the envelope function of the mth sub-band that satisfies

$$\sum_{\mu=0}^{6}\left[\tilde{H}_{v\mu}(k_x, k_y, -i\partial/\partial z) + (v_h(z) + eF_z z)\delta_{v\mu}\right]g_m^{(\mu)}(k_x, k_y, z) = E_m(k_x, k_y)g_m^{(\mu)}(k_x, k_y, z) \tag{II.12}$$

where the potential $v_h(z)$ $(v_c(z))$ is the potential for the valence-band (conduction-band) offset of the QW F_z is the internal electric fields and e is the electron charge.

II.3.1 Built in Electric fields in the well and barrier

If a stress τ_{jk} is applied to ZnO or GaN crystals, there is an induced piezoelectric polarization with a magnitude proportional to the applied stress τ_{jk} [19]:

$$P_i = d_{ijk}T_{jk,} \tag{II.13}$$

where d_{ijk} are the piezoelectric moduli or piezoelectric tensor elements. The stress τ_{ij} is related to the strain by

$$T_{ij} = C_{ijk}\varepsilon_{kl,} \tag{II.14}$$

where C_{ijkl} are the stiffness constants of the Wurtzite GaN crystal. Here, it is convenient to replace the tensor notation with the engineering notation for d_{ijk} and C_{ijkl}

using their symmetry properties. That is, the second and third subscripts in d_{ijk}, and the first two and the last two subscripts in C_{ijkl}, are replaced by a single subscript running from 1 to 6 as follows:

$$\begin{pmatrix} \text{tensor notation} & 11 & 22 & 33 & 23,32 & 31,13 & 12,21 \\ \text{matrix notation} & 1 & 2 & 3 & 4 & 5 & 6 \end{pmatrix}.$$

Then, the piezoelectric polarization in the (x, y, z) coordinates for a general crystal orientation is given by

$$\begin{pmatrix} P_x \\ P_y \\ P_z \end{pmatrix} = \begin{pmatrix} 0 & 0 & 0 & 0 & d_{15} & 0 \\ 0 & 0 & 0 & d_{15} & 0 & 0 \\ d_{31} & d_{31} & d_{33} & 0 & 0 & 0 \end{pmatrix} \begin{pmatrix} c_{11} & c_{12} & c_{13} & 0 & 0 & 0 \\ c_{12} & c_{11} & c_{13} & 0 & 0 & 0 \\ c_{13} & c_{13} & c_{33} & 0 & 0 & 0 \\ 0 & 0 & 0 & c_{44} & 0 & 0 \\ 0 & 0 & 0 & 0 & c_{44} & 0 \\ 0 & 0 & 0 & 0 & 0 & c_{66} \end{pmatrix} \begin{pmatrix} \varepsilon_{xx} \\ \varepsilon_{yy} \\ \varepsilon_{zz} \\ 0 \\ 2\varepsilon_{xz} \\ 0 \end{pmatrix} \quad \text{(II.15)}$$

The polarization components along x, y and z axes for the (0001)-WZ structure is written as [36, 37]

$$P_{PZ} \begin{cases} P_{PZ}^{x} = 2d_{15}C_{44}\varepsilon_{xz} \\ P_{PZ}^{y} = 0 \\ P_{PZ}^{z} = 2d_{31}(C_{11} + C_{12} + \dfrac{2C_{13}^{2}}{C_{33}})\varepsilon_{xx}^{(0)} \end{cases} \quad \text{(II.16)}$$

Using the periodic boundary condition for a superlattice structure, the build in electric fields in the well and barrier can be written as [37, 38]:

$$F_z^{w} = \frac{\left(P_{SP}^{b} + P_{PZ}^{b} - P_{SP}^{w} - P_{PZ}^{w}\right)}{\varepsilon^{w} + \varepsilon^{b}\left(L_w / L_b\right)}$$

$$F_z^{b} = -\frac{L_w}{L_b} F_z^{w} \quad \text{(II.17)}$$

where L_w (L_b) and ε_w (ε_b) are the length of well (barrier) and the static dielectric constant, respectively.

II.3.2 Finite Difference Method

In the case of quantum well QW, there are several techniques used to solve the effective mass equations for instance the finite difference method (FDM) [19], the propagation matrix method [3, 39] , and the basis expansion method [40].FDM is used here because of its simplicity and the easy implementation especially for non-complex geometries .Firstly we will apply the FDM to find numerical solutions for the simple form Hamiltonian for conduction band in equation (II.10) which can be written as:

$$H_c(k,\varepsilon)=\frac{\hbar^2}{2}\left(\frac{k_x^2+k_y^2}{m_e^t}+\frac{k_z^2}{m_e^z}\right)+\Delta_1+\Delta_2+E_g+a_{cz}\varepsilon_{zz}+a_{ct}\left(\varepsilon_{xx}+\varepsilon_{yy}\right) \tag{II.18}$$

We rewrite the Hamiltonian so it takes the form:

$$H_c(k_x,k_z,k_z,r)=H_0+H_1k_z+H_1k_z^2 \tag{II.19}$$

with

$$\begin{aligned} H_0&=\frac{\hbar^2}{2}\left(\frac{k_x^2+k_y^2}{m_e^t}\right)+\Delta_1+\Delta_2+E_g+a_{cz}\varepsilon_{zz}+a_{ct}\left(\varepsilon_{xx}+\varepsilon_{yy}\right)\\ H_1&=0\\ H_1&=\frac{\hbar^2}{2}\left(\frac{1}{m_e^z}\right)\end{aligned} \tag{II.20}$$

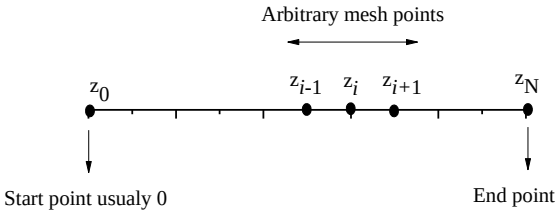

Figure 12 Discretization of z axis that coincide with growth direction.

Then we change the change wave vector k_z to its derivative form $-i\partial/\partial z$ as it is illustrated in equation (II.10) .The first order total derivative $d\Psi/dz$ at a point z = z_i can be approximated as

$$\left(\frac{\partial \psi}{\partial z}\right)_i = \frac{\psi_{i+1} - \psi_{i-1}}{2\Delta z} \tag{II.21}$$

where Δz is the difference between adjacent grid points i and $i+1$ corresponding to mesh point z_i and z_{i+1} as illustrated in Figure (12).

Using a three - point central difference representation for the second -order derivatives, the central difference is

$$\left(\frac{\partial^2 \psi}{\partial z^2}\right)_i = \frac{\psi_{i+1} - 2\psi_i + \psi_{i-1}}{\Delta z^2} \tag{II.22}$$

To ensure that Hamiltonian is Hermitian and the continuity of the probability current density in the heterostructure [39], if transformations are done as below: i.e.

$$\frac{\partial^2}{\partial z^2} H_2(z) \rightarrow \left(\frac{\partial}{\partial z} H_2(z) \frac{\partial}{\partial z}\right)$$

$$\frac{\partial}{\partial z} H_1(z) \rightarrow \frac{1}{2}\left(\frac{\partial}{\partial z} H_1(z) + H_1(z) \frac{\partial}{\partial z}\right)$$

The term containig H_1 vanish because H_1 =0 which left the remaining two term and only the term H_2 is associated with derivation ,we Then obtain

$$\begin{aligned}
\left[\frac{\partial}{\partial z}\left(H_2(z)\frac{\partial}{\partial z}\right)\right]\phi(z) &= \left(\frac{\partial}{\partial z} H_2(z)\right)\left(\frac{\partial \phi(z)}{\partial z}\right) + H_2(z)\frac{\partial^2 \phi(z)}{\partial z^2} \\
&= \left(\frac{H_2(z_{i+1}) - H_2(z_{i-1})}{2\Delta z}\right) \cdot \left(\frac{\phi(z_{i+1}) - \phi(z_{i-1})}{2\Delta z}\right) \\
&\quad + H_2(z_i)\left(\frac{\phi(z_{i+1}) - 2\phi(z_i) + \phi(z_{i-1})}{\Delta z^2}\right) \\
&= \frac{1}{\Delta z^2}\begin{pmatrix} \left(\frac{H_2(z_{i+1}) - H_2(z_{i-1})}{4}\right)\phi(z_{i+1}) \\ -\left(\frac{H_2(z_{i+1}) - H_2(z_{i-1})}{4}\right)\phi(z_{i-1}) + H_2(z_i)\phi(z_{i+1}) \\ -2H_2(z_i)\phi(z_i) + H_2(z_i)\phi(z_{i-1}) \end{pmatrix}
\end{aligned} \tag{II.23}$$

Now we rearrange the terms to have this sequence i-1 , i and i+1 i.e.

$$\left[\frac{\partial}{\partial z}\left(H_2(z)\frac{\partial}{\partial z}\right)\right]\phi(z)=\frac{1}{\Delta z^2}\begin{pmatrix} H_2(z_i)\phi(z_{i-1})-\left(\frac{H_2(z_{i+1})-H_2(z_{i-1})}{4}\right)\phi(z_{i-1}) \\ -2H_2(z_i)\phi(z_i) \\ +H_2(z_i)\phi(z_{i+1})+\left(\frac{H_2(z_{i+1})-H_2(z_{i-1})}{4}\right)\phi(z_{i+1})\end{pmatrix} \quad \text{(II.24)}$$

Then equation (II.24) become of this form

$$H_0(z_i)\phi(z_i)+\frac{1}{\Delta z^2}\begin{pmatrix} H_2(z_i)\phi(z_{i-1})-\frac{(H_2(z_{i+1})-H_2(z_{i-1}))}{4}\phi(z_{i-1}) \\ -2H_2(z_i)\phi(z_i) \\ +H_2(z_i)\phi(z_{i+1})+\frac{(H_2(z_{i+1})-H_2(z_{i-1}))}{4}\phi(z_{i+1})\end{pmatrix}=E\phi(z_i) \quad \text{(II.25)}$$

We move the left side of equation (II.25) to be grouped with the i^{th} term in the right side and the same for the terms in H_0.

$$\frac{1}{\Delta z^2}\begin{pmatrix} H_2(z_i)\phi(z_{i-1})-\frac{(H_2(z_{i+1})-H_2(z_{i-1}))}{4}\phi(z_{i-1}) \\ -2H_2(z_i)\phi(z_i)+\Delta z^2H_0(z_i)\phi(z_i)+\Delta z^2E\phi(z_i) \\ +H_2(z_i)\phi(z_{i+1})+\frac{(H_2(z_{i+1})-H_2(z_{i-1}))}{4}\phi(z_{i+1})\end{pmatrix}=0 \quad \text{(II.26)}$$

$$\begin{pmatrix} \frac{4H_2(z_i)-H_2(z_{i+1})+H_2(z_{i-1})}{4}\phi(z_{i-1})+ \\ \left(-2H_2(z_i)+\Delta z^2H_0(z_i)+\Delta z^2E\right)\phi(z_i)+ \\ \frac{H_2(z_i)+H_2(z_{i+1})-H_2(z_{i-1})}{4}\phi(z_{i+1})\end{pmatrix}=0 \quad \text{(II.27)}$$

$$\begin{pmatrix} \frac{4H_2(z_i)-H_2(z_{i+1})-H_2(z_i)+H_2(z_{i-1})+H_2(z_i)}{4}\phi(z_{i-1})+ \\ \left(-2H_2(z_i)+\Delta z^2H_0(z_i)+\Delta z^2E\right)\phi(z_i)+ \\ \frac{4H_2(z_i)+H_2(z_{i+1})+H_2(z_i)-H_2(z_{i-1})-H_2(z_i)}{4}\phi(z_{i+1})\end{pmatrix}=0 \quad \text{(II.28)}$$

We define the two average values of $H_2(z_{i+1/2})$ and $H_2(z_{i-1/2})$ as

$$H_2(z_{i+1/2})=\frac{H_2(z_{i+1})+H_2(z_i)}{2} \quad \text{(II.29)}$$

$$H_2\left(z_{i-1/2}\right)=\frac{H_2\left(z_{i-1}\right)+H_2\left(z_i\right)}{2} \tag{II.30}$$

We replace the values in equations (II.29) and (II.30) in equation (II.28).

$$\left(\begin{array}{l}\frac{2H_2(z_i)-H_2\left(z_{i+1/2}\right)+H_2\left(z_{i-1/2}\right)}{2}\phi(z_{i-1})+\\ \left(-2H_2\left(z_i\right)+\Delta z^2 H_0\left(z_i\right)+\Delta z^2 E\right)\phi(z_i)+\\ \frac{2H_2(z_i)+H_2\left(z_{i+1/2}\right)-H_2\left(z_{i-1/2}\right)}{2}\phi(z_{i+1})\end{array}\right)=0 \tag{II.31}$$

$$\left(\begin{array}{l}H_2(z_i)\phi(z_{i-1})+\frac{H_2\left(z_{i-1/2}\right)-H_2\left(z_{i+1/2}\right)}{2}\phi(z_{i-1})+\\ \left(-2H_2\left(z_i\right)+\Delta z^2 H_0\left(z_i\right)+\Delta z^2 E\right)\phi(z_i)+\\ H_2(z_i)\phi(z_{i-1})-\frac{H_2\left(z_{i-1/2}\right)-H_2\left(z_{i+1/2}\right)}{2}\phi(z_{i+1})\end{array}\right)=0 \tag{II.32}$$

We define $H_2\left(z_{i\pm1/4}\right)$ as

$$H_2\left(z_{i\pm1/4}\right)=\frac{H_2\left(z_{i-1/2}\right)-H_2\left(z_{i+1/2}\right)}{2} \tag{II.33}$$

We insert (II.33) into (II.32) to obtain:

$$\left(\begin{array}{l}\left(H_2\left(z_i\right)+H_2\left(z_{i\pm1/4}\right)\right)\phi(z_{i-1})+\\ \left(-2H_2\left(z_i\right)+\Delta z^2 H_0\left(z_i\right)+\Delta z^2 E\right)\phi(z_i)+\\ \left(H_2\left(z_i\right)-H_2\left(z_{i\pm1/4}\right)\right)\phi(z_{i+1})\end{array}\right)=0 \tag{II.34}$$

We substitute each part multiplied by $\phi(z_{i-1}), \phi(z_i)$ and $\phi(z_{i+1})$ with $a_{(i-1)\,(i-1)}$, a_{ii} and $a_{(i+1)\,(i+1)}$ to reduce equation (II.34) to:

$$\left(a_{i-1}\phi(z_{i-1})+a_i\phi(z_i)+a_{i+1}\phi(z_{i+1})\right)=0 \tag{II.35}$$

Substituting node numbers from i = 1 to i = N into Equation (II.35), we get a homogeneous system of equations written as follow:

$$\begin{pmatrix} a_{11} & a_{12} & 0 & 0 & & & \cdots & 0 \\ a_{21} & a_{22} & a_{23} & & & & & \\ 0 & a_{32} & a_{33} & a_{34} & & & & \\ 0 & 0 & \ddots & \ddots & \ddots & & & \\ & & & a_{(i-1)\,i} & a_{i\,i} & a_{(i+1)\,i} & & \vdots \\ & & & & \ddots & \ddots & \ddots & 0 \\ \vdots & \vdots & & & & a_{(N-1)(N-2)} & a_{(N-1)(N-1)} & a_{(N-1)N} \\ 0 & 0 & & & \cdots & 0 & a_{N(N-1)} & a_{NN} \end{pmatrix} \begin{pmatrix} \phi_1 \\ \phi_2 \\ \vdots \\ \vdots \\ \phi_i \\ \vdots \\ \phi_N \\ \phi_N \end{pmatrix} = 0 \tag{II.36}$$

Here, we apply the Dirichlet condition that the wave functions at the boundaries are set to zero although there other boundary condition that could be used for instance Neumann boundary conditions:

$$\phi_i = 0 \tag{II.37}$$

Now the system is reduced to an eigenvalue problem where the eigenvalues obtained from solving the determinant of the matrix in equation (II.36) then the founded eigenvalues are inserted into Equation (II.35) to find the Eigen functions.

A Fortran language code of conduction band calculation using finite difference method is given in Appendix (E) and similar program with multi-quantum well ability and self-consistent calculations is implemented in an open source code called Aestimo (in versions 0.8 , 0.9 and 1.0 FDM ,0.7 Shouting method which is out of the scope of this work) written in Python language [41].

In a multiband case such as in Hamiltonian of equation (II.12) every Hamiltonian element spans on the grid to become an N × N block. If the element does not contain k_z, then the N × N block is just a constant matrix. If the element contains k_z or k^2_z , then the N ×N block follows the same form as in equation (II.18). Thus the 6×6 Chaung Hamiltonian on a 1D grid with N points see figure (12), becomes a 6N × 6N matrix. Diagonalizing this Hamiltonian gives 6N eigenenergies and corresponding

wave functions, each of which is composed of six components (the Chaung basis), which are spanned on the N grid points.

The Hamiltonian has the following form (here is the 3x3 block diagonalized Hamiltonian mentioned in chapter I):

$$\begin{pmatrix} \begin{pmatrix} \cdots & \cdots & \cdots \\ \cdots & H^{11} & \cdots \\ \cdots & \cdots & \cdots \end{pmatrix} & \begin{pmatrix} \cdots & \cdots & \cdots \\ \cdots & H^{12} & \cdots \\ \cdots & \cdots & \cdots \end{pmatrix} & \begin{pmatrix} \cdots & \cdots & \cdots \\ \cdots & H^{13} & \cdots \\ \cdots & \cdots & \cdots \end{pmatrix} \\ \begin{pmatrix} \cdots & \cdots & \cdots \\ \cdots & H^{21} & \cdots \\ \cdots & \cdots & \cdots \end{pmatrix} & \begin{pmatrix} \cdots & \cdots & \cdots \\ \cdots & H^{22} & \cdots \\ \cdots & \cdots & \cdots \end{pmatrix} & \begin{pmatrix} \cdots & \cdots & \cdots \\ \cdots & H^{23} & \cdots \\ \cdots & \cdots & \cdots \end{pmatrix} \\ \begin{pmatrix} \cdots & \cdots & \cdots \\ \cdots & H^{31} & \cdots \\ \cdots & \cdots & \cdots \end{pmatrix} & \begin{pmatrix} \cdots & \cdots & \cdots \\ \cdots & H^{32} & \cdots \\ \cdots & \cdots & \cdots \end{pmatrix} & \begin{pmatrix} \cdots & \cdots & \cdots \\ \cdots & H^{33} & \cdots \\ \cdots & \cdots & \cdots \end{pmatrix} \end{pmatrix} \begin{pmatrix} \begin{pmatrix} \cdots \\ \Phi^{(1)} \\ \cdots \end{pmatrix} \\ \begin{pmatrix} \cdots \\ \Phi^{(2)} \\ \cdots \end{pmatrix} \\ \begin{pmatrix} \cdots \\ \Phi^{(3)} \\ \cdots \end{pmatrix} \end{pmatrix} = 0 \tag{II.38}$$

where H^{ij} and $\Phi^{(i)}$ take the same form in equation (II.36).

Table 1 Classification of the 3x3 Hamiltonian elements according to k_z power.

k_z power/ Element	k_z^2	k_z^1	k_z^0
λ	$\frac{\hbar^2}{2m_0}A_1k_z^2$	0	$\frac{\hbar^2}{2m_0}\left[A_2\left(k_x^2+k_y^2\right)\right]+\lambda_{\varepsilon}$
θ	$\frac{\hbar^2}{2m_0}A_{31}k_z^2$	0	$\frac{\hbar^2}{2m_0}\left[A_4\left(k_x^2+k_y^2\right)\right]+\theta_{\varepsilon}$
K	0	0	$\frac{\hbar^2}{2m_0}A_5(k_x+ik_y)^2+D_5\varepsilon_{\pm}$
H	0	$\frac{\hbar^2}{2m_0}A_6(k_x+ik_y)k_z$	$D_6\varepsilon_{z\pm}$
$\Delta_1 and\ \Delta_2$	0	0	$\Delta_1 and\ \Delta_2$

Note that the 3x3 Hamiltonian is numerically implemented in Aestimo 0.9 and 1.0 with self-consistent solution for zinc blende and Wurtzite materials [41].

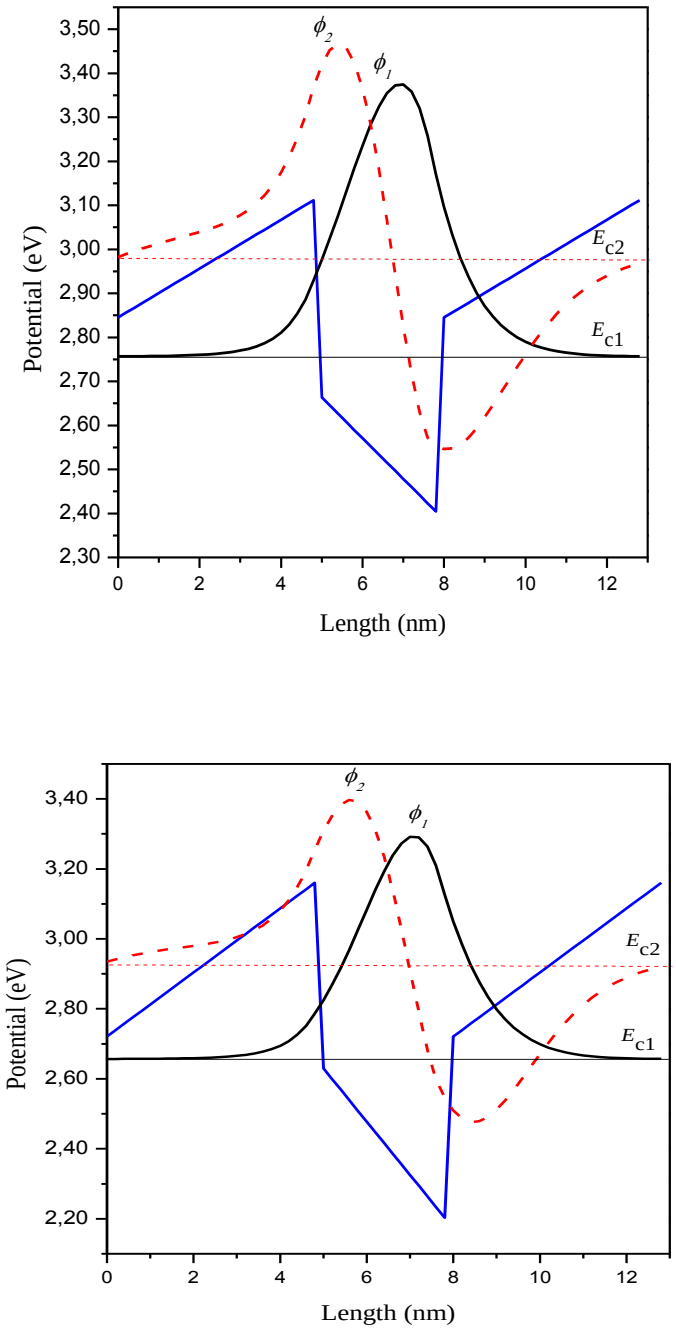

Figure 13 conduction band edges and wave functions at the zone center with piezoelectric and spontaneous polarizations for $ZnO/Cd_{15}Zn_{85}O$ (a) and $GaN/In_{15}Ga_{85}N$ (b) QW structures [21].

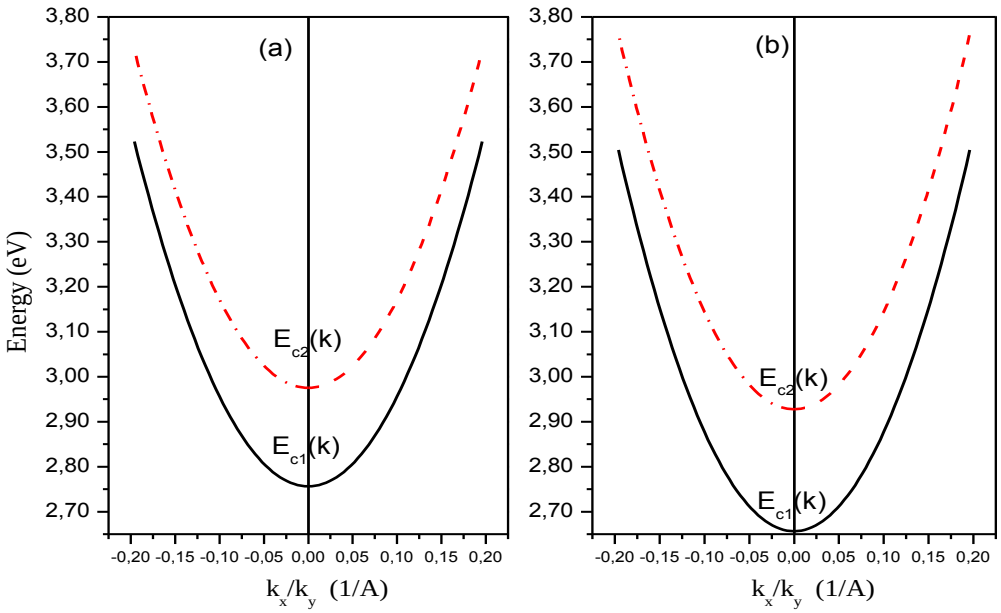

Figure 14 Conductions-band structures of Wurtzite $ZnO/Cd_{15}Zn_{85}O$ (a) and $GaN/In_{15}Ga_{85}N$ (b) QW.

Figure (13) show conduction band edges and wave functions at the zone center with piezoelectric and spontaneous polarizations for $ZnO/Cd_{15}Zn_{85}O$ (a) and $GaN/In_{15}Ga_{85}N$ (b) QW structures.Note that the length of the well is 3nm with barriers of 5 nm and Cadmium and Indium composition of 15% for CdZnO and InGaN respectively. Stark effect is present in the well region and causing the wave function shift from the center of the well .The first subband is total confined unlike the second subband which is confined in one side of the well barriers.

Figure (14) show Conductions-band structures of Wurtzite $ZnO/Cd_{15}Zn_{85}O$ (a) and $GaN/In_{15}Ga_{85}N$ (b) QW.Both band structures are parabolic because we used the parabolic model and we are only interested in the strain shifts and transition strength.

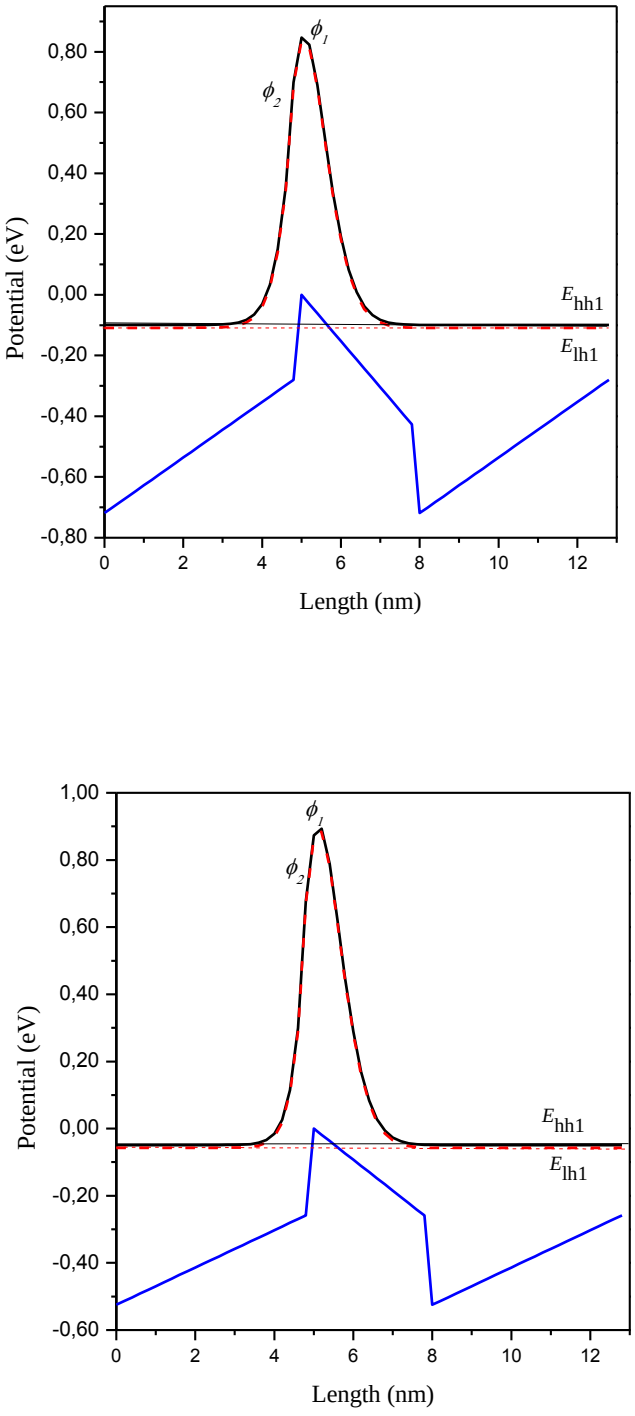

Figure15 Valence band edges and wave functions at the zone center with piezoelectric and spontaneous polarizations for $ZnO/Cd_{15}Zn_{85}O$ (a) and $GaN/In_{15}Ga_{85}N$ (b) QW structures [21].

Figure (15) shows Valence-band structures of Wurtzite $ZnO/Cd_{15}Zn_{85}O$ (continuous line) and $GaN/In_{15}Ga_{85}N$ (dashed line) QW structures Stark effect is present in the well region and causing the wave function shift from the center of the well .

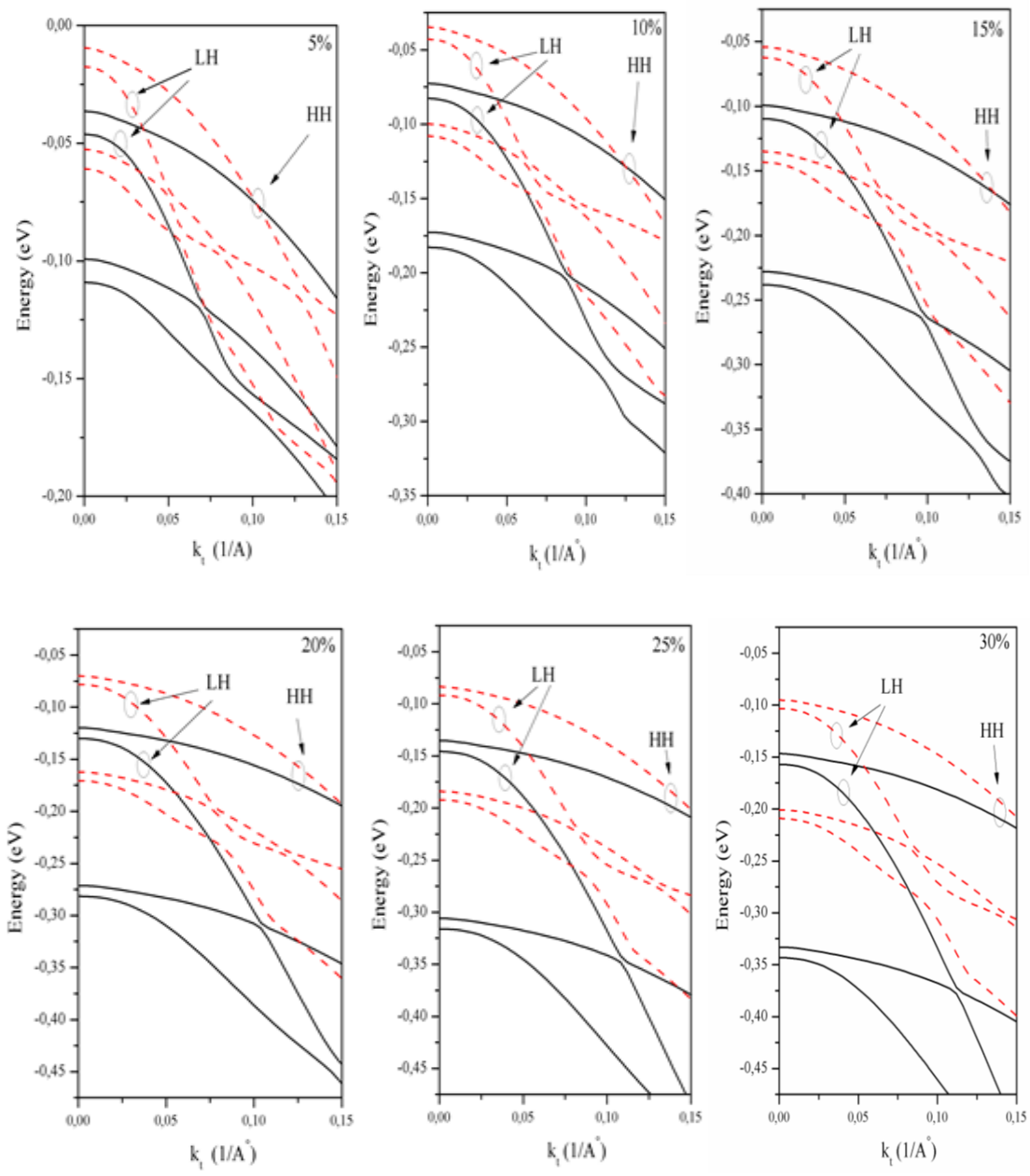

Figure 16 Valence-band structures of Wurtzite $GaN/In_xGa_{1-x}N$ (continuous line) and $ZnO/Cd_xZn_{1-x}O$ (dashed line) QW structures as function of the in-plane wave vector k_t in different x values[21].

In Figure (16), the valence band structure of Wurtzite $ZnO/Cd_xZn_{1-x}O$ in dashed line and $GaN/In_xGa_{1-x}N$ in continuous line QW structures as function of the in-plane wave vector k_t for both band structures are calculated for different values of the ratio x of Cd (Cadmium) and In (Indium).The first two subbands are heavy hole and light hole for both structures and they almost have the same subband distance which is very important in density of state estimation. Band wrapping occurs in greater values in GaN based structure than in ZnO based structure, which is consistent with the distance of the second two subbands in both band structures. Increasing the ratio of Cd (In) is consistent with an increase in compressive strain applied to the well region in both structures starting from −0.61% (−1.05%) to −1.8% (−3.1%) for ZnO (GaN) based structures with Cd (In) ratio of 10% to 30%, respectively. For ZnO based structure, strain values are consistent with experimental results. We can see that the value of compressive strain in GaN base structure is larger than in ZnO based structure due to greater mismatch between barrier and well in GaN base structure. Thus, a larger band shifting is expected, the first two subbands in each structure receive a similar energy shift ensuing from D_1, D_2, D_3 and D_4 deformation potentials, where the two first ones tend to decrease energy levels and the last two do the opposite but the dominant shift is the one that decrease energy levels with larger amount in GaN case compared to ZnO [21].

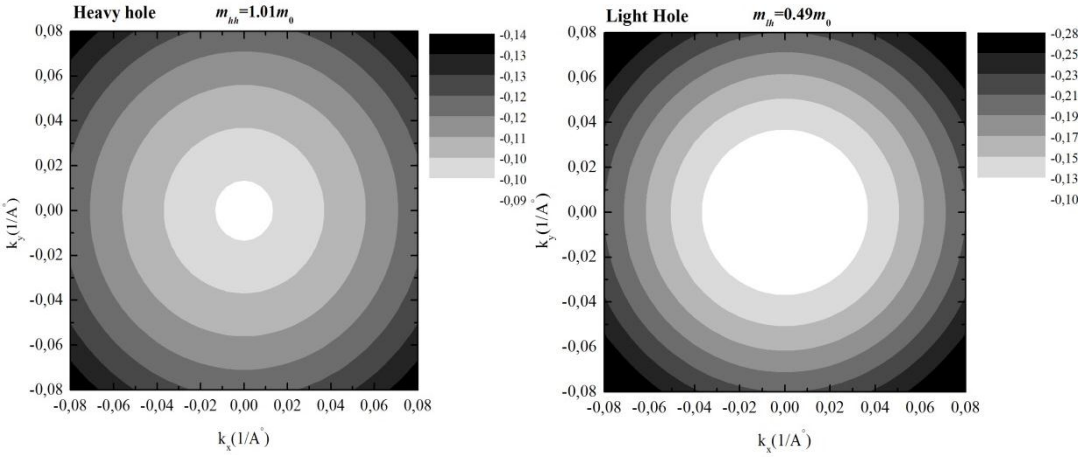

Figure 17 Isoenergy plot of the GaN/InGaN heavy- and light-hole bands in the k_x-k_y plane near the Γ point color scale in (eV) [21].

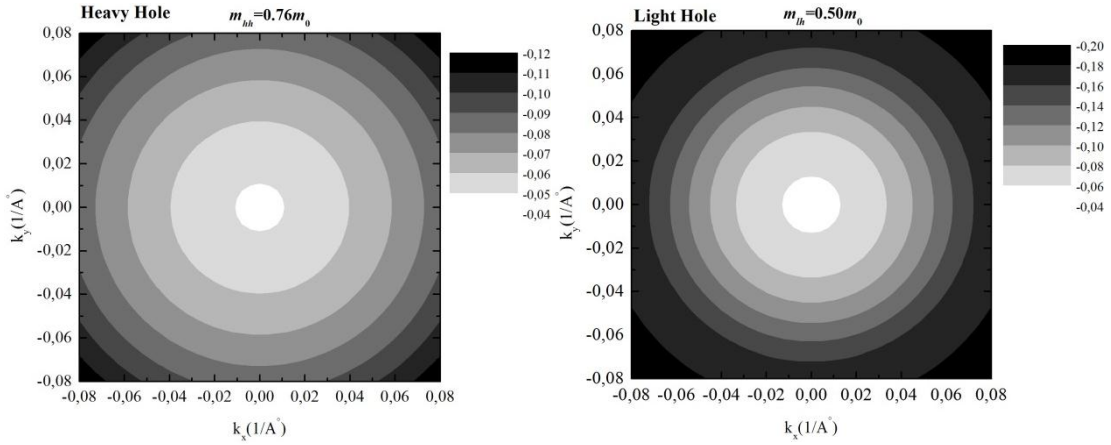

Figure18 Isoenergy plot of the ZnO/CdZnO heavy- and light-hole bands in the k_x−k_y plane near the Γ point colour scale in (eV) [21].

Figure (17) and (18) show constant energy contour of GaN/InGaN and ZnO/CdZnO heavy- and light-hole bands in the k_x−k_y plane near the Γ point, respectively. Both plots illustrate the isotropic nature of heavy hole and light hole bands. Thus, the averaged effective masses are also isotropic with heavy hole mass of $0.76m_0$ ($1.01m_0$) and light hole mass of $0.50m_0$ ($0.49m_0$) for ZnO (GaN) based structure, respectively. The method used to obtain these masses is by shiefting their energy level to coincide with a null energy level then considering a parabolic form of energy band and calculating the effective mass for every k point to have an averaged value at the end. To determine the strain effect on effective masses, we calculated the latter without strain influence and found an increase in all effective masses with heavy hole mass of $0.85m_0$ ($1.08m_0$) and light hole mass of $0.56m_0$ ($0.81m_0$) for ZnO (GaN) based structure, respectively. The main raison for this increase is the change in energy levels spacing which in turn is responsible for energy band coupling that affects the curvatures of energy levels [21].

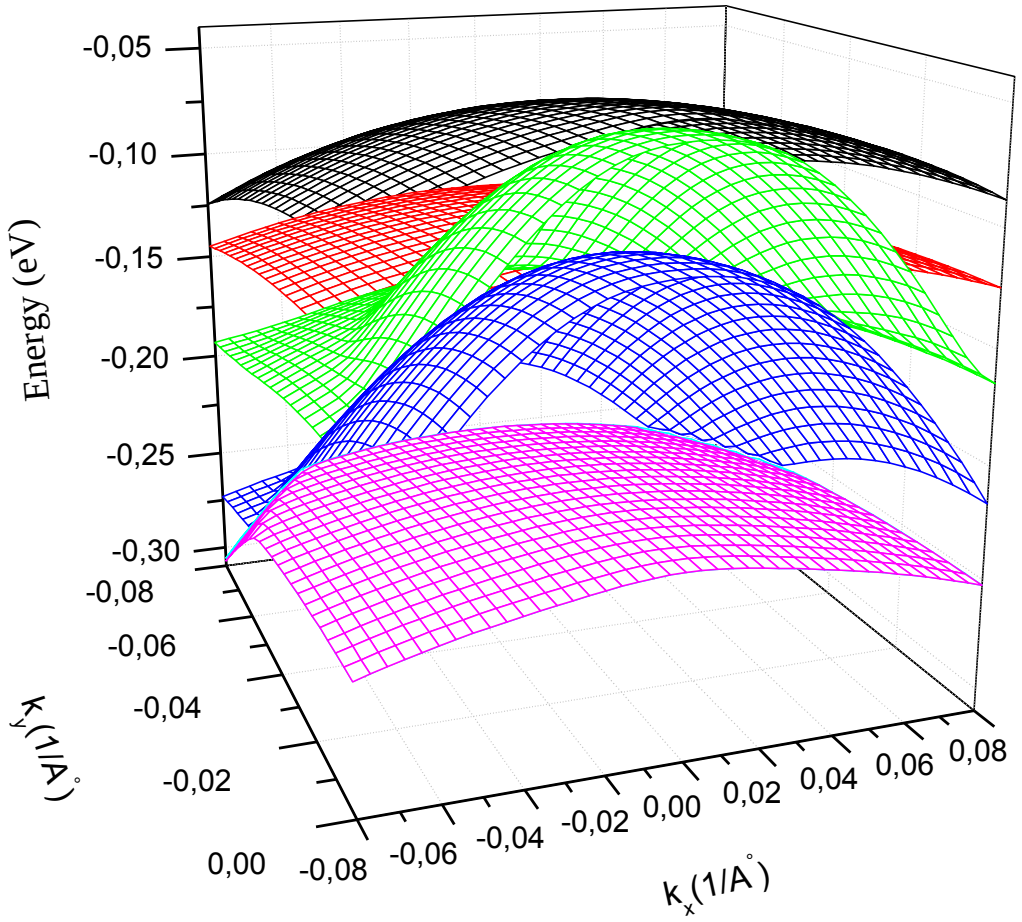

Figure 19 Energy dispersion in the (k_x-k_y) plane at the valence band edge of ZnO.

Figure (19) is the same as figure (18) but in three dimensions to illustrate clearly the isotropic nature of the valence band structure which means also isotropic effective masses which effect the electronic and the optical properties of the structure.

II.4 Summary:

In this chapter, we introduced the basic formalism of EFA and its direct application to our ZnO based quantum well structure and presented the comparison of the ZnO's results with its counterpart GaN based structure, such as band edges profiles, band structures and isoenergy counters, using numerical means such as finite difference method.

Chapter III

Theory of Optical Gain in Semiconductors

III.1 Introduction:

Optical gain is one of the most important basic properties of semiconductor lasers. Optical gain is simply defined as the growth ratio of light intensity (photon density) per unit length of light propagation. In a semiconducting material, the electrons and holes do not move as free particles, so the relation between energy, momentum and mass is different from that of a free particle. However, in many cases, the relation between energy and momentum is still nearly parabolic; hence an *effective mass* can be defined. In most of the materials of interest for semiconductor lasers, we find that the effective mass for the electrons in the conduction band, m_C, is smaller than the effective mass for the holes in the valence band, m_v.

In a semiconductor hetero structure, which is small in one or more dimensions, the carriers (electrons and holes) do not behave like particles. Instead, they start to display wave nature, and their behavior must be treated according to the rules of quantum mechanics.

In this chapter we will be discussing the basic optical gain formalism starting from the definition of optical transition and their transition strength or as called momentum matrix elements to broadening effect, where a different type from the conventional Lorentzian function is presented and thus the Gaussian or non-Markovian line shape function .Numerous effects on optical gain are will be discussed in this chapter for instance built in electric field due to piezoelectric and spontaneous polarization , many body effects , strain effect and carrier concentration effect.

III.2 Optical transitions:

Transitions of electrons from the conduction band to the valence band induced by photons are the main cause of optical gain in semiconductors. Therefor to understand the latter one we have to examine its transitions.

The interaction between the photons and the electrons in semiconductor using Fermi Golden Rule are described by the Hamiltonian [42]:

$$H = \frac{p^2}{2m_0} + V(r) - \frac{e}{2m_0}(p \cdot A + A \cdot p) + \frac{e^2 A^2}{2m_0} \quad \text{(III.1)}$$

where A (r, t)is the vector potential accounting for the presence of the electromagnetic field.After using the coulomb gauge where $\nabla A(r,t) = 0$ and neglecting the last term against linear terms in A(r, t), the final form of the Hamiltonian is

$$H = -\frac{e}{m_0} A(r,t) \cdot p \quad \text{(III.2)}$$

$$H = H'(r)e^{-iwt} + H'^{+}(r)e^{+iwt} \quad \text{(III.3)}$$

where $H'(r)$ is

$$H'(r) = -\frac{eA_0 e^{ik_{op}r}}{2m_0}\hat{e} \cdot p \quad \text{(III.4)}$$

The plus sign in the second $H'(r)$ means Hermitian adjoint and k_{op} is the wave vector, w is the optical angular frequency and $\hat{e}$ is a unit vector in the direction of optical electric field.

The optical matrix element discussed in section (III.3) is the projection of resulted interaction Hamiltonian of electromagnetic field and mater in their bases and it is the basic element in the description of optical transition properties such as spontaneous emission spectrum, optical gain and refractive index and the first two will be discussed in this work.

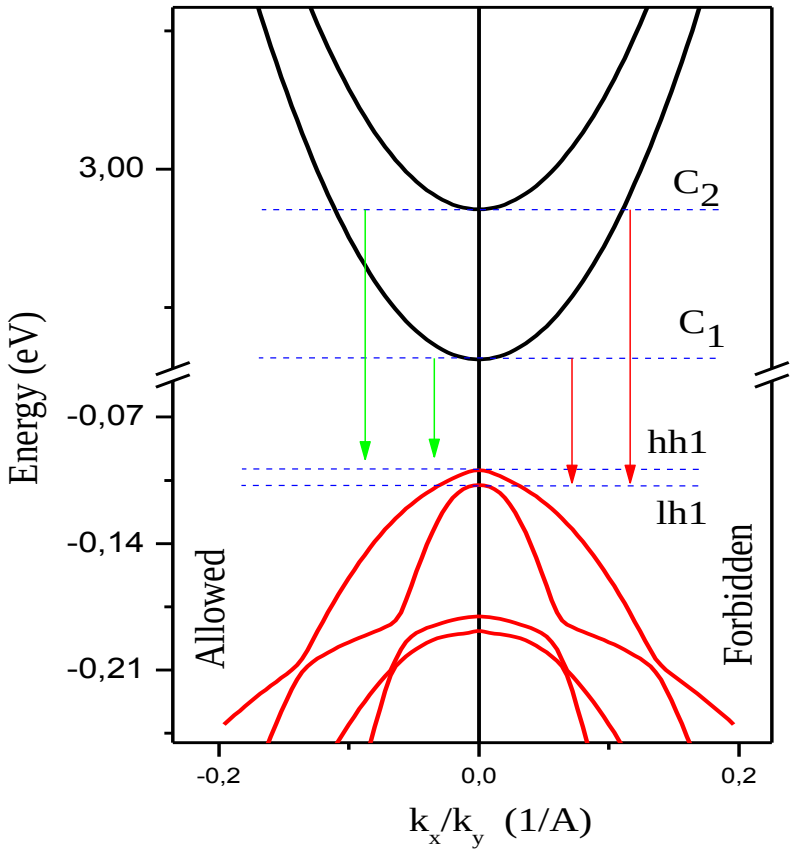

Figure 20 Allowed and forbidden transitions in a quantum well (C#, conduction band; HH#, heavy-hole band; LH#, light-hole band; #, subband number) [43].

The allowed transitions in figure (20) have very strong transition probabilities, whereas the forbidden transitions have zero transition probability in an infinite barrier quantum well and weak probability at best in a finite barrier quantum well.

III.3 Interband Optical Momentum Matrix Elements

In order to calculate the optical transition rates in quantum wells we will need momentum matrix element between the valence and conduction band states. We assume that the valence band and the conduction band states are,

$$|\Psi_m\rangle = \sum_{u=1}^{6}\left[e^{ik_x x+ik_y y} g_m^{(u)}(z)|v\rangle\right] \tag{III.5}$$

and

$$|\phi_n^{\eta}\rangle = e^{ik_x x'+ik_y y}\phi_n(z)|S\eta\rangle \tag{III.6}$$

The optical momentum matrix elements are given by

$$\left|\hat{e}\cdot M^{\eta}\right|^2 = \left|\left\langle \Psi_l^{c\eta}\left|\hat{e}\cdot p\right|\Psi_m^{v}\right\rangle\right|^2 \tag{III.7}$$

where $\Psi_l^{c\eta}$ (Ψ_m^{v}) is the wave function for the conduction (valence) band, and $\eta = \uparrow$ and $\downarrow$ for both electron spins. The indexes and stand for the electron states in the conduction band and the heavy-hole (light hole) subband states in the valence band, respectively. The interband momentum matrix elements for each spin orientation can be written as follows. For TE- polarization ($\hat{e} = \cos\phi\hat{x} + \sin\phi\hat{y}$) [44]:

$$\begin{aligned}
\left|\hat{e}\cdot M^{\uparrow}\right|^2 &= \left|\cos\phi\frac{p_x}{\sqrt{2}}\left\{-\left\langle g_m^{(1)}\middle|\phi_l\right\rangle + \left\langle g_m^{(2)}\middle|\phi_l\right\rangle\right\} - i\sin\phi\frac{p_y}{\sqrt{2}}\left\{\left\langle g_m^{(1)}\middle|\phi_l\right\rangle + \left\langle g_m^{(2)}\middle|\phi_l\right\rangle\right\}\right|^2 \\
\left|\hat{e}\cdot M^{\downarrow}\right|^2 &= \left|\cos\phi\frac{p_x}{\sqrt{2}}\left\{\left\langle g_m^{(4)}\middle|\phi_l\right\rangle - \left\langle g_m^{(5)}\middle|\phi_l\right\rangle\right\} - i\sin\phi\frac{p_y}{\sqrt{2}}\left\{\left\langle g_m^{(4)}\middle|\phi_l\right\rangle + \left\langle g_m^{(5)}\middle|\phi_l\right\rangle\right\}\right|^2
\end{aligned} \tag{III.8}$$

where $g_m^{(v)}$ (v =1, 2,3,4,5 and 6) is the wave function for the mth subband in (x,y,z) coordinates, note that we use only the TE polarized momentum matrix elements because it was found that optical gain is by far larger in TE polarization than TM [44].Also

$$\begin{aligned}
P_z &= \langle S|p_z|Z\rangle = \frac{m_0}{\hbar}P_1 \\
P_x &= P_y = \langle S|p_x|X\rangle = \langle S|p_y|Y\rangle = \frac{m_0}{\hbar}P_2 \\
P_1^2 &= \frac{\hbar^2}{2m_0}\left(\frac{m_0}{m_e^z}-1\right)\frac{\left(E_g+\Delta_1+\Delta_2\right)\left(E_g+2\Delta_2\right)-2\Delta_3^2}{E_g+2\Delta_2} \\
P_2^2 &= \frac{\hbar^2}{2m_0}\left(\frac{m_0}{m_e^t}-1\right)\frac{E_g\left[\left(E_g+\Delta_1+\Delta_2\right)\left(E_g+2\Delta_2\right)-2\Delta_3^2\right]}{\left(E_g+\Delta_1+\Delta_2\right)\left(E_g+\Delta_2\right)-\Delta_3^2}
\end{aligned} \tag{III.9}$$

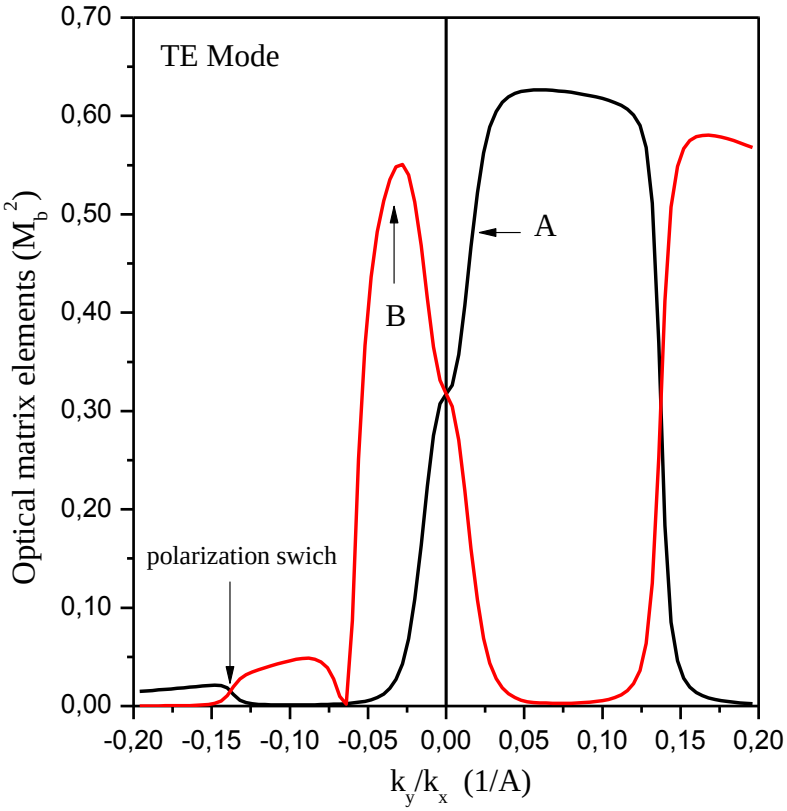

Figure 21 y-polarized optical matrix elements as a function of and wave vectors and of wurtzite $ZnO/Cd_{15}Zn_{85}O$ QW structures with transition A (continuousline) and transition B (dashed line) [43].

Figure (21) shows the y-polarized optical matrix elements as a function of and wave vectors and of wurtzite $ZnO/Cd_{15}Zn_{85}O$ QW structures with transition A (continuousline) and transition B (dashed line). We only plotted the y-polarized optical matrix elements without the x -polarized optical matrix elements because we the latter is very small compared to y-polarized one. Polarization switching is very obvious and happens several times between transition A and B (the crossing of the two optical matrix elements) [45].

III.4 Quantum Well Density of States:

One of the most important objectives in describing a semiconductor in relation to its electrical and optical properties is to determine both the carrier concentrations and the energy distributions. These require knowledge of (i) the probability of carrier occupancy of a state at energy E which we will see later and (ii) the density of

available states, or density of states (DOS), we will be dealing with only the 2D density of states in quantum well. The 2D density of states is defined as the number of states per energy per unit surface of real space [46].

In order to evaluate the number of electronic states (*dN*) over the range between *k* and *k* + *dk*, in figure (23) the spherical surface between *k* and *dk*, i.e. $\pi k^2 dk$, is divided by $(2\pi)^2/S$.(the result should also be multiplied by a factor of two in order to account for the fact that each state with a specific value of *k* can be occupied by two electrons with opposite spins.) Thus, the expression for *dN* can be written as [46]

$$dN = S\frac{k^2 dk}{2\pi} \tag{III.10}$$

For the parabolic bands, we can write $k = \left[2m_e^*(E_v - E)/\hbar^2\right]^{1/2}$, and $kdk = 2m_e^* dE/\hbar^2$ and thus, the DOS can be written as

$$D(E) = \frac{m_{eff}}{\pi\hbar^2} \tag{III.11}$$

with units of number per unit energy per unit area. Notice that it is a constant.

Actually, The dispersion relation of a band given by *E* = *E* (*k*) is not always parabolic. Thus, if several non-parabolic bands overlap, the densities of state of all bands need to be summed up. The density of states at the energy E for the given band is [47]

$$D(E')dE = 2\int \frac{d^2k}{(2\pi/L)^2}\delta(E'-E(k)) \tag{III.12}$$

The surface integral can be converted to a length integral over the isoenergy surface (see figure (17) and (18) in chapter (II)) $S(E')$ the surface element d^2k is written as d^2ld $k_\perp$ The vector $k_\perp$ is perpendicular to *l*(E') and proportional to $\nabla_k E$(k), i.e. d*E* = $|\nabla_k$ *E*(k)|d $k_\perp$

$$D(E') = 2\oint_{l(E')} \frac{d^2l}{(2\pi/L)^2}\frac{1}{\nabla_k E(k)}$$

$$D(E) = \frac{L^3}{4\pi^3}\oint_{l(E)} \frac{d^2l}{\nabla_k E(k)} \tag{III.13}$$

There are several methods in calculating 2D density of states and the simplest one is so called Gilat-Raubenheimer method [48] developed by Gilat *et al* for cubic crystals [49] and Wurtzite hcp [50].For the gradient of energy appearing in the above equations we use Hellmann-Feynman theorem [51] to find it.

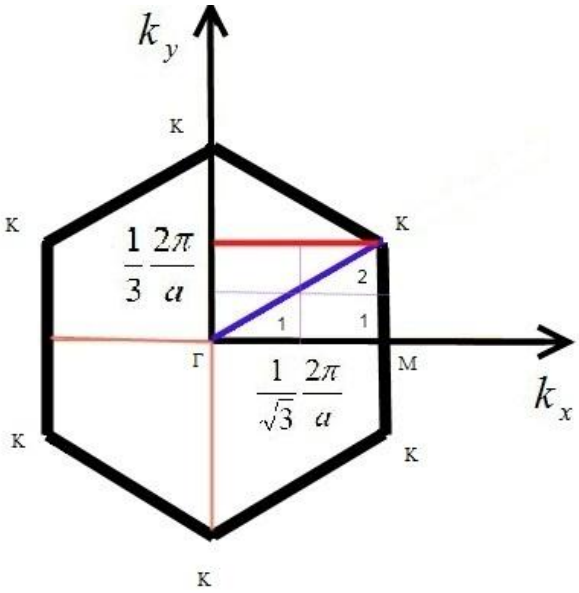

Figure 22 First Brillouin zone of Wurtzite crystals with symmetry points Γ, M and K, Illustration of discretization choice in DOS calculations [52].

We avoid the use of fluctuating weighting factor proposed by Gilat *et al* by choosing the number of discretization along k_y double the one along k_x and fixing the weighting factor to 0.5 for $i=j$ and 1 otherwise, this choice allow us to limit our calculation in energy dispersion and energy gradient to half the total number see figure (22), where a simple discretization scheme is plotted.

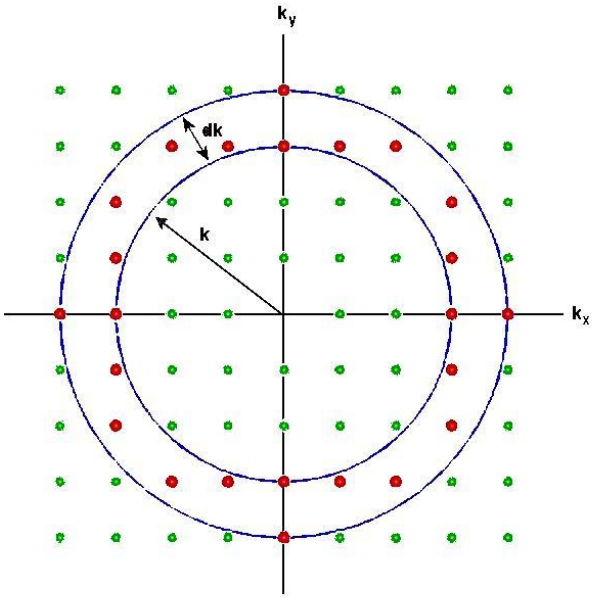

Figure 23 A two-dimensional k-space in which the states are equally spaced on the k_x-and k_y-axes.

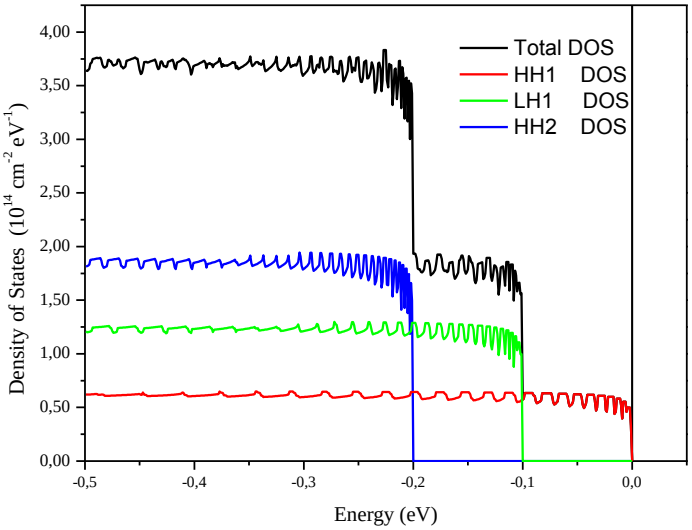

Figure 24 2D density of states of for $ZnO/Cd_{15}Zn_{85}O$ structure for parabolic bands [52].

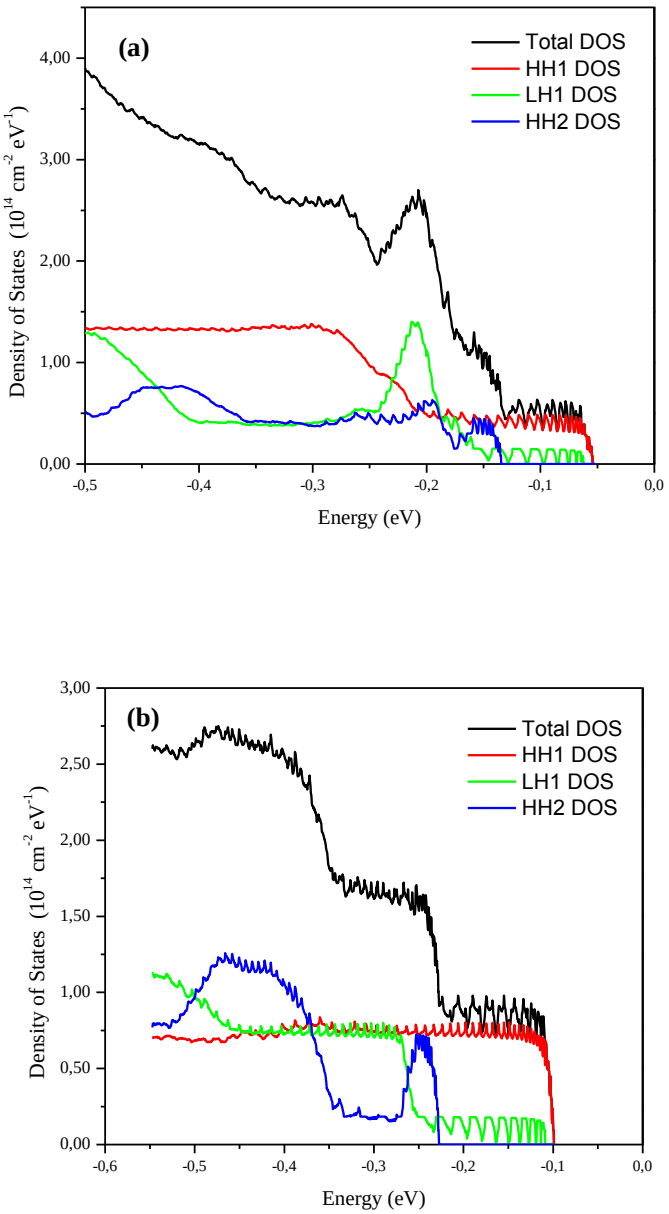

Figure 25 2D density of states of for $ZnO/Cd_{15}Zn_{85}O$ (a) and $GaN/In_{15}Ga_{85}N$ (b) QW structures [52].

As result of numerical calculation the 2D density of states of for $ZnO/Cd_{15}Zn_{85}O$ (a) and $GaN/In_{15}Ga_{85}N$ (b) QW structures are plotted in figure (25) and to verify the correctness of programming also 2D density of states for parabolic bands are plotted too, the latter are the same as predicted by equation (III.), the three first subbands density of states are plotted separately along with the total density of states and showed more parabolic behavior in $GaN/In_{15}Ga_{85}N$ (b) QW structure than that of

$ZnO/Cd_{15}Zn_{85}O$ due to step shape of density of states . The relatively high density of states in both structures near the band edge is attributed to the small subband difference between the first two subbands and this is a key factor in enhanced laser performance [52].

III.5 Fermi levels:

Electrons and holes are *fermions*, and the probability that a certain energy state is occupied is therefore given by a *Fermi–Dirac distribution*. The number of occupied states with a given energy in the conduction band (unoccupied states, i.e. holes, in the valence band) is given by the product of the density of states in the conduction (valence) band, multiplied by the probability of occupation f_c (the probability of finding an empty state is 1 - f_v). These probabilities are given by [3]

$$f_c(E) = \frac{1}{1+\exp\left(\frac{E-\varepsilon_c}{k_B T}\right)} \text{ and } 1-f_v(E) = \frac{1}{1+\exp\left(-\frac{E-\varepsilon_v}{k_B T}\right)} \qquad \text{(III.14)}$$

where the Fermi level ε_c (ε_v) (cf figure 18) is found by requiring that the integral (over all energies) of the product of the density of states and the occupation probability is equal to the total number of electrons (holes). In the case of charge neutrality and no doping, the number of electrons must be equal to the number of holes.

For a given injection level, the electron and hole concentrations are related by the charge neutrality condition [3]

$$n + N_A = p + N_D \qquad \text{(III.15)}$$

where N_A and N_D are the ionized acceptor and donor concentrations, respectively, in the active region and are assumed to be zero for an undoped active layer. The electron concentration n and the hole concentration p are related to the quasi-Fermi levels, f_c and f_v in (III.14), by [44]

$$n = \frac{2}{L_w}\sum_n \int \frac{k_t dk}{2\pi} f_n^c(k_t) \qquad \text{(III.16)}$$

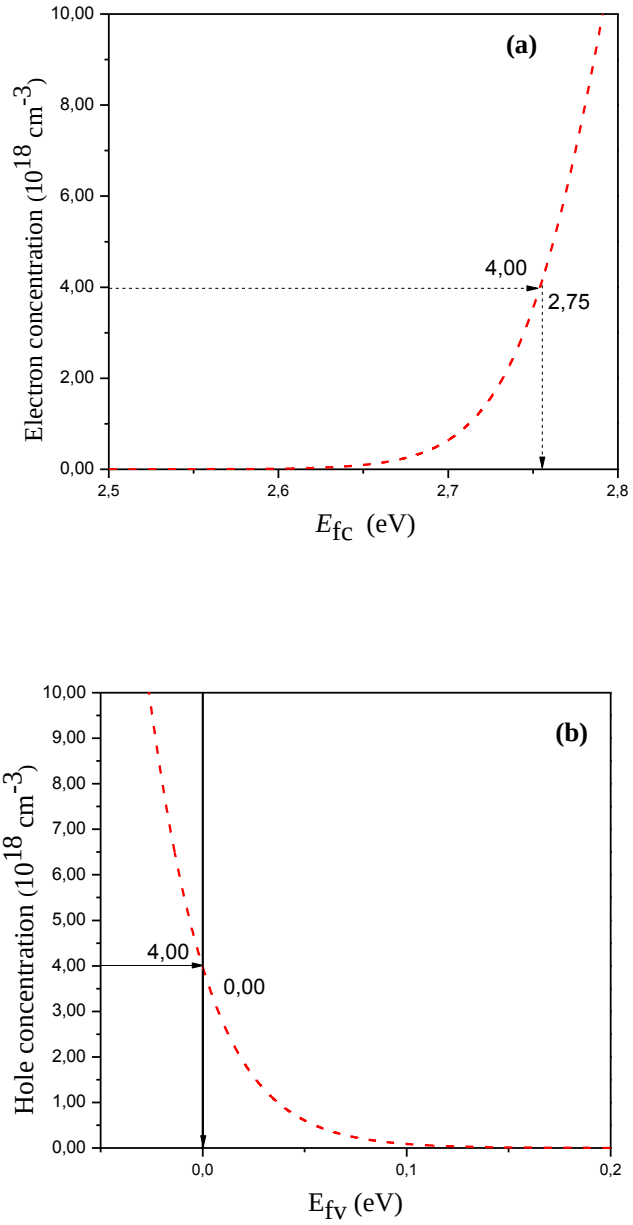

Figure 26 Electron (a) and Hole (b) concentration in the CdZnO conduction band as a function of Fermi level position at room temperature which represent the result of the exact Fermi integral (equations (III.16) and (III.17)).

for electrons and for holes

$$p = \frac{2}{L_w}\sum_m \int \frac{k_t dk}{2\pi}\left(1 - f_n^v(k_t)\right) \qquad \text{(III.17)}$$

As indicated in figure (26), we use the geometric method [3] to find the Fermi level of electrons and holes found in optical gain and spontaneous emission formula.for exemple electron and hole concentration equal to $4x10^{18}$ correspond to E_{fc}=2.75 eV and E_{fv}=0 eV Fermi energy level for electrons and holes, respectively.

III.6 Spontaneous Emission:

The spontaneous emission spectrum can be given as [44]

$$g_{sp}(\omega)=\sqrt{\frac{\mu_0}{\varepsilon}}\left(\frac{e^2}{m_0^2\omega}\right)\int_0^{\infty}dk_{\parallel}\,\frac{k_{\parallel}}{\pi^2 L_w}\cdot\left|M_{nm}(k_{\parallel})\right|^2\left[1-f_m^{v}(k_{\parallel})\right]f_n^{c}(k_{\parallel})L(\omega,k_{\parallel}) \qquad \text{(III.18)}$$

where ω represents the angular frequency, μ_0 is the vacuum permeability, ε is the dielectric constant, e is the charge of an electron, m_0 is the free electron mass, $k_{||}$ is the magnitude of the in-plane wave vector in the QW plane, M_{nm} is the momentum matrix element in the strained QW, $f_n^{c}(k_{||})$ and $f_m^{v}(k_{||})$ are the Fermi functions for occupation probability by the electrons in the conduction subband states and the valence subband states, respectively. The indexes l and m stand for the electron (hole) states in conduction (valence), respectively.

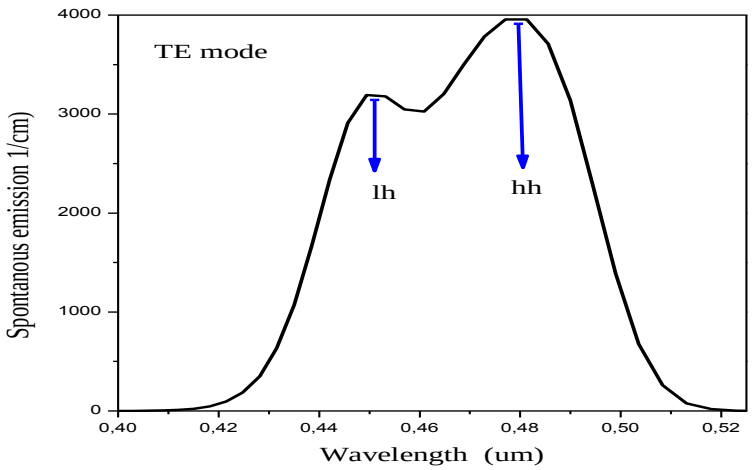

Figure 27 Spontaneous emission spectrum of ZnO/CdZnO quantum well structure.

Figure (27) shows the spontaneous emission spectrum of ZnO/CdZnO quantum well structure. The first two subbands peaks are clearly shown in spontaneous emission spectrum in figure (27), where the rate is greater in the peak of heavy hole subband than light hole subband and it is consistent with their density of states.

III.7 Optical gain:

The optical gain is proportional to the probability that a given photon triggers an electron transition from a higher energy level *j* to a lower energy level *i*. The photon energy *hv* must be equal to the transition energy $E_{ij} = E_j - E_i$. The quantum-mechanical calculation of this probability for semiconductors has been described in many publications (see, e.g., [3, 22, 44 and 53]). To provide a more intuitive understanding, we skip most of the quantum mechanics here and evaluate the simple gain function [44]

$$g(\omega) = \sqrt{\frac{\mu_0}{\varepsilon}}\left(\frac{e^2}{m_0^2\omega}\right)\int_0^\infty dk_{\parallel}\,\frac{k_{\parallel}}{\pi^2 L_w}\cdot\left|M_{nm}(k_{\parallel})\right|^2\left[f_n^c(k_{\parallel}) - f_m^v(k_{\parallel})\right]L(\omega,k_{\parallel}) \tag{III.19}$$

Same definition of symbols provided earlier in the spontaneous spectrum formula in equation (20). D. Ahn provides a detailed description of the theory of non-Markovian gain model in Ref. [19].

III.7.1 Line shape function:

Park *et al* introduced the phenomenological non-Markovian gain model with many-body effects [19, 54], which is used here with including the effects of anisotropy on both the valence band dispersion and the momentum matrix element, and it is based on considering a Gaussian broadening in rather than the conventional Lorentizian broadening line-shape function which is given by [54, 55]

$$L(k_{\parallel},\hbar\omega) = \frac{\gamma/\pi}{\left(E_{lm}(k_{\parallel},\hbar\omega)\right)^2 - \gamma^2} \tag{III.20}$$

And the non-Markovian line-shape function [54, 55]

$$L(k_{\parallel},\hbar\omega)=\sqrt{\frac{\pi\tau_{in}(k_{\parallel},\hbar\omega)\tau_c}{2\hbar^2}}\times\exp\left(-\frac{\pi\tau_{in}(k_{\parallel},\hbar\omega)\tau_c}{2\hbar^2}E_{lm}^2(k_{\parallel},\hbar\omega)\right) \quad \text{(III.21)}$$

the intraband relaxation time τ_{in} and the correlation time τ_c are taken to be constant. $\tau_{in}=10\,\text{fs}$ and $\tau_c=25\,\text{fs}$ are used in the calculation.

$$E_{lm}(k_{\parallel},\hbar\omega)=E_l^c(k_{\parallel})-E_m^v(k_{\parallel})+E_g+\Delta E_{SX}+\Delta E_{CH}-\hbar\omega \quad \text{(III.22)}$$

is the renormalized transition energy between electrons and holes, where E_g is the bandgap of the material, ΔE_{SX} and ΔE_{CH} are the screened exchange and the coulomb-hole contributions to the bandgap renormalization, respectively [53].

According to figure (28), where the line-shape functions for a full line width of both Gaussian (solid line) and Lorentzian (dashed line) are presented, Ahn *et al* assertions [19] of the limitation of Lorentizian line shape function choice to the non-Markovian broadening function are verified though the absorption tail in the long wave side of the gain spectrum and also the optical gain enhancement received with that type of broadening shown in figure (28) and in the broadening function plotting versus the wave vector or energy which made it more suitable to be compared with experimental results [56].

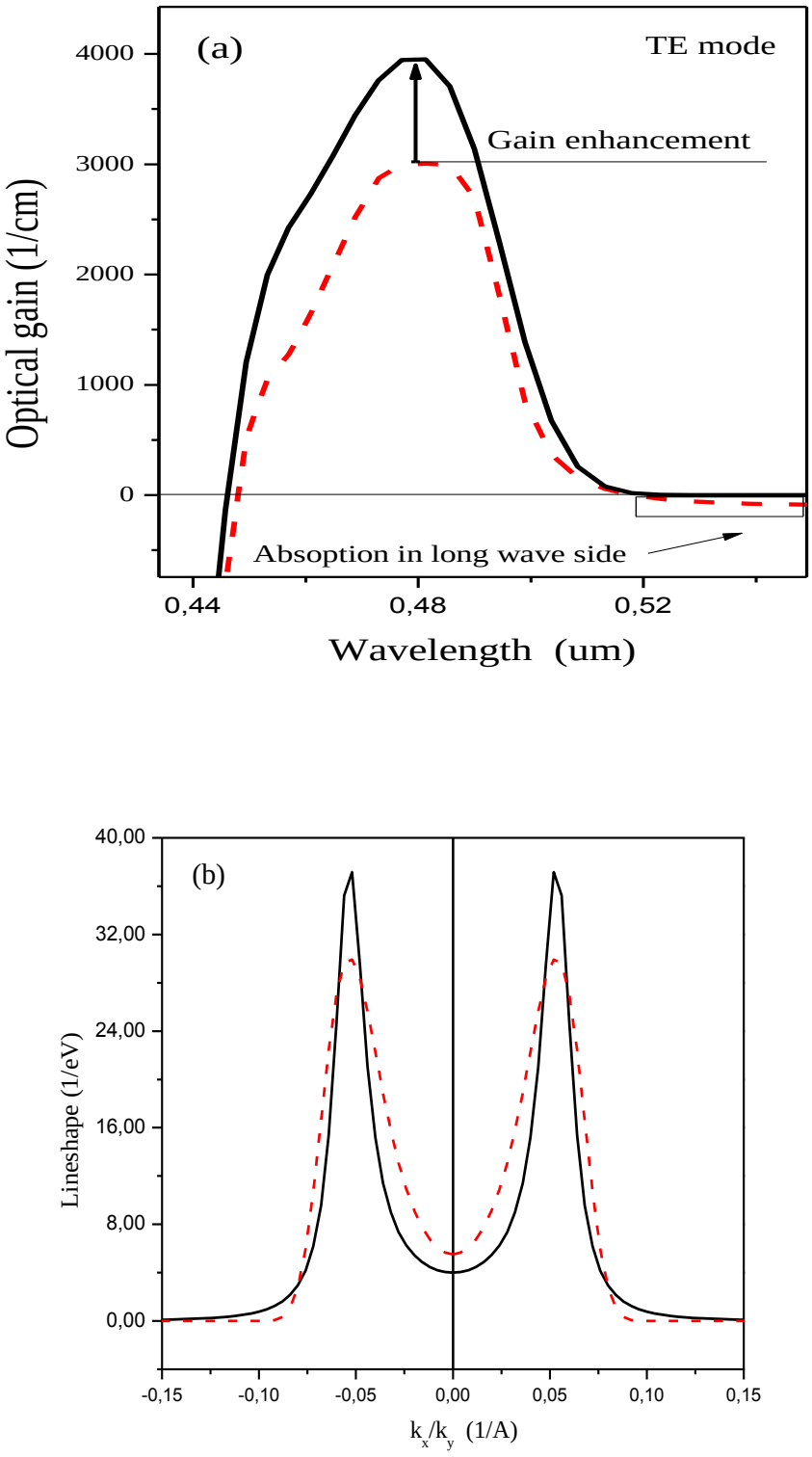

Figure 28 Optical gain (a) and Line shape functions (b) for a full line width of both Gaussian (solid line) and Lorentzian (dashed line) type [43].

III.7.2 Many body effects:

The bandgap renormalization include the sum between the Coulomb-hole self-energy and the screened-exchange shift [53]. The Coulomb-hole contribution to the bandgap renormalization is written as

$$\Delta E_{CH} = -2E_R a_0 \int_0^{\infty} dk_{\parallel} \frac{1}{1+\frac{k_{\parallel}}{\lambda_s}+\frac{Ca_0 k_{\parallel}^{\ 3}}{32\pi NL_Z}} \tag{III.23}$$

Where N is the carrier density and C is the constant usually taken between 1 and 4. The Rydberg constant E_R and the exciton Bohr radius a_0 are given by

$$a_0 = \frac{4\pi\hbar^2\varepsilon}{e^2 m_r}, E_R = \frac{\hbar^2}{2m_r a_0^2} \tag{III.24}$$

Where m_r is the reduced electron–hole mass defined by $1/m_r = 1/m_e + 1/m_h$. The exchange contribution to the bandgap renormalization is given by

$$\Delta E_{SX} = \frac{-2E_R a_0}{\lambda_s} \int_0^{\infty} dk_{\parallel} k_{\parallel} \frac{1+\frac{Ca_0 k_{\parallel}^{\ 2}}{32\pi NL_Z}}{1+\frac{k_{\parallel}}{\lambda_s}+\frac{Ca_0 k_{\parallel}^{\ 3}}{32\pi NL_Z}} \left[f_n^c(k_{\parallel}) + 1 - f_m^v(k_{\parallel}) \right] \tag{III.25}$$

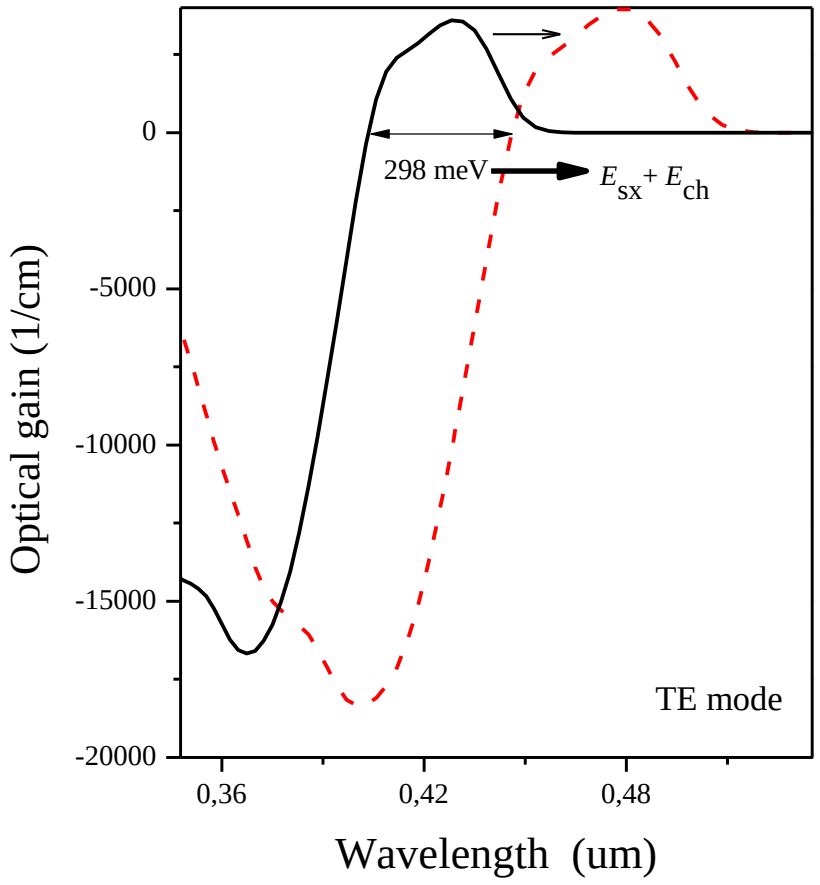

Figure 29 optical gain spectrum of ZnO/CdZnO quantum well structure with (solid line) and without many body effects -exchange correlation and coulomb interactions - (dashed line) [43].

In figure (29) we see the optical gain spectrum of ZnO/CdZnO quantum well structure with (solid line) and without many body effects -exchange correlation and coulomb interactions - (dashed line).Including many body effect cause a red shift of the optical gain in the spectrum with a slighter increase in gain maximum this type of shifting also known as band gap renormalization is increased with the increase of carrier concentrations [43].

In numerical implementation, we use at first pure Python code for the calculation of many body effect but we encounter a problem of the huge time spent for calculation (nearly 2 days), finally we changed the code to more quick procedure by using an

integrated C language in Python interpreter which is called Cython and the time for calculation is reduced dramatically to reach 30 minutes in long time cases [57, 58].

III.7.3 Piezoelectric effect:

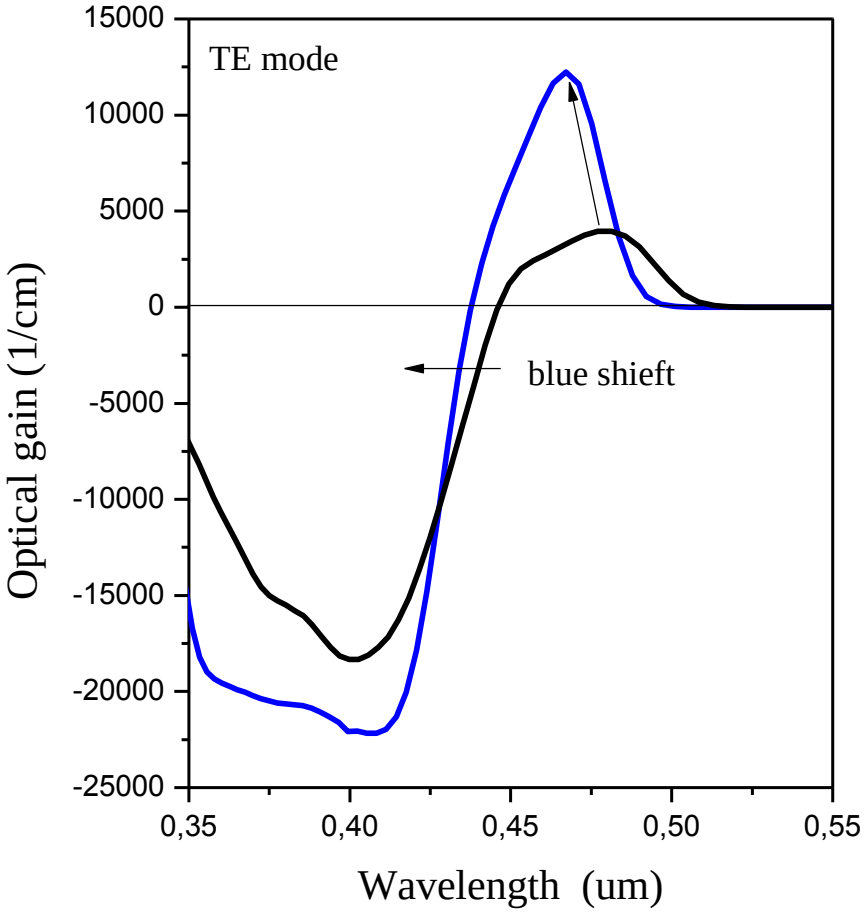

Figure 30 Optical gain spectrum in the presence (continuous line) and absence (dashed line) of piezoelectric and spontaneous polarization built in field [43].

Figure (30) shows the optical gain spectrum in the presence (continuous line) and absence (dashed line) of piezoelectric and spontaneous polarization built in field. note that in the absence of this field the optical gain is similar to the one found in non-polar crystal orientation as we are going to see in chapter V. Obviously the negative effect of the piezoelectric and spontaneous polarization built in field is shown clearly, where the optical gain in absence of the latter is greater by more than double the value

in normal case and this is a direct consequence of the decrease seeing in transition strength due to weak overlap integral caused by special separation of both conduction and valence bands wave functions.

III.7.4 Strain effect:

The use of strained layers has been a very important milestone in the development of quantum well lasers. We turn off the strain effect either by considering a perfect lattice match of simply by attributing a null value to the basic strain components.

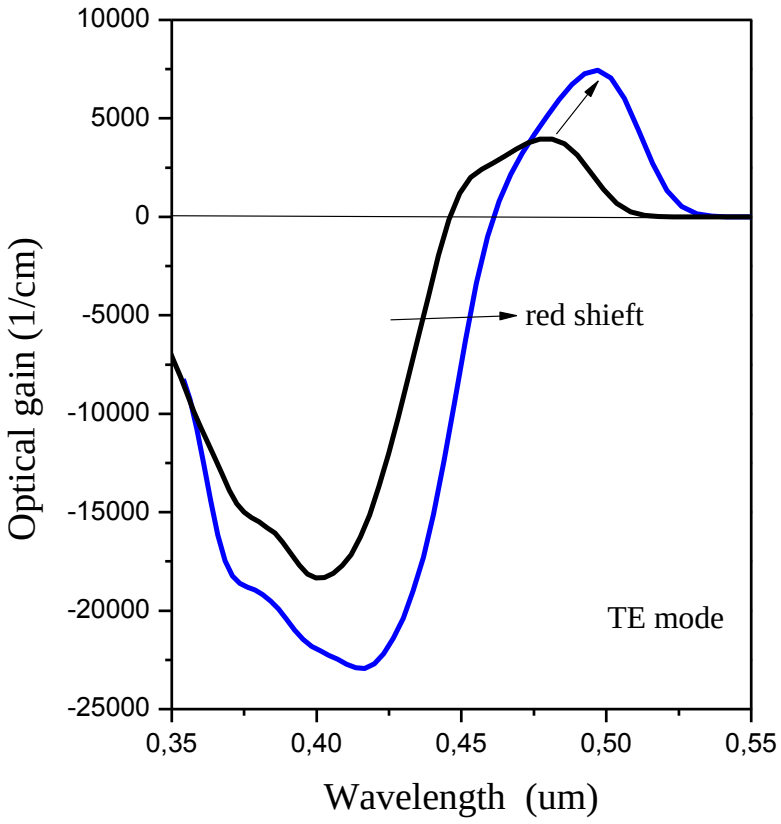

Figure 31 Optical gain spectrum of ZnO/CdZnO quantum well structure with (solid line) and without strain effects (dashed line) [43].

Figure (31) illustrates the optical gain spectrum of ZnO/CdZnO quantum well structure with (solid line) and without strain effects (dashed line).Strain and built in electric field due to piezoelectric and spontaneous polarization are linked to each

other by the same components i.e. strain elements and both have the same undesirable effect on optical properties such as weak transition strength and also optical gain, the only difference is the amount of energy shifting observed in optical gain spectrum which is greater with strain effect because it adds up with the one from built in electric field.

III.7.5 carrier concentration effect:

Carrier concentration increase is a straight consequence of increase injected carriers and confinement due to quantum well structure. Figure (32) displays Optical gain spectrum in different carrier concentration (a) and the optical gain maximum versus carrier concentration (b).Carrier concentrations are divided equally from $1x10^{26}$ to $7x10^{26}$ cm^{-3}, optical gain maximum is increasing with the increase of carrier concentrations because of its direct effect on Fermi levels for both electrons and holes that favor recombination weight through high density of states especially near band edges.

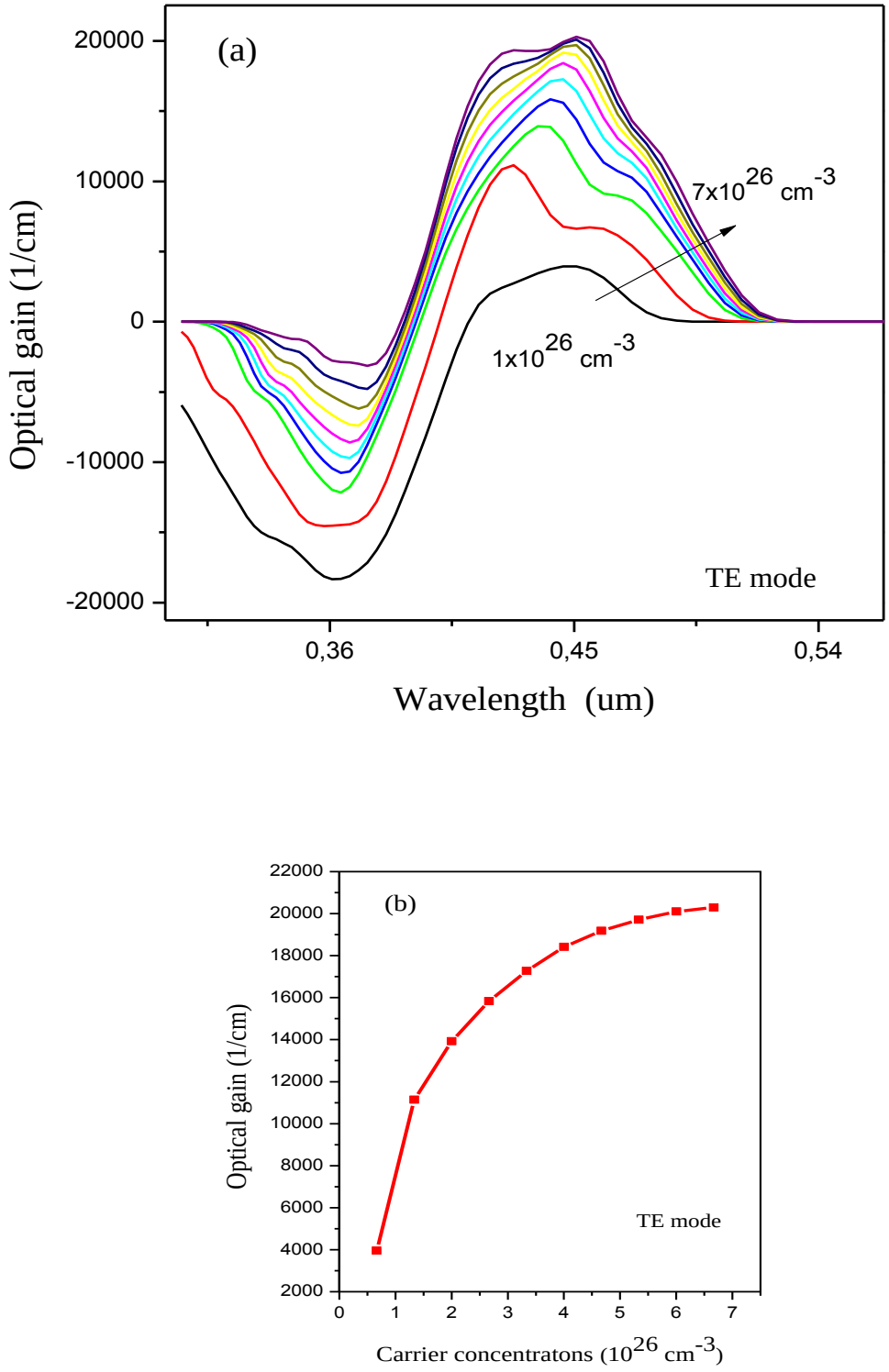

Figure 32 Optical gain maximum versus carrier concentration (a) and Optical gain spectrum in different carrier concentration (b).

III.8 Summary:

The main objectives of this chapter have been firstly to provide an introduction to the basic concepts of optical transitions and their transition strength combined with Fermi-Dirac probability and broadening function to form the basic formalism of optical gain. Lorentzian line shape function is presented and also the Gaussian or non-Markovian lineshape function. Numerous effects on optical gain are studied in this chapter for like built in electric field due to piezoelectric and spontaneous polarization, many body effects, strain effect and carrier concentration effect.

Chapter IV

Crystal Orientation Effects on Wurtzite Hamiltonian

IV.1 Introduction:

Quantum wells (QWs) based on zinc oxide (ZnO) and related alloys have gained an important amount of interest as an active region in short wavelength light-emitting diodes and laser diodes competing with GaN-based QW structures in the same field with many distinctive properties [59–61]. Due to the large exciton binding energy (60 meV) of ZnO which allows excitonic recombination even above room temperature ZnO system renewed the interest in its usage in blue and ultraviolet wavelengths [59]. Experimentally, numerous groups succeeded in depositing $Cd_xZn_{1-x}O$ alloy thin films, mostly on sapphire substrates like Makino *et al.* using PLD with 7% Cd content [62], Ma *et al.* by dc reactive magnetron sputtering method [63], and Vigil *et al.* with the spray pyrolysis method [64].

Theoretically, ZnO and GaN based quantum structures are studied extensively, specially by Park *el al* [65, 66, 44 and 36], also the use of quantum structures with non-polar crystal orientation is covered by the same group, but there was a focusing on (Al and In)-GaN and (Mg) -ZnO based quantum structures [66–69], where there is no sufficient investigation on (Cd)-ZnO based quantum structures with crystal orientation.

In this chapter, we consider the theoretical electronic and optical properties of ZnO/CdZnO QW structures as object of studying [19] .To obtain the band structures and the wave functions ,we solve (a finite difference method was used in numerical

calculations, un example for zincblende is implemented in the open source code called Aestimo 0.9 and for wurtzite in coming version 1.0 [41]) the Schrodinger equation for electrons and the 6×6 Hamiltonian for holes for arbitrary crystal orientation considering the electric field due to build in polarization [67]. These results are compared with those for GaN/InGaN QW structures.

IV.2 Hamiltonian for Arbitrary Crystal Orientation

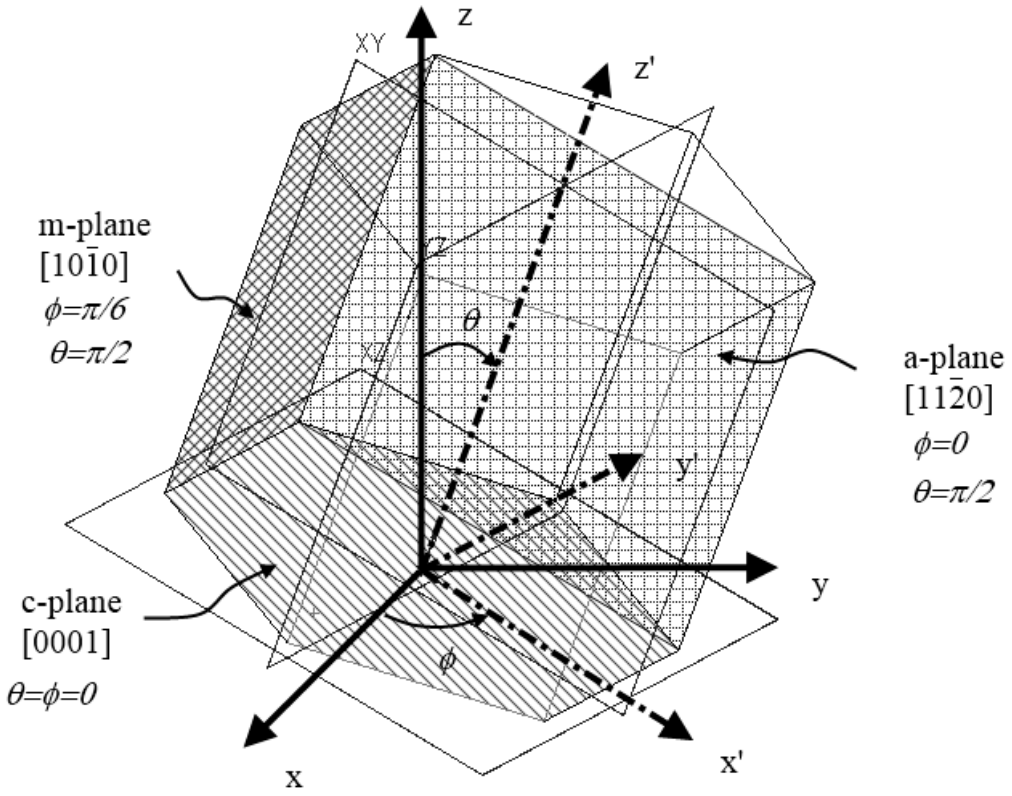

Figure 33 c-, a- and m-planes with the growth direction parallel to the c-axis. With $\theta = \pi/2$ and $\varphi = 0$ (a-plane) corresponds to the z = $(11\bar{2}0)$ growth direction and $\theta = \pi/2$ and $\varphi = \pi/6$ (m-plane) corresponds to the z =$(10\bar{1}0)$ growth direction [hamza et al 43].

We use the same approach done by D. Ahn *et al* [69] where a rotation matrix of the Euler angles φ and θ is use to give the physical quantities representation in coordinates (x′, y′,z′) The z-axis corresponds to the c-axis (0001) and the growth axis (defined as the z'-axis) is normal to the QW plane [*h k i l*], as shown in Figure (33). The relation between the coordinate systems for vectors and tensors are given by [70, 71]:

$$U = \begin{pmatrix} \cos\theta\cos\varphi & \cos\theta\sin\varphi & -\sin\varphi \\ -\sin\varphi & \cos\theta & 0 \\ \cos\theta\sin\varphi & \sin\phi\sin\varphi & \cos\theta \end{pmatrix} \quad \text{(IV.1)}$$

which is the inverse of the rotation R = $R_y(\phi)R_z(\theta)$, where $R_i(\alpha)$ is a counter-clockwise rotation of angle α with respect to the axis $i = x, y, z$.

Rotations of the Euler angles θ and φ transform the physical quantities from (x, y, z) coordinates to (x′, y′,z′) coordinates (figure 1). The z-axis corresponds to the c-axis [0 0 0 1], and the growth axis (defined as the z'-axis) is normal to the QW plane (*hk i l*). The polar angle θ is defined as the angle between z' and c-axes. Here we assume that z′ and k'_z are perpendicular to the (*h k i l*) plane with $i = -h - k$. For simplicity, we assume that $k = 0$ and we further have $(h0il) = (h0\bar{i}l)$. Then the polar angle θ is given by [66]

$$\cos\theta = \frac{\sqrt{a/c}l}{\sqrt{4h^2/3 + al^2/c}}$$

(IV.2) with a and c being the usual hexagonal lattice parameters. Equation (IV.2) is obtained for the case of ϕ = 0 and k = 0. Once the crystal orientation angle θ is determined from equation (IV.2), the following coordinate transformation can be calculated from equation (IV.1).

$$k'_i = U_{i\alpha}k_\alpha \quad \text{(IV.3)}$$

$$k_\alpha = U_{i\alpha}k'_i \quad \text{(IV.4)}$$

$$\varepsilon'_{ij} = U_{i\alpha}U_{j\beta}\varepsilon_{\alpha\beta} \quad \text{(IV.5)}$$

$$\varepsilon_{\alpha\beta} = U_{i\alpha}U_{j\beta}\varepsilon'_{ij} \quad \text{(IV.6)}$$

The strain coefficients in the (x,y,z) coordinates for a general crystal orientation are determined under pseudomorphic growth condition, and these strain coefficients correspond to the lowest strain energy of the layer simultaneously [36].

where the summation over repeated indices is assumed. The strain coefficients in the (x, y, z) coordinates for a general crystal orientation are determined from the condition that the layer is grown pseudomorphically and these strain coefficients should minimize the strain energy of the layer simultaneously. To obtain the new Hamiltonian for an arbitrary crystal orientation, one should rotate the crystal momentum and the angular momentum (or spin) of that Hamiltonian to the desired

position. This should be equivalent to rotating the basis functions at the same time when the crystal momentum k_s are rotated to the new direction. We denote the rotation of the crystal momentum, strain tensors and basis functions in the following compact notation:

$$\begin{aligned}&\vec{k}' = U\vec{k},\\ &\bar{\varepsilon}' = U\bar{\varepsilon}U,\\ &|\alpha'\rangle = \tilde{U}|\alpha\rangle,\end{aligned} \tag{IV.7}$$

where $\bar{\varepsilon} = \varepsilon_{ij}$ for i, j = x, y, z is a strain tensor, $|\alpha\rangle$ is the basis function for α = 1, 2,… 6 and $\tilde{U} = \begin{pmatrix} U & 0 \\ 0 & U \end{pmatrix}$ is a block diagonalized extended rotation operator for the basis functions. Then the original Hamiltonian $H(\vec{k}', \bar{\varepsilon}')$ for the (0 0 0 1) crystal orientation and the Hamiltonian $H(\vec{k}, \bar{\varepsilon})$ should satisfy

$$\begin{aligned}\langle\alpha|H(\vec{k},\bar{\varepsilon})|\beta\rangle &= \langle\alpha'|H'(\vec{k}',\bar{\varepsilon}')|\beta'\rangle\\ &= \langle\alpha'|\tilde{U}^{-1}H'(\vec{k}',\bar{\varepsilon}')\tilde{U}|\beta'\rangle\end{aligned}. \tag{IV.8}$$

From this we obtain

$$\begin{aligned}H'(\vec{k}',\bar{\varepsilon}') &= \tilde{U}H(\vec{k},\bar{\varepsilon})\tilde{U}^{-1}\\ &= \tilde{U}H(U^{-1}\vec{k}, U^{-1}\bar{\varepsilon}U^{-1})\tilde{U}^{-1}\end{aligned} \tag{IV.9}$$

The Hamiltonian for the valence-band structure with general crystal orientation is very complicated. Instead, we use the matrix representation $H'(\vec{k}', \bar{\varepsilon}')$ in the old basis denoted as $\tilde{H}'(\vec{k}', \bar{\varepsilon}')$

$$\tilde{H}'(\vec{k}',\bar{\varepsilon}') = \tilde{U}^{-1}H(\vec{k},\bar{\varepsilon})\tilde{U} = H(U^{-1}\vec{k}, U^{-1}\bar{\varepsilon}U^{-1}) \tag{IV.10}$$

We consider the θ and ϕ dependence of physical quantities in the following [72] . Figure (32) shows (a) a configuration of the coordinate systems (x′, y′, z′) in (*hkil*)-oriented crystals, and (b) a coordinate system in a wurtzite primitive cell and nonpolar a - and m - planes with the growth direction parallel to the c - axis. The z-axis corresponds to the c-axis (0001), and the growth axis (defined as the z ′-axis) is normal to the quantum well plane (*hkil*). The coordinate system (x, y, z) denotes the primary crystallographic axes. The relation between the coordinate systems for vectors and tensors is given by Equations (IV.3) to (IV.6). The strain coefficients in

the (x, y, z) coordinates for a general crystal orientation are determined from the condition that the layer is grown pseudomorphically, and these strain coefficients should minimize the strain energy of the layer simultaneously. We define the unit vectors x^′, y^′, and z^′ along the x′-, y′-, and z′-axes, and they are related to unit vectors x^, y^, and z^ along the x-, y-, and z-axes through the rotation matrix Equation (IV.1). The hexagonal primitive translational vectors are

$$\begin{aligned}\alpha_i &= a_i \hat{x},\\ \beta_i &= -\frac{a_i}{2}\hat{x} + \frac{\sqrt{3a_i}}{2}\hat{y},\\ \gamma_i &= c_i \hat{z},\end{aligned} \tag{IV.11}$$

where a is the lattice constant, and *i* labels the epilayer (e) and the substrate (s). When the crystal is translated, the primitive translational vectors become

$$\begin{aligned}\alpha_i^{''} &= a_i \hat{x}^{''},\\ \beta_i^{''} &= -\frac{a_i}{2},\hat{x}^{''} + \frac{\sqrt{3a}_i}{2}\hat{y}^{''},\\ y_i^{''} &= c_i \hat{z}^{''},\end{aligned} \tag{IV.12}$$

where

$$\begin{aligned}\hat{x}^{''} &= (1+\varepsilon_{xx})\hat{x} + \varepsilon_{xy}\hat{y} + \varepsilon_{xz}\hat{z},\\ \hat{y}^{''} &= \varepsilon_{yx}\hat{x} + (1+\varepsilon_{yy})\hat{y} + \varepsilon_{yz}\hat{z},\\ \hat{z}^{''} &= \varepsilon_{zx}\hat{x} + \varepsilon_{zy}\hat{y} + (1+\varepsilon_{zz})\hat{z}.\end{aligned} \tag{IV.13}$$

When the first atomic layers are deposited on the substrate, these layers will be strained to match the substrate, and a pseudomorphic (or coherent) interface will be formed. Thus, the condition for a pseudomorphic interface means that the projections of the strain - distorted primitive translational vectors of the epilayer and the substrate on the growth plane should be equal:

$$\alpha_e^{''} \cdot \hat{x}^{'} = \alpha_s^{''} \cdot \hat{x}^{'},$$

$$\alpha_e^{''} \cdot \hat{y}^{'} = \alpha_s^{''} \cdot \hat{y}^{'}, \tag{IV.14}$$

with similar conditions are applied on β″ and γ″. Then, the constraints (Equation (IV.14)) yield the following relations for the strain tensors:

$$\varepsilon_{xx} = \varepsilon_{xx}^{(0)} + \varepsilon_{xz} \frac{\sin\theta\cos\varphi}{\cos\theta}$$

$$\varepsilon_{xy} = \frac{\sin\theta\cos\varphi}{\cos\theta}\varepsilon_{xy}$$

$$\varepsilon_{yy} = \varepsilon_{xx}^{(0)} + \varepsilon_{xz} \frac{\sin\theta\sin^2\varphi}{\cos\theta\cos\varphi}$$

$$\varepsilon_{zz} = \varepsilon_{xz} \frac{\cos\theta}{\sin\theta\cos\varphi} + \varepsilon_{zz}^{(0)}, \tag{IV.15}$$

$\varepsilon_{xx}^{(0)} = (a_s - a_e)/a_e$ and $\varepsilon_{zz}^{(0)} = (c_s - c_e)/c_e$. Under the engineering notation, the strain energy density is given by

$$W = \frac{1}{2}\left[c_{11}\varepsilon_{xx}^2 + c_{11}\varepsilon_{yy}^2 + c_{33}\varepsilon_{zz}^2 + 2c_{12}\varepsilon_{xx}\varepsilon_{yy} + 2c_{13}\left(\varepsilon_{xx}\varepsilon_{zz} + \varepsilon_{yy}\varepsilon_{zz}\right) + 4c_{44}\varepsilon_{xz}^2\right] \tag{IV.16}$$

Using the above relations, the strain energy can be expressed through only one strain component, ε_{xz}, which can be found by minimizing the strain energy with respect to the variable ε_{xz}. This procedure gives the following expression for ε_{xz}

$$\varepsilon_{xz\_n} = -\left(\left((C_{11} + C_{12})\varepsilon_{xx}^{(0)} C_{13}\varepsilon_{zz}\right)\sin^2\theta + \left(2C_{13}\varepsilon_{xx}^{(0)} + C_{33}\varepsilon_{zz}^{(0)}\right)\cos^2\theta\right)$$

$$\varepsilon_{xz\_d} = \begin{pmatrix} \left(C_{11}\left(\sin^4\varphi + \cos^4\varphi\right) + 2C_{12}\sin^2\varphi\cdot\cos^2\varphi\right)\sin^4\theta \\ + 2\left(C_{13} + 2C_{44}\cos^2\varphi\right)\sin^2\theta\cdot\cos^2\theta + C_{33}\cos^4\varphi \end{pmatrix}$$

$$\varepsilon_{xz} = \frac{\varepsilon_{xz\_n}}{\varepsilon_{xz\_d}} \tag{IV.17}$$

Hence, we obtain a 6 × 6 Hamiltonian in the (x′, y′, z′) coordinates by substituting the transformation relation for the vector k in Equation (IV.4), and the strain coefficients for a general crystal orientation into the Hamiltonian for the (0001) orientation.

$$H(K',\varepsilon')=\begin{pmatrix} F' & -K'^{*} & -H'^{*} & 0 & 0 & 0 \\ -K' & G' & H' & 0 & 0 & \Delta \\ -H' & H'^{*} & \lambda' & 0 & \Delta & 0 \\ 0 & 0 & 0 & F' & -K' & H' \\ 0 & 0 & \Delta & -K'^{*} & G' & -H'^{*} \\ 0 & \Delta & 0 & H'^{*} & -H' & \lambda' \end{pmatrix}\begin{matrix} |U_1\rangle \\ |U_2\rangle \\ |U_3\rangle \\ |U_4\rangle \\ |U_5\rangle \\ |U_6\rangle \end{matrix} \quad \text{(IV.18)}$$

$$F'=\Delta_1+\Delta_2+\lambda'+\theta'$$

$$G'=\Delta_1-\Delta_2+\lambda'+\theta'$$

$$\lambda'=\frac{\hbar^2}{2m_0}A_1\left[k'^2_x\sin^2\theta-2k'_x k'_z\sin\theta\cos\theta+k'^2_z\cos^2\theta\right]+$$
$$\frac{\hbar^2}{2m_0}A_2\left[k'^2_x\cos^2\theta+2k'_x k'_z\sin\theta\cos\theta+k'^2_z\sin^2\theta\right]+\lambda'_{\varepsilon}$$

$$\theta'=\frac{\hbar^2}{2m_0}A_3\left[k'^2_x\sin^2\theta-2k'_x k'_z\sin\theta\cos\theta+k'^2_z\cos^2\theta\right]+$$
$$\frac{\hbar^2}{2m_0}A_4\left[k'^2_x\cos^2\theta+2k'_x k'_z\sin\theta\cos\theta+k'^2_z\sin^2\theta\right]+\theta'_{\varepsilon}$$

$$K'=\frac{\hbar^2}{2m_0}e^{2i\varphi}A_5\begin{bmatrix}k'_x\cos^2\theta+2k'_x k'_z\cos\theta\sin\theta+2ik'_x k'_z\sin\theta \\ +2ik'_y k'_z\sin\theta+k'^2_z\sin^2\theta-k'^2_y\end{bmatrix}+K'_{\varepsilon}$$

$$H'=\frac{\hbar^2}{2m_0}e^{2i\varphi}A_6\begin{bmatrix}-k'^2_x\cos\theta\sin\theta-ik'_x k'_y\sin\theta-k'_x k'_z\sin^2\theta \\ +k'_x k'_z\cos^2\theta+ik'_y k'_z+k'^2_z\cos\theta\sin\theta\end{bmatrix}+H'_{\varepsilon} \quad \text{(IV.19)}$$

Where

$$\lambda'_{\varepsilon}=\mathrm{D}_2\left(2\varepsilon^{(0)}_{xx}+\varepsilon_{xz}\sin^2\theta\right)+\mathrm{D}_1\left(\varepsilon^{(0)}_{zz}+\varepsilon_{xz}\cos^2\theta\right)$$

$$\theta'_{\varepsilon}=\mathrm{D}_4\left(2\varepsilon^{(0)}_{xx}+\varepsilon_{xz}\sin^2\theta\right)+\mathrm{D}_3\left(\varepsilon^{(0)}_{zz}+\varepsilon_{xz}\cos^2\theta\right)$$

$$K'_{\varepsilon}=\mathrm{D}_5\varepsilon_{xz}\sin^2\theta\cdot(\cos\varphi+i\cdot\sin\varphi)^2$$

$$H'_{\varepsilon}=\mathrm{D}_6\varepsilon_{xz}(\cos\phi+i\cdot\sin\varphi)\cos\theta\cdot\sin\theta/\cos^2\varphi$$

$$P_{c\varepsilon}^{'} = a_c\left(\varepsilon_{\mathrm{xx}}^{(0)} + \varepsilon_{\mathrm{yy}}^{(0)} + \varepsilon_{\mathrm{zz}}^{(0)} + \varepsilon_{xz}\sin^2\theta\right) \tag{IV.20}$$

The A_i's represents the valence band effective mass parameters or Luttinger like parameters, the D_i's stand for the deformation potentials for Wurtzite crystals, k_i is the wave vector, ε_{ij} is the strain tensor, Δ_1 is the crystal-field split energy, Δ_2 and Δ_3 are the spin-orbit interactions. $\varepsilon_{xx}^{(0)} = (a_s - a_e)/a_e$ and $\varepsilon_{zz}^{(0)} = (c_s - c_e)/c_e$ are caused by mismatches in the lattice constants of the well (a_e and c_e) and the substrate (a_s and c_s).

IV.3 Momentum Matrix elements (MME):

The general crystal orientation of optical matrix elements is given by

$$\left|\hat{e}'\cdot M'^{\eta}\right|^2 = \left|\left\langle \Psi_l'^{c\eta}\left|\hat{e}'\cdot p'\right|\Psi_m'^{v}\right\rangle\right|^2 \tag{IV.21}$$

where $\Psi_{\mathrm{l}}'^{\mathrm{c}\eta}$ ($\Psi_{\mathrm{m}}'^{\mathrm{v}}$) is the wave function for the conduction (valence) band , and $\eta = \uparrow$ and $\downarrow$ for both electron spins. The indexes and stand for the electron states in the conduction band and the heavy-hole (light hole) subband states in the valence band, respectively. The interband momentum matrix elements for each spin orientation can be written as follows. For TE- polarization ($\hat{e}' = \cos\phi\hat{x}' + \sin\phi\hat{y}'$):

$$\left|\hat{e}'\cdot M'^{\uparrow}\right|^2 = \left|-\cos\phi'\sin\theta P_z'\left\langle g_m'^{(3)}\middle|\phi_l'\right\rangle - \cos\phi'\cos\varphi\cos\theta\frac{p_x}{\sqrt{2}}\left\{(1+i)\left\langle g_m'^{(1)}\middle|\phi_l'\right\rangle - (1-i)\left\langle g_m'^{(2)}\middle|\phi_l'\right\rangle\right\}\right.$$
$$\left. + \sin\phi'\frac{p_x}{\sqrt{2}}\left\{\sin\varphi\left(\left\langle g_m'^{(1)}\middle|\phi_l'\right\rangle - \left\langle g_m'^{(2)}\middle|\phi_l'\right\rangle\right) - i\cos\varphi\left(\left\langle g_m'^{(1)}\middle|\phi_l'\right\rangle + \left\langle g_m'^{(2)}\middle|\phi_l'\right\rangle\right)\right\}\right|^2 \tag{IV.22}$$

$$\left|\hat{e}'\cdot M'^{\downarrow}\right|^2 = \left|-\cos\phi'\sin\theta P_z'\left\langle g_m'^{(6)}\middle|\phi_l'\right\rangle - \cos\phi'\cos\varphi\cos\theta\frac{p_x}{\sqrt{2}}\left\{(1+i)\left\langle g_m'^{(4)}\middle|\phi_l'\right\rangle - (1-i)\left\langle g_m'^{(5)}\middle|\phi_l'\right\rangle\right\}\right.$$
$$\left. + \sin\phi'\frac{p_x}{\sqrt{2}}\left\{\sin\varphi\left(\left\langle g_m'^{(4)}\middle|\phi_l'\right\rangle - \left\langle g_m'^{(5)}\middle|\phi_l'\right\rangle\right) - i\cos\varphi\left(\left\langle g_m'^{(4)}\middle|\phi_l'\right\rangle + \left\langle g_m'^{(5)}\middle|\phi_l'\right\rangle\right)\right\}\right|^2 \tag{IV.23}$$

TM-polarization ($\hat{e}' = \hat{z}'$):

$$\left|\hat{e}'\cdot M'^{\uparrow}\right|^2 = \left|-\left\langle g'^{(3)}_m \middle| \phi'_l \right\rangle + \frac{p_x}{\sqrt{2}}\sin\theta\cos\varphi\left\{-\left\langle g'^{(1)}_m \middle| \phi'_l \right\rangle + \left\langle g'^{(2)}_m \middle| \phi'_l \right\rangle\right\}\right.$$
$$\left. - \frac{ip_x}{\sqrt{2}}\sin\theta\sin\varphi\left\{\left\langle g'^{(1)}_m \middle| \phi'_l \right\rangle + \left\langle g'^{(2)}_m \middle| \phi'_l \right\rangle\right\}\right|^2 \quad \text{(IV.24)}$$

$$\left|\hat{e}'\cdot M'^{\downarrow}\right|^2 = \left|-\left\langle g'^{(6)}_m \middle| \phi'_l \right\rangle + \frac{p_x}{\sqrt{2}}\sin\theta\cos\varphi\left\{-\left\langle g'^{(4)}_m \middle| \phi'_l \right\rangle + \left\langle g'^{(5)}_m \middle| \phi'_l \right\rangle\right\}\right.$$
$$\left. - \frac{ip_x}{\sqrt{2}}\sin\theta\sin\varphi\left\{\left\langle g'^{(4)}_m \middle| \phi'_l \right\rangle + \left\langle g'^{(5)}_m \middle| \phi'_l \right\rangle\right\}\right|^{2^2} \quad \text{(IV.25)}$$

where $g'^{(v)}_m$ (v =1, 2,3,4,5 and 6) is the wave function for the m^{th} subband in (x', y', z') coordinates. The use of old bases in equation (III.9) results in the same known quantities p_x and p_z.

IV.4 Piezoelectric and Spontaneous polarization

The polarization components along *x*, *y* and *z* axes for the (0001)-WZ structure is written as [36]

$$P_{PZ}\begin{cases} P^x_{PZ} = 2d_{15}C_{44}\varepsilon_{xz} \\ P^y_{PZ} = 0 \\ P^z_{PZ} = 2d_{31}(C_{11}+C_{12}+\dfrac{2C^2_{13}}{C_{33}})\varepsilon^{(0)}_{xx} \end{cases} \quad \text{(IV.26)}$$

The strain induced piezoelectric polarization normal with respect to the growth plane (along the growth direction) in an arbitrary crystal orientation can be expressed as [36]

$$P'_{PZ}\begin{cases} P'^x_{PZ} = P^x_{PZ}\cos\theta - P^z_{PZ}\sin\theta \\ P'^y_{PZ} = 0 \\ P'^x_{PZ} = P^x_{PZ}\sin\theta + P^z_{PZ}\cos\theta \end{cases} \quad \text{(IV.27)}$$

The spontaneous polarization P_{SP} along the growth direction in the arbitrary crystal orientation is estimated by the relation [73]

$$P'_{SP} = P^{[0001]}_{SP}\cos\theta \quad \text{(IV.29)}$$

Using the periodic boundary condition for a superlattice structure, the build in electric fields in the well and barrier can be written as [37, 38]:

$$F_z^{'w} = \frac{\left(P_{SP}^{'b} + P_{PZ}^{'b} - P_{SP}^{'w} - P_{PZ}^{'w}\right)}{\varepsilon^w + \varepsilon^b\left(L_w / L_b\right)} \qquad (IV.30)$$

$$F_z^{'b} = -\frac{L_w}{L_b} F_z^{'w}$$

where L_w (L_b) and ε_w (ε_b) are the length of well (barrier) and the static dielectric constant, respectively.

IV.5 Results and discussions:

Figures (34) and (35) show the strain components as functions of the crystal angle θ with $\phi = 0$ (a) and $\phi = \pi/6$ (b) for wurtzite $ZnO/Cd_{15}Zn_{85}O$ (34) and $GaN/In_{15}Ga_{85}N$ (35) QW structures ($L_W = 30A^\circ$). Both plotted strain components seem to be similar for each component with the two values of ϕ, but there is a difference in the starting angle which represents the c-plane orientation, where it is -0.9% for $ZnO/Cd_{15}Zn_{85}O$ QW structure while it is -1.6% for $GaN/In_{15}Ga_{85}N$ QW structure in ε_{xx}. The latter has a great effects on all properties of both structures and this explains the difference seen between both c-plane oriented structures. The same thing occurs at the ending angle represented by a- and m-planes oriented structures but with different values.

The variation of all strain components of the same structure with crystal orientation angles is not the same i.e. the ε_{xx} tends to increase from negative value which stand for compressive strain to positive value in a tensile strain state unlike ε_{zz} strain component which decreases to a compressive strain state due to the negative sign between the two strain components.

In the case of ε_{xz} strain component, it has a null value in both beginning and ending angles and also this has a large effect on all properties of QW structures especially band structure and optical gain.

Figures (36) and (37) show the total polarization components as functions of the crystal angle θ with $\phi = 0$ (a) and $\phi = \pi/6$ (b) for well (continuous line), barrier (dashed line) of Wurtzite $ZnO/Cd_{15}Zn_{85}O$ (36) and $GaN/In_{15}Ga_{85}N$ (37) QW structures ($L_W = 30A^\circ$). The polarization components are strongly affected by the strain components and in general follow ε_{xx} strain component in its increase, but into a null value which gives us a structure without piezoelectric and spontaneous effect.

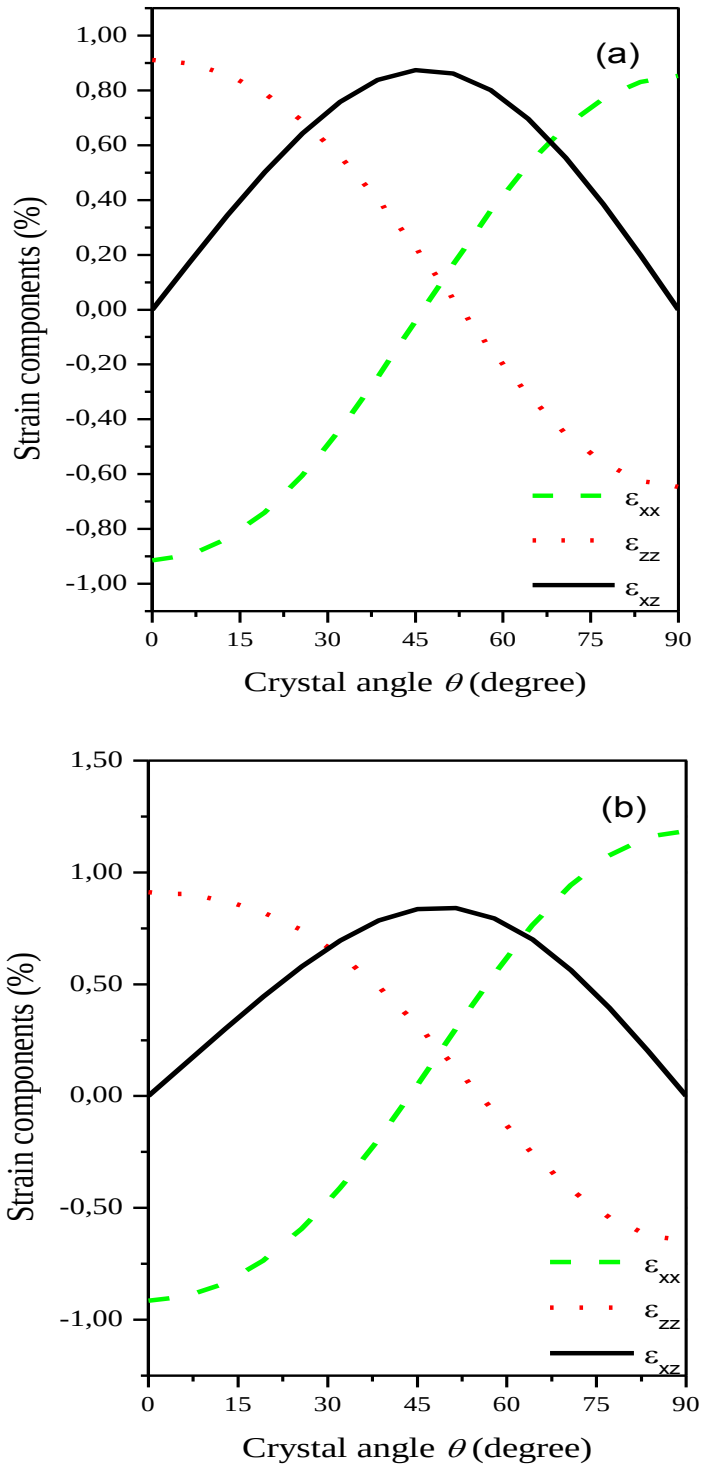

Figure 34 Strain components as functions of the crystal angle θ with $\phi = \theta$ (a) and $\phi = \pi/6$ (b) for wurtzite $ZnO/Cd_{15}Zn_{85}O$ QW structures $(L_W = 30A^\circ)$.

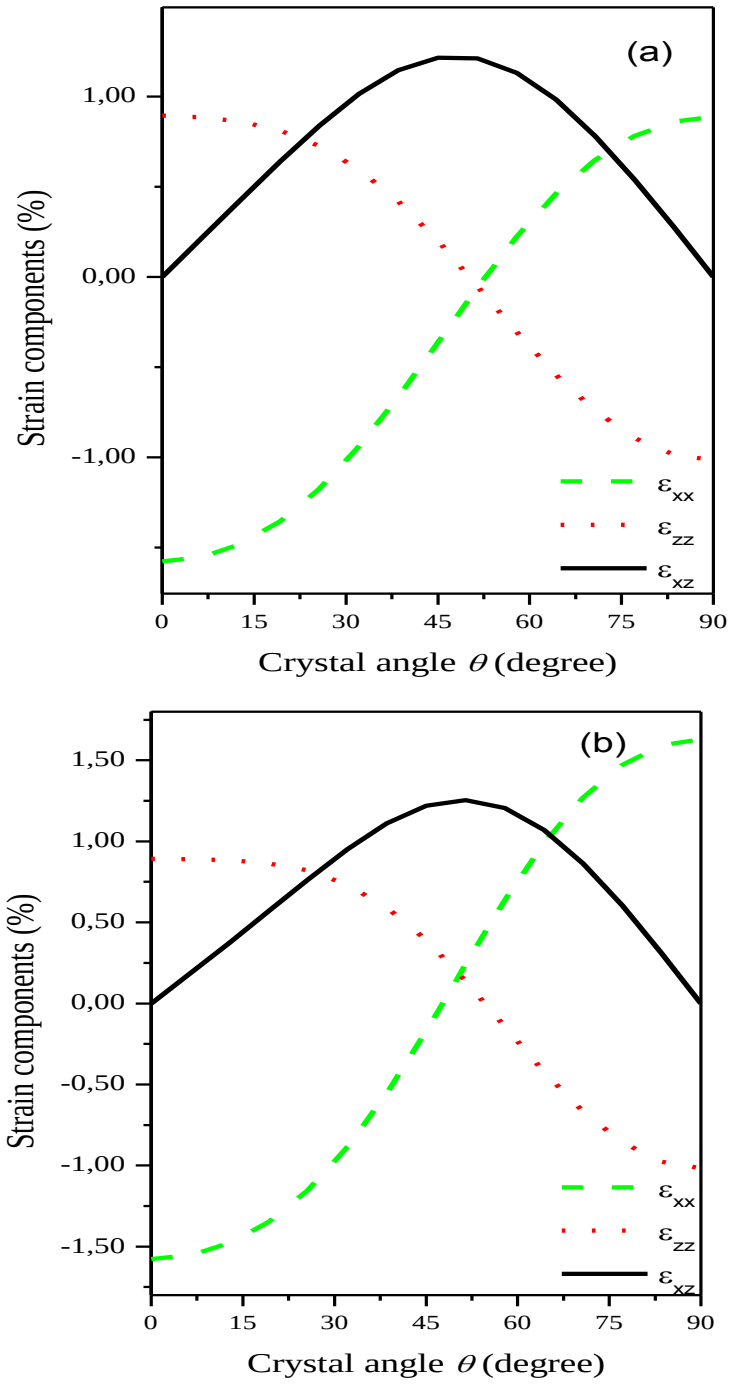

Figure 35 Strain components as functions of the crystal angle θ with $\phi = 0$ (a) and $\phi = \pi/6$ (b) for Wurtzite $GaN/In_{15}Ga_{85}N$ QW structures $(L_W = 30A^\circ)$.

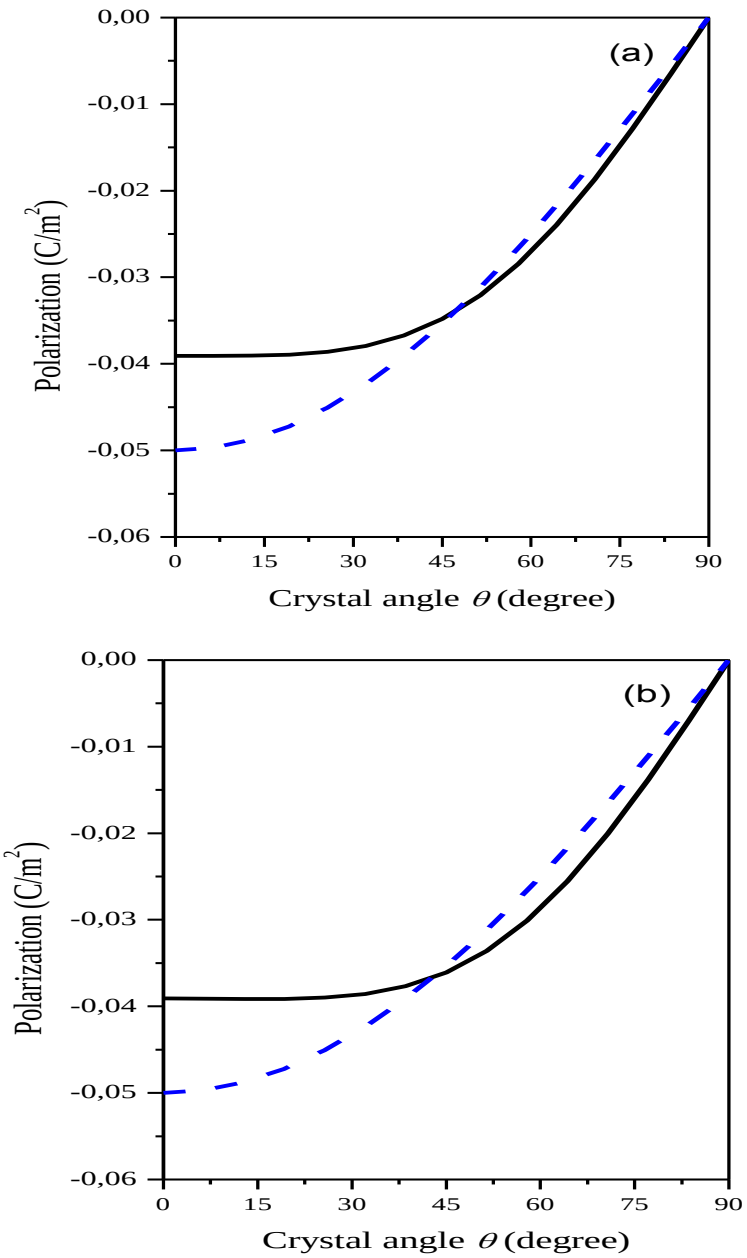

Figure 36 total polarization components as functions of the crystal angle θ with $\phi = 0$ (a) and $\phi = \pi/6$ (b) for well (continuousline), barrier (dashed line b) of wurtzite $ZnO/Cd_{15}Zn_{85}O$ QW structures $(L_W = 30A^\circ)$.

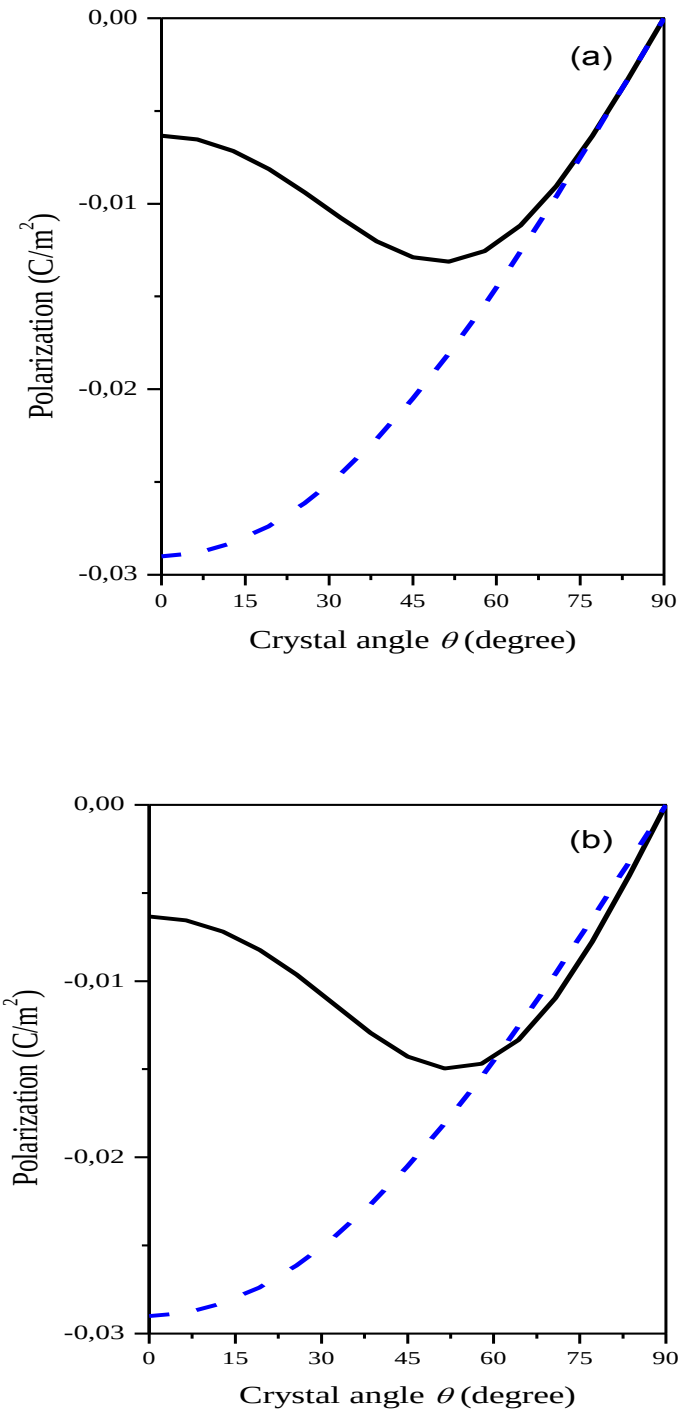

Figure 37 total polarization components as functions of the crystal angle θ with $\phi = 0$ (a) and $\phi = \pi/6$ (b) for well (continuousline), barrier (dashed line) of Wurtzite $GaN/In_{15}Ga_{85}N$ QW structures $(L_W = 30A^\circ)$.

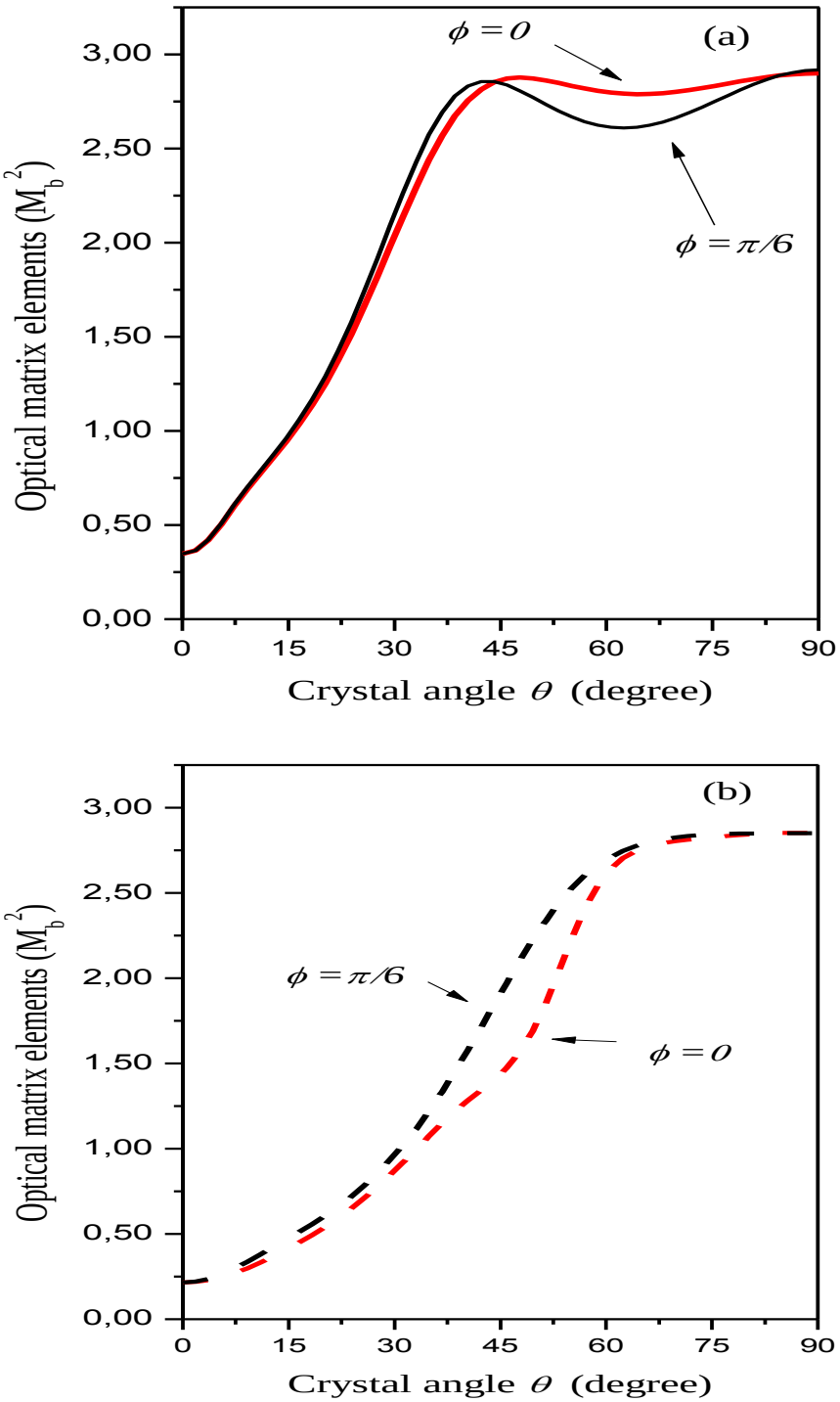

Figure 38 the y-polarized optical matrix element at the band edges as functions of the crystal angle θ (a) for wurtzite $ZnO/Cd_{15}Zn_{85}O$ and (b) $GaN/In_{15}Ga_{85}N$ QW structures $(L_w = 30A^\circ)$ [43].

Figure 38 shows the y-polarized optical matrix element at the band edges as functions of the crystal angle θ (a) for wurtzite $ZnO/Cd_{15}Zn_{85}O$ and (b) $GaN/In_{15}Ga_{85}N$ QW

structures ($L_w = 30A^\circ$). The OME of a- and m-planes are exhibiting similar behavior in $GaN/In_{15}Ga_{85}N$ structure unlike the case of $ZnO/Cd_{15}Zn_{85}O$ structure, we see a decrease between the angles $\theta = \pi/6$ and $\theta = \pi/2$ in the case of $\phi = \pi/6$.The increase in the OME become larger when we increase the crystal angle θ until it saturates after an angle of $\theta = \pi/4$ for $ZnO/Cd_{15}Zn_{85}O$ structure and $\theta = \pi/6$ for $GaN/In_{15}Ga_{85}N$ structure, the main benefit from this increase is seen in a larger optical gain peak in a- and m-planes[43].

Figure (39) shows Interband transition wavelength as functions of the crystal angle θ (a) for wurtzite $ZnO/Cd_{15}Zn_{85}O$ and (b) $GaN/In_{15}Ga_{85}N$ QW structures. The transition wavelength of the c-planes is much larger than that of the a- or m-plane in both structures because the red shifting of the transition energy due to the internal field in well region. The difference between the transition energy of the m-plan oriented structure and the a-plan is bigger in $GaN/In_{15}Ga_{85}N$ structure than $GaN/In_{15}Ga_{85}N$ structure, but in both cases the transition of m-plan structure is greater than the a-plan by 10 nm for $GaN/In_{15}Ga_{85}N$ structure and 2 nm for $ZnO/Cd_{15}Zn_{85}O$ structure. Thus, the transition energy defines the spectral window for the optical gain [43].

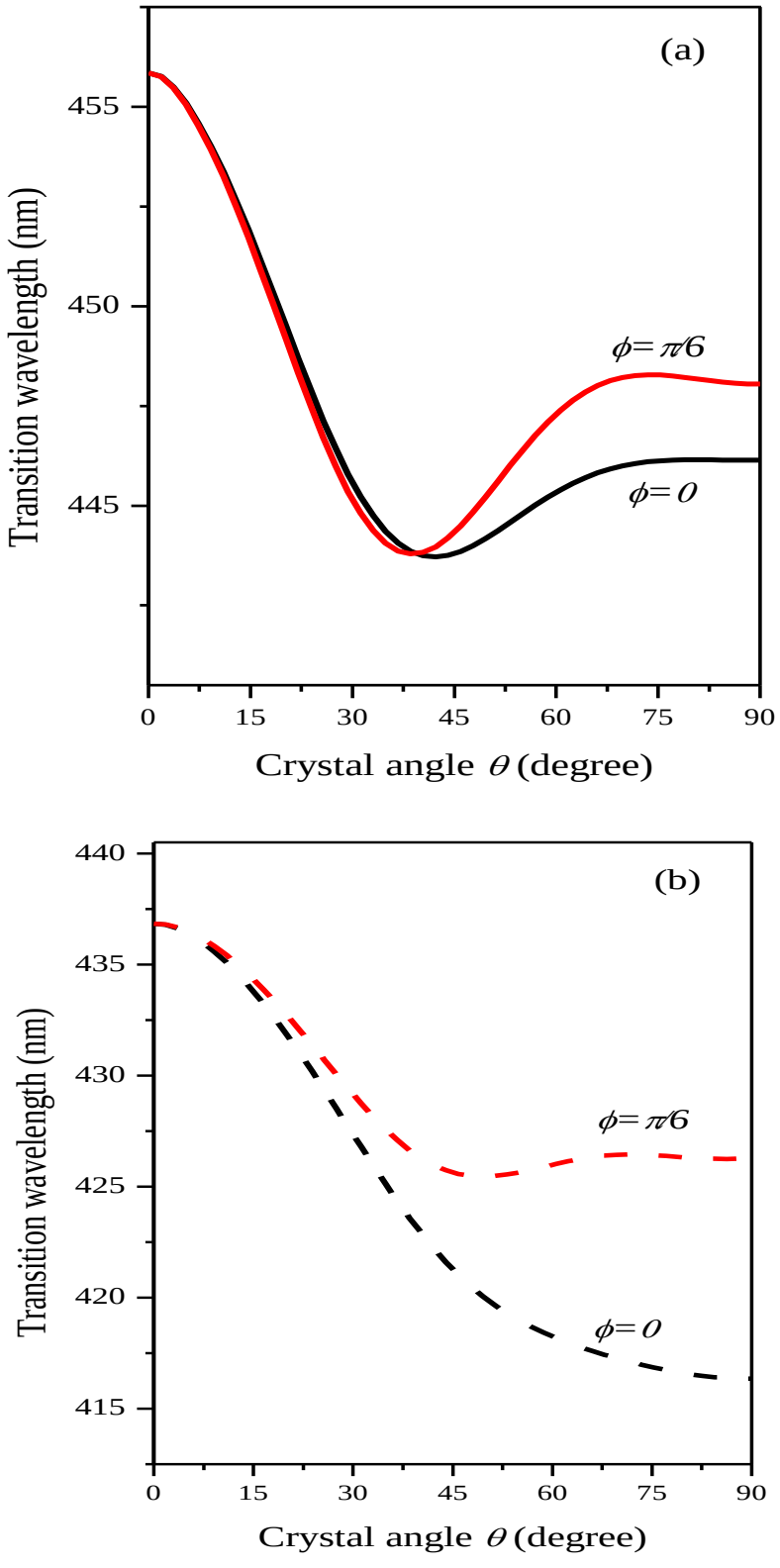

Figure 39 interband transition wavelengths as functions of the crystal angle θ (a) for wurtzite $ZnO/Cd_{15}Zn_{85}O$ and (b) $GaN/In_{15}Ga_{85}N$ QW structures $(L_w = 30A^\circ)$ [43].

IV.6 Summary:

In this chapter, we studied the crystal orientation dependence of electronic and optical properties of $ZnO/Cd_{15}Zn_{85}O$ and $GaN/In_{15}Ga_{85}N$ QW structures. The K.P method based on effective mass theory was used to calculate electronic and optical properties with including the many body effects. These results are used to establish comparisons primarily between polar and non-polar structures and secondly between $ZnO/Cd_{15}Zn_{85}O$ and $GaN/In_{15}Ga_{85}N$ QW structures. We used the c-plane Hamiltonian to extract the arbitrary crystal orientation Hamiltonian by applying a rotational matrix and thus their momentum matrix elements. Both the angle θ and ϕ have a tremendous influence on electronic and optical properties of $ZnO/Cd_{15}Zn_{85}O$ and $GaN/In_{15}Ga_{85}N$ QW structures whether on transition energy or transition strength.

Chapter V

Electronic and Optical Properties of ZnO/CdZnO QW Structures with m- and a-planes Orientations

V.1 Introduction

After studying the general case in the preVous chapter ,where an arbitrary crystal orientation Hamiltonian was drived for wurtzite materials such as Cd-ZnO and In-GaN along with their optical transition stranght elements .We will be focusing on non-polar oriented structures for the raison of their fanishing piezoelectric and spontaneous polarization and also their larger optical gain compaired to conventional structrure in this case c-plane oriented structrues.

Although the internal field created by piezoelectric (PZ) and spontaneous (SP) polarizations of strain origin for ZnO [0001] wurtzite (WZ) QW structures is found to be smaller than that of GaN [74], it still has the same influence of increasing carrier density needed to generate an optical gain compared to zincblende (ZB) materials [75 and 76]. Studies showed that the major effect of the built-in electric fields due to quantum confined Stark effects is the spatial separation of the wave functions of both electrons and holes, which has an effect on carrier recombination efficiency and thus optical properties in general [77–79]. Therefore, to reduce the quantum confined Stark effects of the field, structures that are non-polar are suggested by many groups [77 and 78].

In this chapter, we consider the theoretical electronic and optical properties of ZnO/CdZnO QW structures as object of studying using a Gaussian line shape function

in the gain model including many-body effects [19].To obtain the band structures and the wave functions ,we solve (a finite difference method was used in numerical calculations, un example for zincblende is implemented in the open source code called Aestimo 0.9 and for wurtzite in coming version 1.0 [41]) the Schrodinger equation for electrons and the 6×6 Hamiltonian for holes for c-, a- and m-plane considering the electric field due to build in polarization [67]. These results are compared with those for GaN/InGaN QW structures.

V.2 Electronic band structures and momentum matrix elements

The valence band structure of strained wurtzite semiconductors with piezoelectric field is determined by the 6×6 Hamiltonian given by Park and Chuang [67] for c-plane, the latter Hamiltonian is used to obtain those for the m- and a-planes. We use the same approach done by D. Ahn *et al* [69] where a rotation matrix of the Euler angles θ and ϕ is use to give the physical quantities representation in coordinates (x',y',z') see Appendix A. The energy bands E'_c, E'_v and wave functions φ'^{η}_n and Ψ'_m of conduction and valence states respectively, are obtained from a numerical solution of the Schrödinger equations for electrons with the electron wave function is given by

$$\left|\phi'^{\eta}_n\right\rangle = e^{ik'_x x'+ik'_y y'}\phi'_n(z')\left|S\eta\right\rangle \tag{V.1}$$

Where $\eta=\uparrow or\downarrow$ and S is a spherically symmetric wave function and $\phi'_n(z')$ is the envelope function that satisfies

$$\left[\tilde{H}'_c\left(k'_x,k'_y,-i\partial/\partial z'\right)+\left(v_c(z')+eF'_z z'\right)\delta_{vu}\right]=E'_c\left(k'_x,k'_y\right)\phi'_n\left(k'_x,k'_y,z'\right) \tag{V.2}$$

and for holes with the hole wave function is given by

$$\left|\Psi'_m\right\rangle=\sum_{u=1}^{6}\left[e^{ik'_x x'+ik'_y y'}g'^{(u)}_m(z')\left|v\right\rangle\right] \tag{V.3}$$

where $g'^{(u)}_m(z')$ is the envelope function of the m^{th} sub-band that satisfies

$$\sum_{\mu=0}^{6}\left[\tilde{H}'_{v\mu}\left(k'_x,k'_y,-i\partial/\partial z'\right)+\left(v_h(z')+eF'_z z'\right)\delta_{v\mu}\right]g'^{(\mu)}_m\left(k'_x,k'_y,z'\right)= E'_m\left(k'_x,k'_y\right)g'^{(\mu)}_m\left(k'_x,k'_y,z'\right) \tag{V.4}$$

where the potential $v_h(z')$ $(v_c(z'))$ is the potential for the valence-band (conduction-band) offset of the QW, F'_z is the internal electric fields and e is the electron charge.

V.2.1 [10$\bar{1}$0] Orientation (m-Plane)

The m-plane Hamiltonian can be obtained by inserting $\phi = \pi/6$ and $\theta = \pi/2$ into equation (V.18) defined in the chapter (IV) to return:

$$F' = \Delta_1 + \Delta_2 + \lambda' + \theta'$$

$$G' = \Delta_1 - \Delta_2 + \lambda' + \theta'$$

$$\lambda' = \frac{\hbar^2}{2m_0}\left[A_1 k'^2_x + A_2\left(k'^2_z + k'^2_y\right)\right] + D_1\varepsilon^{(0)}_{zz} + D_2(2\varepsilon^{(0)}_{zz} - 2(\frac{(4C_{12}+3C_{11})\varepsilon^{(0)}_{xx} + 4C_{13}\varepsilon^{(0)}_{zz}}{5C_{11}+3C_{12}}))$$

$$\theta' = \frac{\hbar^2}{2m_0}\left[A_3 k'^2_x + A_4\left(k'^2_z + k'^2_y\right)\right] + D_3\varepsilon^{(0)}_{zz} + D_4(2\varepsilon^{(0)}_{zz} - 2(\frac{(4C_{12}+3C_{11})\varepsilon^{(0)}_{xx} + 4C_{13}\varepsilon^{(0)}_{zz}}{5C_{11}+3C_{12}}))$$

$$K' = \frac{\hbar^2}{2m_0}(i\sqrt{3}+1)A_5\left[-\frac{1}{2}k'^2_y + ik'_y k'_z + \frac{1}{2}k'^2_z\right] - D_5(1+3i)(\frac{(4C_{12}+3C_{11})\varepsilon^{(0)}_{xx} + 4C_{13}\varepsilon^{(0)}_{zz}}{5C_{11}+3C_{12}}))$$

$$H' = \frac{\hbar^2}{2m_0}\left[A_6\frac{1-i\sqrt{3}}{2}k'_y k'_x - A_6\frac{\sqrt{3}-i}{2}k'_x k'_z\right] \qquad \text{(V.5)}$$

In equation (IV.18), we maintain the same approach [69], where the same old bases defined in equations (I.13) are used here. The optical momentum matrix elements for the m-plane are given by [72]

$$\left|\hat{e}'\cdot M'^{\eta}\right|^2 = \left|\left\langle \Psi'^{c\eta}_l \left|\hat{e}'\cdot p'\right| \Psi'^{v}_m \right\rangle\right|^2 \qquad \text{(V.6)}$$

where $\Psi'^{c\eta}_l$ (Ψ'^{v}_m) is the wave function for the conduction (valence) band , and $\eta = \uparrow$ and $\downarrow$ for both electron spins. The indexes and stand for the electron states in the conduction band and the heavy-hole (light hole) subband states in the valence band, respectively. The interband momentum matrix elements for each spin orientation can be written as follows. For TE- polarization $(\hat{e}' = \cos\phi\hat{x}' + \sin\phi\hat{y}')$:

$$\left|\hat{e}'\cdot M'^{\uparrow}\right|^2 = \left|-\cos\phi' P'_z \left\langle g'^{(3)}_m \middle| \phi'_l \right\rangle + \sin\phi' \frac{p_x}{2\sqrt{2}}\left\{\left(1-i\sqrt{3}\right)\left\langle g'^{(1)}_m \middle| \phi'_l \right\rangle - \left(1+i\sqrt{3}\right)\left\langle g'^{(2)}_m \middle| \phi'_l \right\rangle\right\}\right|^2$$

(V.7)

$$\left|\hat{e}'\cdot M'^{\downarrow}\right|^2 = \left|-\cos\phi' P'_z \left\langle g'^{(6)}_m \middle| \phi'_l \right\rangle - \sin\phi' \frac{p_x}{2\sqrt{2}} \left\{ \left(1+i\sqrt{3}\right)\left\langle g'^{(4)}_m \middle| \phi'_l \right\rangle - \left(1-i\sqrt{3}\right)\left\langle g'^{(5)}_m \middle| \phi'_l \right\rangle \right\}\right|^2$$

(V.8)

where $g'^{(v)}_m$ (v =1, 2,3,4,5 and 6) is the wave function for the mth subband in (x', y', z') coordinates. The use of old bases in equation (I.13) results in the same known quantities p_x and p_z.

V.2.1 [11$\bar{2}$0] Orientation (a-Plane)

The a-plane Hamiltonian can be obtained by inserting ϕ= 0 and θ = π/2 into equation (IV.1) defined in the Chapter (IV) .The matrix elements in the equation (IV.18) are given by

$$F' = \Delta_1 + \Delta_2 + \lambda' + \theta'$$

$$G' = \Delta_1 - \Delta_2 + \lambda' + \theta' \quad \lambda' = \frac{\hbar^2}{2m_0}\left[A_1 k'^2_z + A_2\left(k'^2_x + k'^2_y\right)\right] + D_1\varepsilon^{(0)}_{zz} + D_2\left(2\varepsilon^{(0)}_{xx} + \frac{C_{12}}{C_{11}}\varepsilon^{(0)}_{xx} - \frac{C_{13}}{C_{11}}\varepsilon^{(0)}_{zz}\right)$$

$$\theta' = \frac{\hbar^2}{2m_0}\left[A_3 k'^2_x + A_4\left(k'^2_z + k'^2_y\right)\right] + D_3\varepsilon^{(0)}_{zz} + D_4\left(2\varepsilon^{(0)}_{xx} + \frac{C_{12}}{C_{11}}\varepsilon^{(0)}_{xx} - \frac{C_{13}}{C_{11}}\varepsilon^{(0)}_{zz}\right)$$

$$K' = \frac{\hbar^2}{2m_0}\left[-A_5 k'^2_y + 2iA_5 k'_y k'_z + A_5 k'^2_z\right] - D_5\left(\frac{C_{12}}{C_{11}}\varepsilon^{(0)}_{xx} + \frac{C_{13}}{C_{11}}\varepsilon^{(0)}_{zz} + \varepsilon^{(0)}_{xx}\right)$$

$$H' = \frac{\hbar^2}{2m_0}\left[-iA_6 k'_y k'_x - A_6 k'_x k'_z\right] \qquad \text{(V.9)}$$

The interband momentum-matrix elements for a-plane for each spin orientation are given as follows. TE–polarization $(\hat{e}' = \cos\phi'\hat{x}' + \sin\phi'\hat{y}')$:

$$\left|\hat{e}'\cdot M'^{\uparrow}\right|^2 = \left|-\cos\phi' P'_z \left\langle g'^{(3)}_m \middle| \phi'_l \right\rangle + \sin\phi' \frac{p_x}{2\sqrt{2}} \left\{ -i\left\langle g'^{(1)}_m \middle| \phi'_l \right\rangle - i\left\langle g'^{(2)}_m \middle| \phi'_l \right\rangle \right\}\right|^2 \qquad \text{(V.10)}$$

$$\left|\hat{e}'\cdot M'^{\downarrow}\right|^2 = \left|-\cos\phi' P'_z \left\langle g'^{(6)}_m \middle| \phi'_l \right\rangle - \sin\phi' \frac{p_x}{2\sqrt{2}} \left\{ -i\left\langle g'^{(4)}_m \middle| \phi'_l \right\rangle - i\left\langle g'^{(5)}_m \middle| \phi'_l \right\rangle \right\}\right|^2 \qquad \text{(V.11)}$$

V.3 Electric fields in *a-* and *m-planes* oriented structures

The polarization components along *x, y* and *z* axes for the arbitrary oriented WZ structure are given in chapter (IV) .The strain induced piezoelectric polarization normal

with respect to the growth plane (along the growth direction) with $\theta = \pi/2$ crystal orientation angle can be expressed as

$$P'_{PZ}\begin{cases} P'^{x}_{PZ} = -P^{z}_{PZ} \\ P'^{y}_{PZ} = 0 \\ P'^{z}_{PZ} = P^{x}_{PZ} \end{cases} \tag{V.12}$$

The spontaneous polarization P_{SP} along the growth direction in the same crystal orientation angle is

$$P'_{SP} = 0 \tag{V.13}$$

Note that only spontaneous polarization is independent of the angle ϕ although we don't find the angle ϕ in the final form of the strain induced piezoelectric polarization explicitly but their polarization components which are in function of strain components.

By inserting polarization components found in equation (V.12) into the build in electric fields in the well and barrier to get

$$F'^{w}_{z} = \frac{\left(P'^{b}_{PZ} - P'^{w}_{PZ}\right)}{\varepsilon^{w} + \varepsilon^{b}\left(L_w / L_b\right)} \tag{V.14}$$

$$F'^{b}_{z} = -\frac{L_w}{L_b} F'^{w}_{z}$$

where L_w (L_b) and ε_w (ε_b) are the length of well (barrier) and the static dielectric constant, respectively.

V.4 Optical gain model

Park *et al* introduced the phenomenological non-MarkoVan gain model with many-body effects [19, 54], which is used here with including the effects of anisotropy on both the valence band dispersion and the momentum matrix element, and it is given by [54]

$$g(\omega) = \sqrt{\frac{\mu_0}{\varepsilon}}\left(\frac{e^2}{m_0^2 \omega}\right)\int_0^{\infty} dk_{\parallel} \frac{k_{\parallel}}{\pi^2 L_w} \cdot \left|M_{nm}(k_{\parallel})\right|^2 \left[f_n^c(k_{\parallel}) - f_m^v(k_{\parallel})\right] L(\omega, k_{\parallel}) \tag{V.15}$$

where ω represents the angular frequency, μ_0 is the vacuum permeability, ε is the

dielectric constant, *e* is the charge of an electron, m_0 is the free electron mass, $k_{||}$ is the magnitude of the in-plane wave vector in the QW plane, M_{nm} is the momentum matrix element in the strained QW, $f_n^c(k_{||})$ and $f_m^v(k_{||})$ are the Fermi functions for occupation probability by the electrons in the conduction subband states and the valence subband states, respectively. The indexes *l* and *m* stand for the electron (hole) states in conduction (valence), respectively. The line-shape function is Gaussian and is given by [54, 55]

$$L(k_{\parallel},\hbar\omega)=\sqrt{\frac{\pi\tau_{in}(k_{\parallel},\hbar\omega)\tau_c}{2\hbar^2}}\times\exp\left(-\frac{\pi\tau_{in}(k_{\parallel},\hbar\omega)\tau_c}{2\hbar^2}E_{lm}^2(k_{\parallel},\hbar\omega)\right) \quad \text{(V.16)}$$

The intraband relaxation time τ_{in} and the correlation time τ_c are taken to be constant. $\tau_{in}=10\,\text{fs}$ and $\tau_c=25\,\text{fs}$ are used in the calculation.

$$E_{lm}(k_{\parallel},\hbar\omega)=E_l^c(k_{\parallel})-E_m^v(k_{\parallel})+E_g+\Delta E_{SX}+\Delta E_{CH}-\hbar\omega \quad \text{(V.17)}$$

is the renormalized transition energy between electrons and holes, where E_g is the bandgap of the material, ΔE_{SX} and ΔE_{CH} are the screened exchange and the Coulomb-hole contributions to the bandgap renormalization, respectively [53] ,see chapter (III). The material parameters for ZnO (GaN) and CdO (InN) are given in Table 3(4) in Appendix (A),respectively. We used an averaged bandgap bowing value of –3.8 eV for CdZnO [79].

V.5 Results and discussion

Figure (40) shows the band edges and the corresponding wave functions at the zone center under the effect of piezoelectric and spontaneous polarizations for ZnO/CdZnO (continuous line) and GaN/InGaN (dashed line) QW structures. For all structures, the well width is set to $L_w=30A^\circ$ and barrier width $L_b=50A^\circ$, the first two wave functions C1 and HH are acronyms for the first subband for lowest conduction band and the first heavy-hole subband for the topmost of the valence band in the case of c-plane (a) ,and for a-plane (b) which is almost the same as m-plane ,with vertical shift in the energy scale, we plot the average between the two dominant components of the wave function ;for example, if the dominant components are heavy hole and light hole ,we use the notation HL and the same goes for the other combinations [80]. The ZnO (GaN) well in c-plane is under a 0.91 % (1.58 %) compressive strain ,and these layers are assumed to

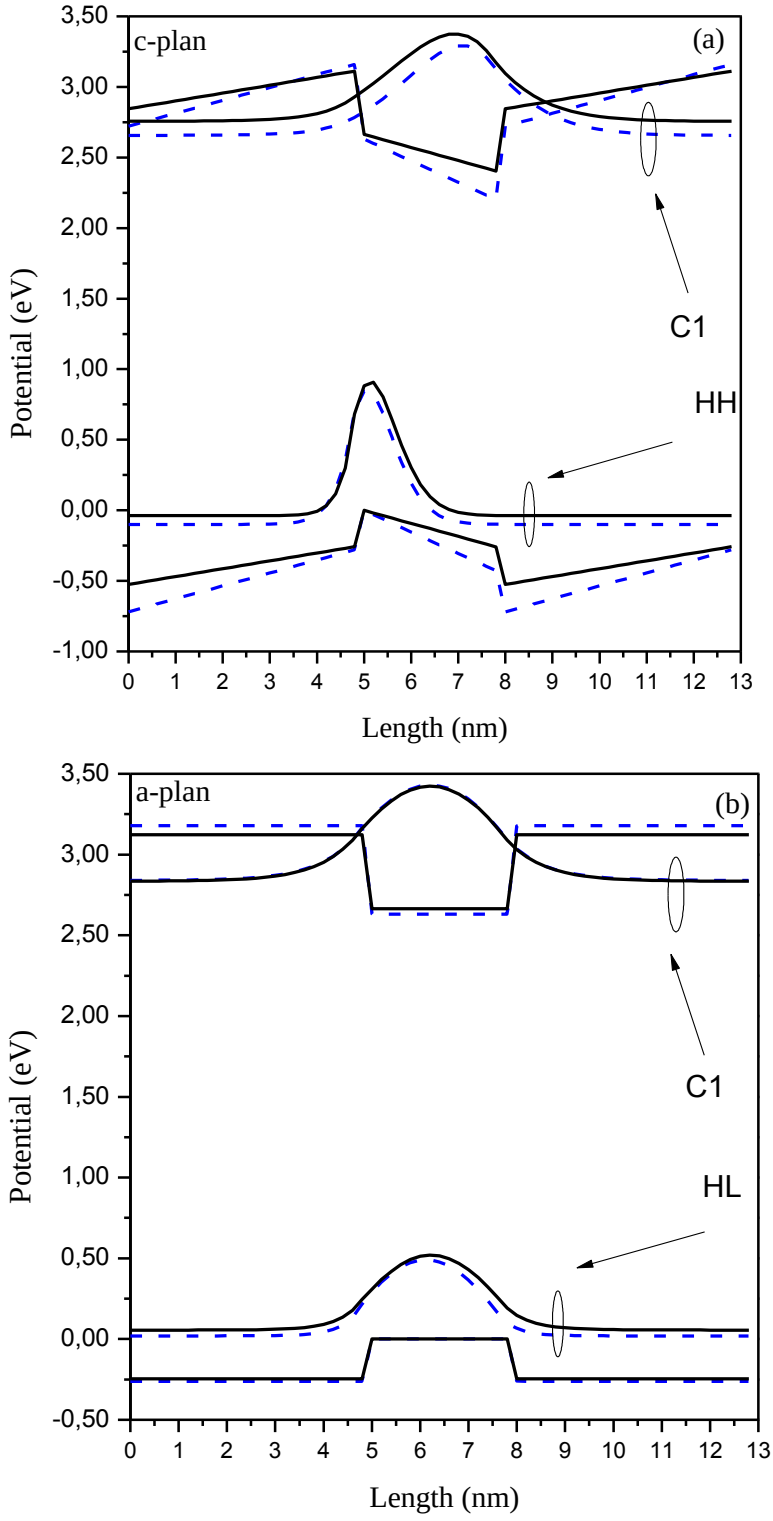

Figur 40 Band edges and wave functions at the zone center with piezoelectric and spontaneous polarizations for $(L_w = 30A^\circ)$ $ZnO/Cd_{15}Zn_{85}O$ (continuous line) and $GaN/In_{15}Ga_{85}N$ (dashed line) QW structures a) for c-plane and b) for a-plane ,the case of m-plane is similar to a-plane with vertical shifts [43].

have a Zn (Ga) face where the SP polarization is pointing towards the substrate because the SP polarization for and ZnO (GaN) is found to be negative [81] , while in a- and m-planes are under less compressive strain 0.64% (1.01 %) in the flat-band (FB) model as the SP and PZ polarization effects cease to exist in the a- and m-planes. Potential profiles show that the slightly larger internal field in the well region of GaN/InGaN than that of ZnO/CdZnO QW structures is owed to the difference in the strain induced PZ polarization ,the latter is the reason for the asymmetric electron and hole wave functions with respect to the well center and thus a large spatial separation between these wave functions in the c-plane ,on the other hand the a- and m-planes structures show symmetric electron and hole wave functions due to the FB model.Since the wave functions are affected by the crystal orientation this implies that the effective mass and the optical moment matrix elements are also affected [43].

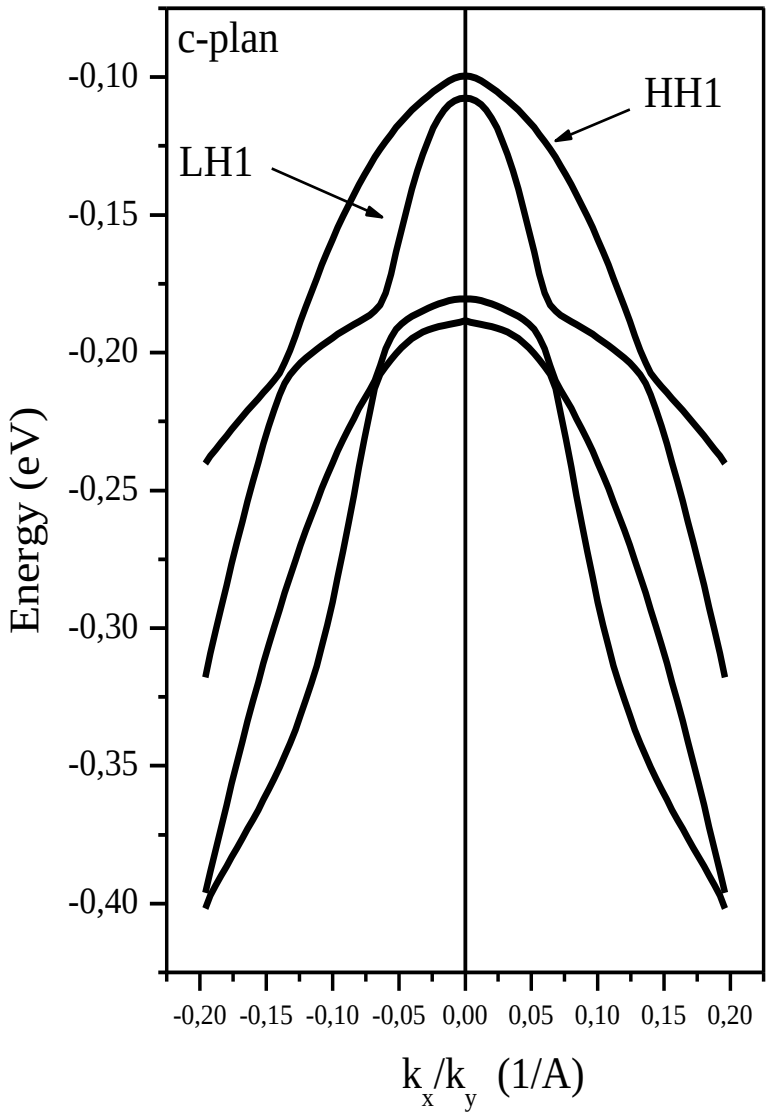

Figure 41 Valence-band structures of Wurtzite $ZnO/Cd_{15}Zn_{85}O$ QW structures $(L_w = 30A^\circ)$ with c-plane [43].

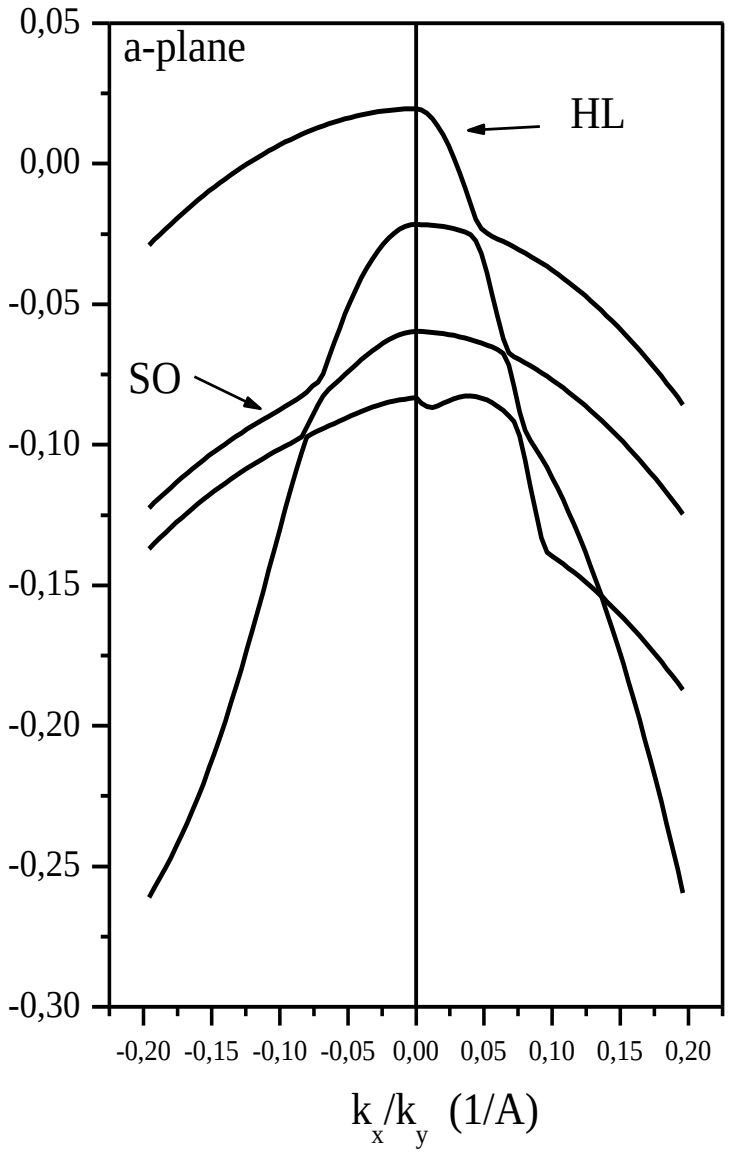

Figure 42 Valence-band structures of Wurtzite $ZnO/Cd_{15}Zn_{85}O$ QW structures ($L_w = 30A^\circ$) with a-plane [43].

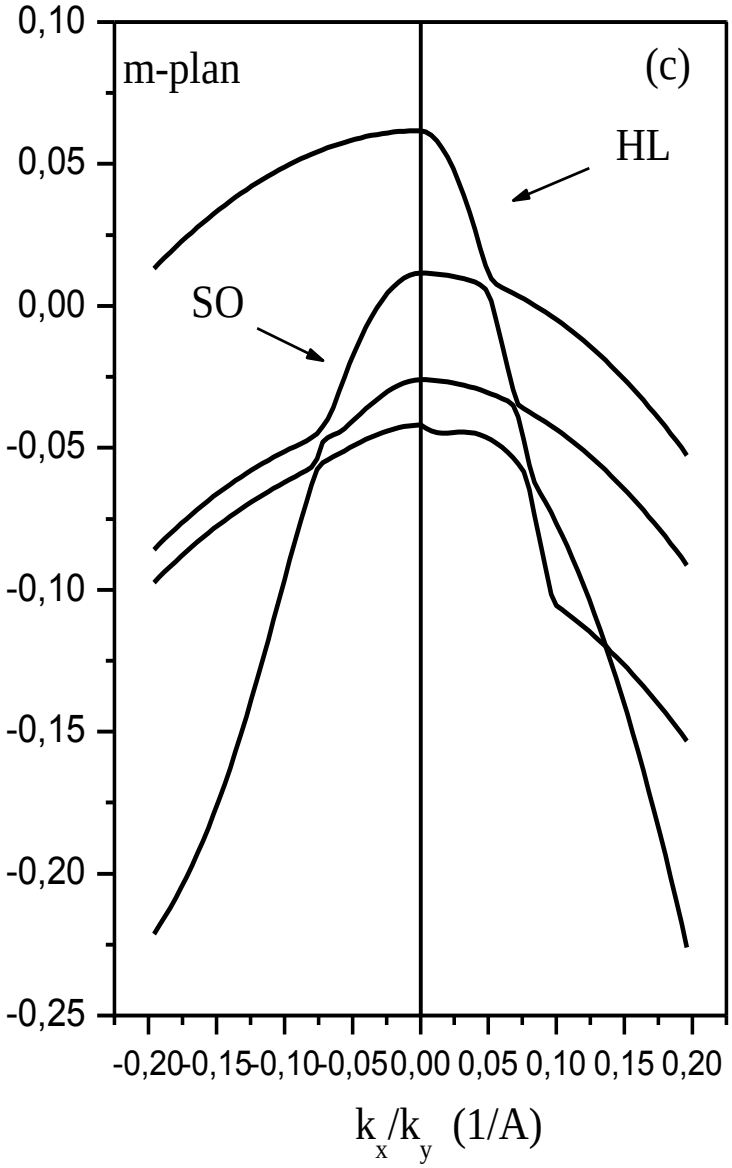

Figure 43 Valence-band structures of Wurtzite $ZnO/Cd_{15}Zn_{85}O$ QW structures $(L_w = 30A^\circ)$ with m-plane [43].

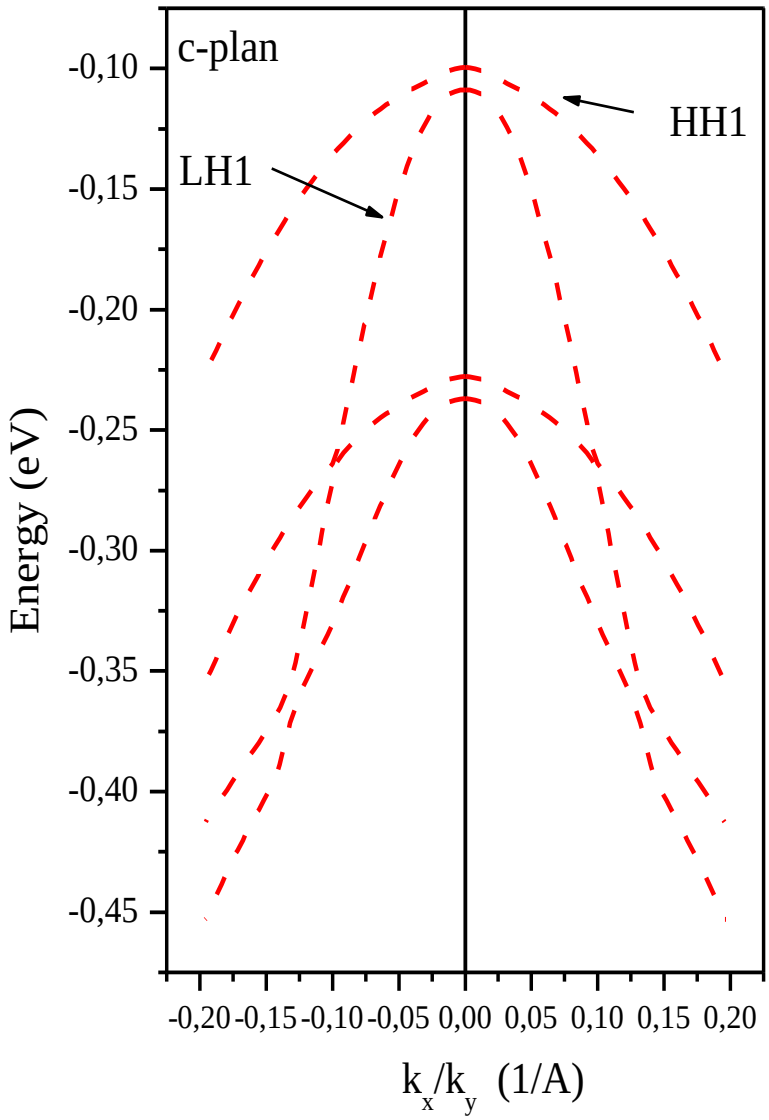

Figure 44 Valence-band structures of Wurtzite $GaN/In_{15}Ga_{85}N$ (dashed line) QW structures $(L_w = 30A^\circ)$ with c-plane [43].

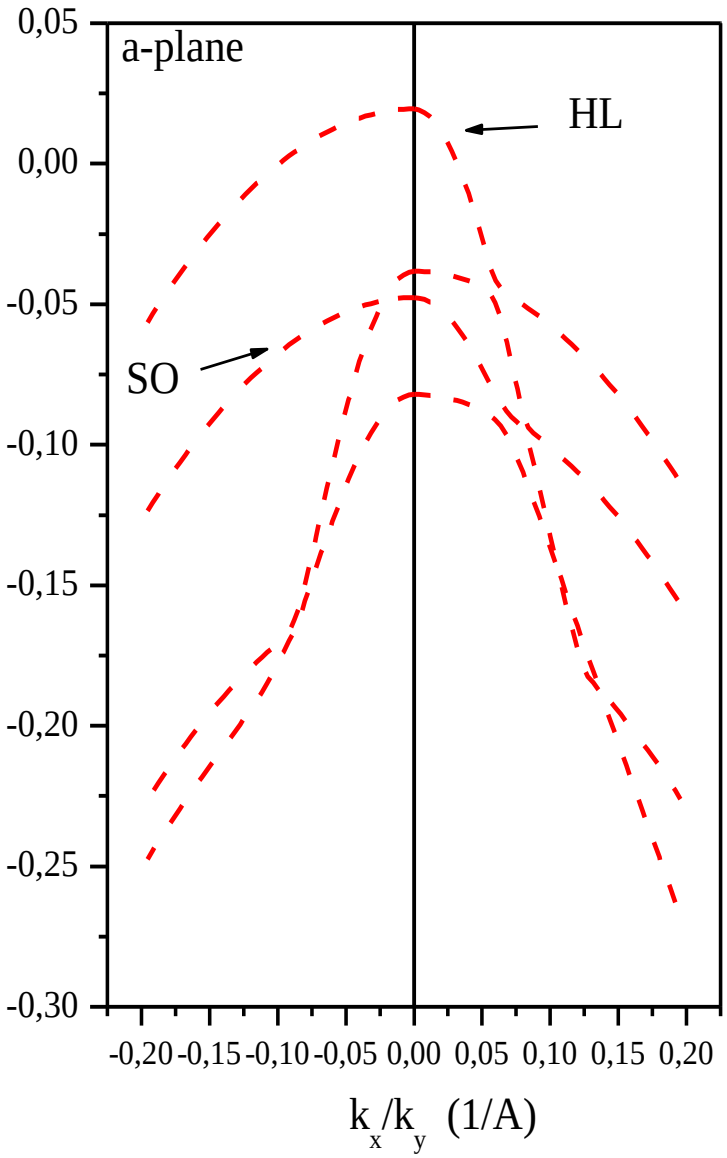

Figure 45 Valence-band structures of Wurtzite $GaN/In_{15}Ga_{85}N$ (dashed line) QW structures ($L_w = 30A^\circ$) with a-plane [43].

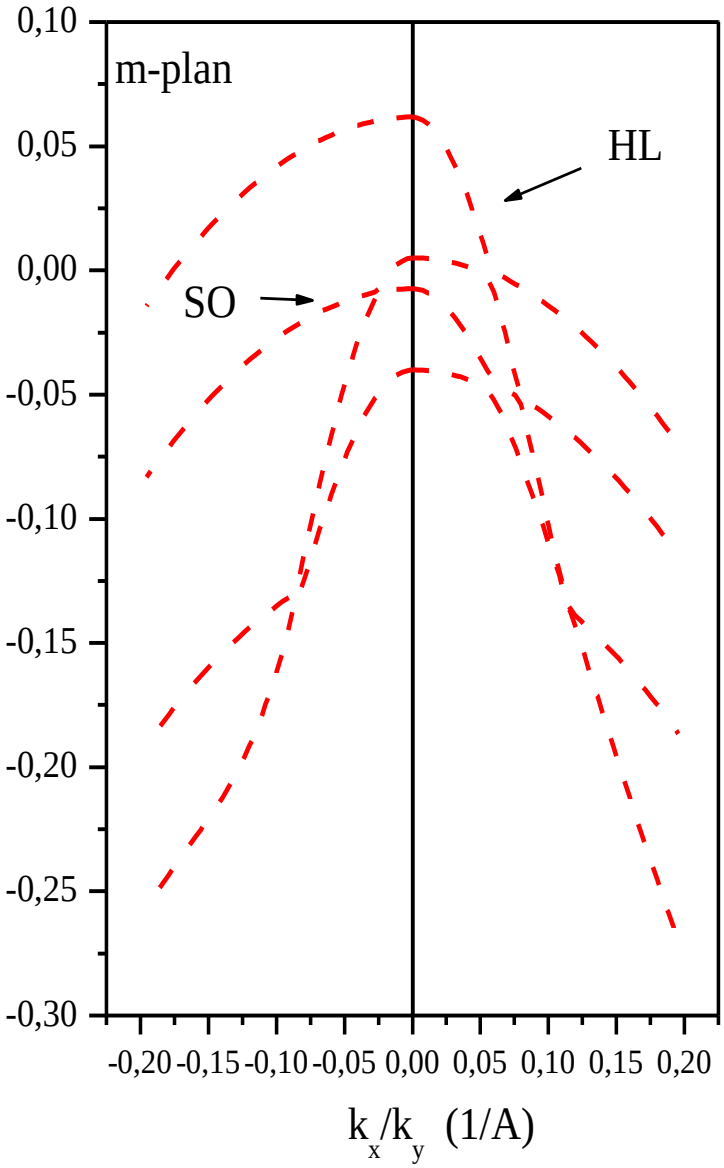

Figure 46 Valence-band structures of Wurtzite (dashed line) QW structures $(L_w = 30A^\circ)$ with m-plane [43].

Figure (41-43) and (43-46) show the valence band structures of $(L_w = 30A^\circ)$ $ZnO/Cd_{15}Zn_{85}O$ (continuous line) and $GaN/In_{15}Ga_{85}N$ (dashed line) QW structures for the (41, 43) c-, (42, 44) a- and (43, 46) m-planes. Here, the naming of the sub-bands for the m- and a-planes is described before. The plotted valence-band structures for $GaN/In_{15}Ga_{85}N$ are consistent with similar works [67] and the material parameters used in the calculation are the same ones used by S-H Park *el al* in Ref [67] except, for the band gap energy of InN was set to 0.78 eV [82].The valence-band structure of the a- and m-planes for $ZnO/Cd_{15}Zn_{85}O$ shows the same strong anisotropy of

$GaN/In_{15}Ga_{85}N$ QW structures in the QW plane unlike the (0001)-oriented c-plane structure. The energies of the $ZnO/Cd_{15}Zn_{85}O$ QWs are rescaled to give the same Γ point energy as that of the $GaN/In_{15}Ga_{85}N$ QWs for the first subband, the added energies are -0.062,-0.036 and 0.011 eV for the (0001), $(11\bar{2}0)$ and $(10\bar{1}0)$ orientations, respectively [43].

Energy deference between the two first subbands (heavy hole and light hole) in the valence band structure of c-plane's oriented structure usually referred as Energy spacing is increased in the cases of a- and m-planes but it is less increased in $ZnO/Cd_{15}Zn_{85}O$ than $GaN/In_{15}Ga_{85}N$ QW structures. The increase of the energy difference is due to the fact that the shift caused by the strain is much larger in a- and m-planes than c-plane, whereas between ZnO and GaN based structures, the deformation potentials of each material are the main reason for this difference [43]. In general, the increase in the subband energy spacing reduces the carrier population in the higher subbands [83,84].The hole effective mass along k_x direction was found in general ($GaN/In_{15}Ga_{85}N$ a- and m-planes) larger than the one along k_y direction [67,83] ,which confirms our calculations for $GaN/In_{15}Ga_{85}N$ as indicated in Table (2).Also, we found that the hole effective mass for $ZnO/Cd_{15}Zn_{85}O$ structure have the same characteristics those of $GaN/In_{15}Ga_{85}N$ structure [43].Between the two strucures, the hole effective mass is found in $ZnO/Cd_{15}Zn_{85}O$ structure larger than in $GaN/In_{15}Ga_{85}N$ structure and this will have a significant effect on the density of state and thus the optical gain. S. Seki *et al* presented a method of estimating the magnitude of the hole effective mass by considering a parabolic band fitted to the topmost valence subband of the exact band structure, where the resulting effective mass (from the parabolic fit) reflects an average density of states [83, 85].

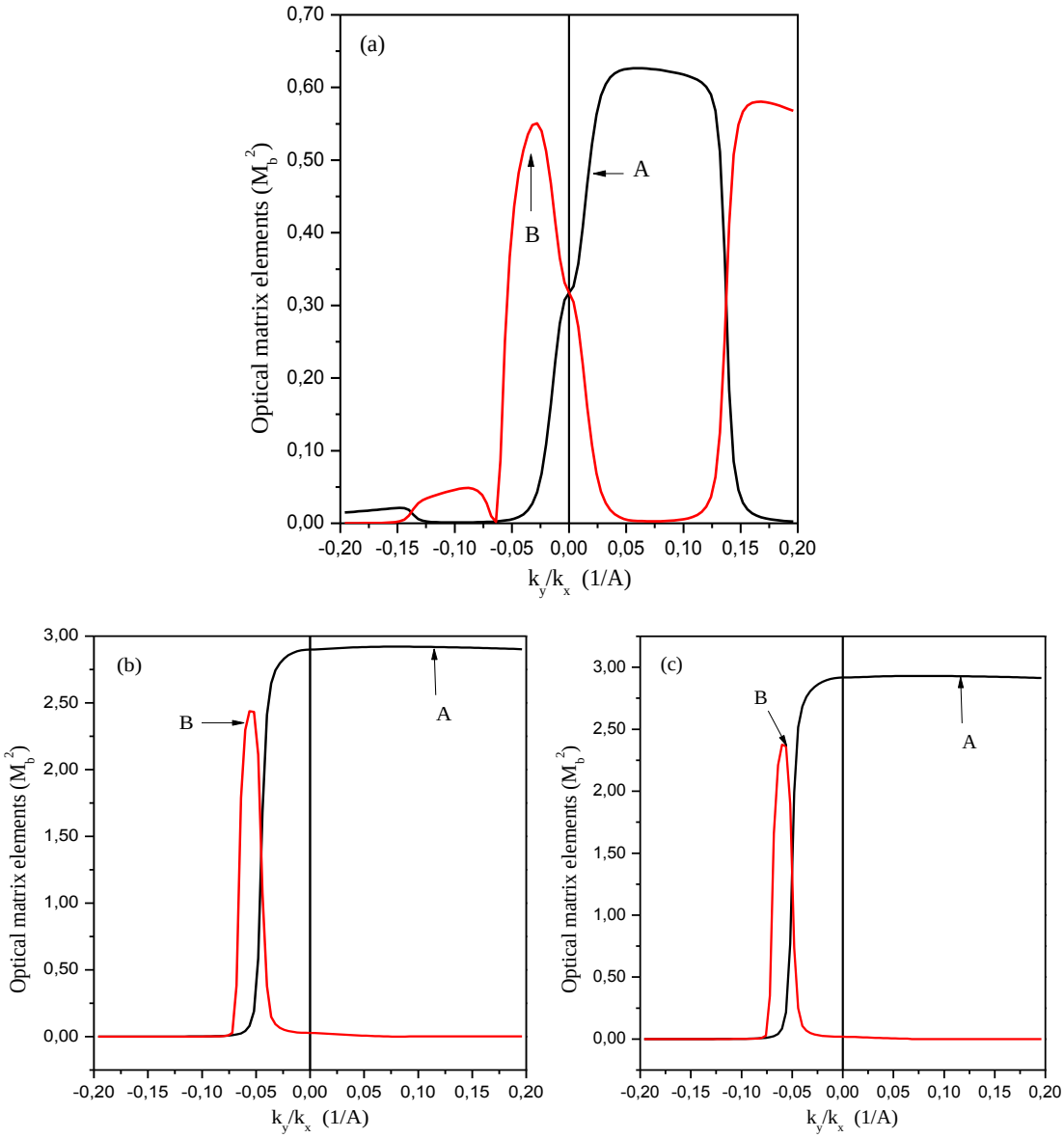

Figure 47 y-polarized (a, b and c) optical matrix elements as a function of k_x and k_y wave vectors and (d) TE optical gain spectra at a carrier density of $N = 20\times10^{12}\,cm^{-1}$ of wurtzite $ZnO/Cd_{15}Zn_{85}O$ (continuous line) and $GaN/In_{15}Ga_{85}N$ (dashed line) QW structures ($L_w = 30A^\circ$) with c-, a-, and m-planes [43].

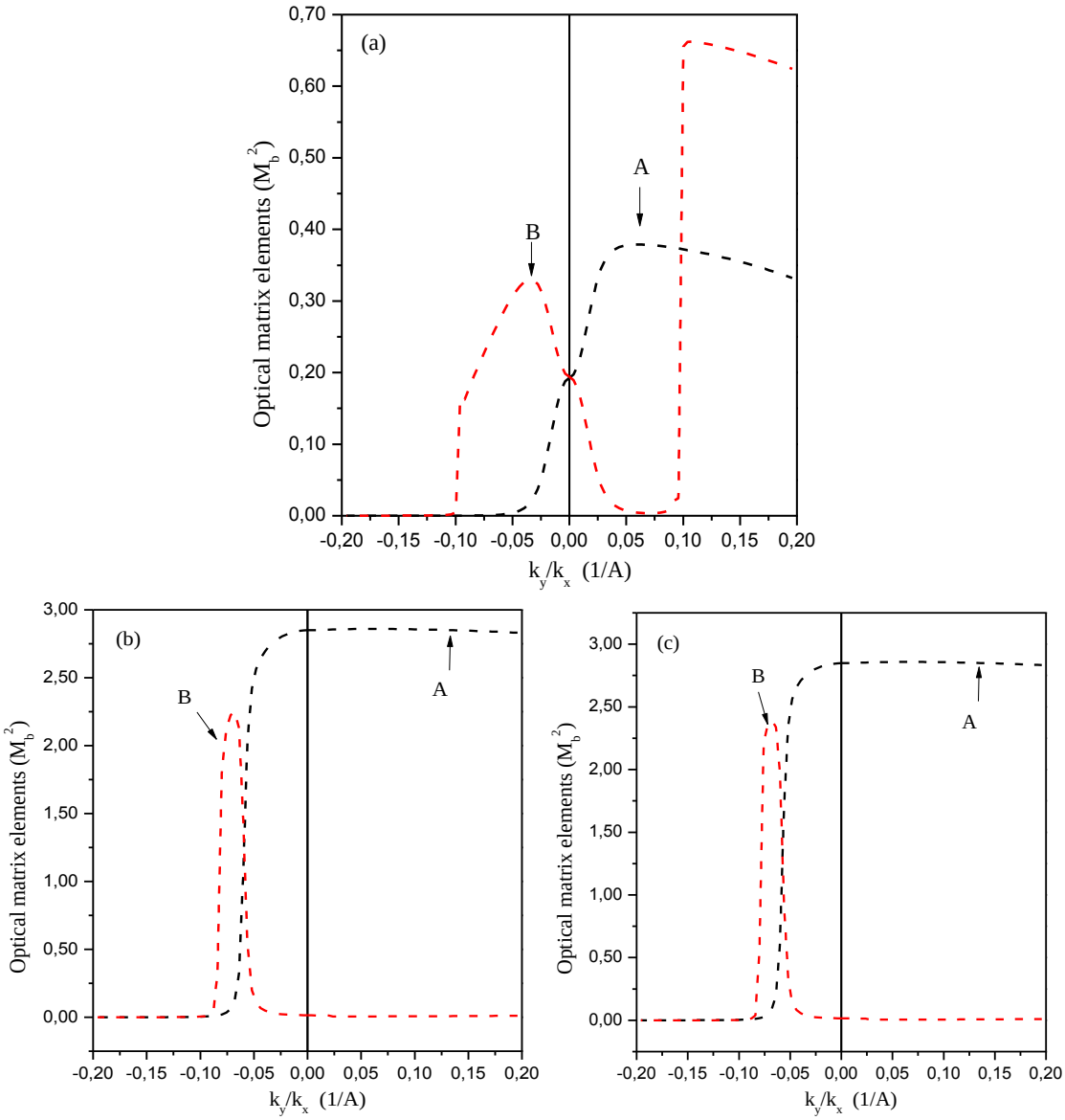

Figure 48 y-polarized (a, b and c) optical matrix elements as a function of k_x and k_y wave vectors and (d) TE optical gain spectra at a carrier density of $N = 20\times10^{12}\,cm^{-1}$ of wurtzite $ZnO/Cd_{15}Zn_{85}O$ (continuous line) and $GaN/In_{15}Ga_{85}N$ (dashed line) QW structures ($L_w = 30A^\circ$) with c-, a-, and m-planes [43].

Figure (48) (a, b and c) shows the y-polarized optical matrix elements as a function of k_x and k_y wave vectors and figure (49) (a, b) the TE optical gain spectra at a carrier density of $N = 20\times10^{12}\,cm^{-1}$ of wurtzite $ZnO/Cd_{15}Zn_{85}O$ (continuous line) and $GaN/In_{15}Ga_{85}N$ (dashed line) QW structures ($L_w = 30A^\circ$) with c-, a- and m-planes. The notations A and B stand for the transition from the lowest conduction band to the two first valence subbands, for example the notation A in the c-plane case means the

transition C1-HH1. The optical matrix elements (OME) show a strong anisotropy and especially in a- and m-planes, where we find that the OME for the transition A is constant in along k_x with larger value in $ZnO/Cd_{15}Zn_{85}O$ structure while along k_y is decreasing till it vanishes at 0.1 $(A^{\circ -1})$ for both planes. Unlike in transition A, the OME in transitions B has a larger value only along k_y with the case of a- and m-planes, in the c-plane oriented structure the OME without the piezoelectric and spontaneous

effects is similar to that obtained in non-polar cases but when we consider those effects as shown in figure 3 (a) we found a total reduction and a stronger anisotropy.

The optical gain for the $ZnO/Cd_{15}Zn_{85}O$ structure is slightly larger than that of $GaN/In_{15}Ga_{85}N$ structure in the a and m-plans and this is due to the deference in the OME but in the c-plane we find that the optical gain of $ZnO/Cd_{15}Zn_{85}O$ structure is nearly double of the value of that in $GaN/In_{15}Ga_{85}N$ structure and this is due to the negative effect of the piezoelectric and spontaneous polarization on the alignment of the electron and hole' wave functions which is higher in $GaN/In_{15}Ga_{85}N$ structure as it is shown in figure (40), the latter effect does not exist in a- and m-planes for both structures which is the raison for higher optical gain compared with c-plane. The results of $GaN/In_{15}Ga_{85}N$ structure agree with those obtained by Park *et al* in ref [67].

Table 2 The hole effective mass along k_x and k_y for both structures in c-,a- and m-planes .

Structure	$GaN/In_{15}Ga_{85}N$			$ZnO/Cd_{15}Zn_{85}O$		
Crystal orientation	c-plane	a-plane	m-plane	c-plane	a-plane	m-plane
Effective mass along k_x (m_0)	1.03	1.89	1.89	1.15	2.94	2.96
Effective mass along k_y (m_0)	1.03	0.89	0.90	1.15	1.12	1.04

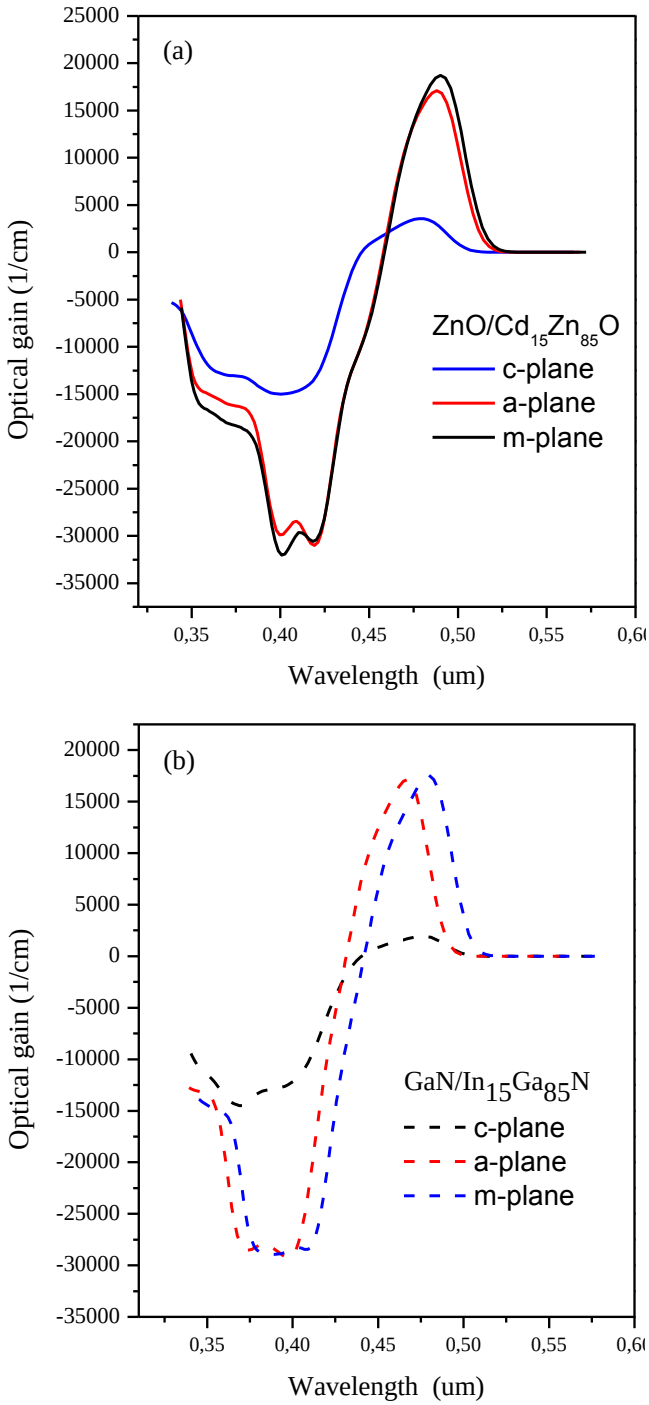

Figure 49 y-polarized (a, b and c) optical matrix elements as a function of k_x and k_y wave vectors and (d) TE optical gain spectra at a carrier density of $N = 20\times10^{12}\,cm^{-1}$ of wurtzite $ZnO/Cd_{15}Zn_{85}O$ (continuous line) and $GaN/In_{15}Ga_{85}N$ (dashed line) QW structures ($L_w = 30A^{\circ}$) with c-, a-, and m-planes [43].

V.6 Summary

In this chapter, we studied the crystal orientation dependence of electronic and optical properties of $ZnO/Cd_{15}Zn_{85}O$ and $GaN/In_{15}Ga_{85}N$ QW structures. We focused on main planes c-, a- and m-planes. The K.P method based on effective mass theory was used to calculate the band structure and optical properties with including the many body effects. These results are used to establish comparisons primarily between polar and non-polar structures and secondly between $ZnO/Cd_{15}Zn_{85}O$ and $GaN/In_{15}Ga_{85}N$ QW structures.In general, the hole effective masses of $ZnO/Cd_{15}Zn_{85}O$ structure for all crystal orientations are relatively larger than the ones in $GaN/In_{15}Ga_{85}N$ structure and for both structures the case of non-polar orientation shows smaller effective masses spatially in k_y direction. Optical gain in non-polar oriented structure is larger than the polar structure due to the retreating effect of built-in field and this is demonstrated in the bigger difference in optical matrix elements.

General Conclusion

In this thesis, we studied the crystal orientation dependence of electronic and optical properties of $ZnO/Cd_{15}Zn_{85}O$ and $GaN/In_{15}Ga_{85}N$ QW structures. we presented the elementary k.p theory to be an introduction to Chuang‘s derivation of the Wurtzite Hamiltonian using Luttinger-Kohn model and showed the its similarity with the one obtained by Bir and Pikus using invariant method. Also we outlined the method to bloc diagonalize the 6x6 Wurtzite Hamiltonian to become a 3x3 matrix which is easy to solve analytically. Band structure for both conduction and valence band were calculated taking into account strain effects, whether it is tensile or compressive and in the same way conduction band edges, valence band edges and effective masses calculated with their parabolic bands that is insufficient to predict a correct band structure. Also we introduced the basic formalism of EFA and its direct application to our ZnO based quantum well structure and presented the comparison of the ZnO’s results with its counterpart GaN based structure, such as band edges profiles, band structures and isoenergy counters, using numerical means such as finite difference method.

The main objectives of this thesis in studying optical properties have been firstly to provide an introduction to the basic concepts of optical transitions and their transition strength combined with Fermi-Dirac probability and broadening function, all to form the basic formalism of optical gain. Lorentzian line shape function is presented and also the Gaussian or non-Markovian lineshape function. Numerous effects on optical gain are studied in this work like built in electric field due to piezoelectric and spontaneous polarization, many body effects, strain effect and carrier concentration effect and all carry a relatively negative effect except for carrier concentration which gave an optical gain enhancement.

We studied the crystal orientation dependence of electronic and optical properties of $ZnO/Cd_{15}Zn_{85}O$ and $GaN/In_{15}Ga_{85}N$ QW structures. The K.P method based on effective mass theory was used to calculate electronic and optical properties with

including the many body effects. These results are used to establish comparisons primarily between polar and non-polar structures and secondly between ZnO/$Cd_{15}Zn_{85}O$ and GaN/$In_{15}Ga_{85}N$ QW structures. We used the c-plane Hamiltonian to extract the arbitrary crystal orientation Hamiltonian by applying a rotational matrix and thus their momentum matrix elements. In c-plane oriented structures, optical gain is relatively larger in the case ZnO/CdxZn1-xO compared to GaN/InxGa1-x N QW structure because of a greater built-in field seen in the well layer that causes a spatial separation between the envelope wave functions of electrons and holes decreasing transition probability and thus reducing optical gain in average by 78% to the case where no built-in field is included. Unlike c-plane case, the built-in field ceases to exist in non-polar cases (i.e. a- and m-planes) due to the change in spontaneous and piezoelectric polarization direction and causes an increase in momentum matrix elements and optical gain with lager value in m-plane compared to a-plane where it is attributed to strain components. A blue shift is observed in both structures between polar and non-polar types with maximum value of 15 nm for ZnO/CdxZn1-xO structure and 25 nm for GaN/InxGa1-x N structure. Energy dispersion, transition strength and the average hole effective masses are anisotropic in non-polar structures. The average hole effective masses are larger along kx direction than ky direction in non-polar structures and larger in general compared to polar structures.

Appendixes

Appendix A: Material parameters

Table 3 Physical parameters of ZnO and CdO [43].

Parameter	ZnO	CdO
Lattice constant (A°)		
a_0	3.2505	3.199
Energy parameters		
$E_g(eV)$	3.35	1.89
$\Delta_1(meV)$	30.5	–
$\Delta_3 = \Delta_2(meV)$	4.2	–
Conduction band effective masses		
m_e/m_0	0.24	–
Valence band effective-mass parameters		
A_1	–3.78	–
A_2	–0.44	–
A_5	–3.13	–
Deformation potentials (eV)		
a_c	–6.05	–
D_1	3.90	–
D_2	4.13	–
D_3	1.15	–
D_4	–1.22	–
D_5	–1.53	–
D_6	–2.83	–
Elastic stiffness constant $(\times 10^{11}\, dyn/cm^2)$		
C_{11}	20.97	–
C_{12}	12.11	–
C_{13}	10.51	–
C_{33}	21.09	–
Dielectric constant		
ε	8.1	-
Piezoelectric constant $10^{-12}(m/V)$		
d_{31}	–5	–1.1
Spontaneous polarization constant		
$P(C/m^2)$	–0.05	–0.099

Table 4 Physical parameters of GaN and InN [67] .

Parameter	GaN	InN
Lattice constant (A°)		
a_0	3.189	3.53
Energy parameters		
$E_g(eV)$	3.44	1.89
$\Delta_1(meV)$	22	41
$\Delta_3 = \Delta_2(meV)$	5	0.11
Conduction band effective masses		
m_e/m_0	0.20	0.32
Valence band effective-mass parameters		
A_1	–6.4	–9.09
A_2	–0.5	–0.63
A_5	–2.56	–4.36
Deformation potentials (eV)		
a_c	–4.6	–1.4
D_1	–1.7	–1.76
D_2	6.3	3.43
D_5	–4	–2.33
Elastic stiffness constant $(\times 10^{11}\, dyn/cm^2)$		
C_{11}	39	27
C_{12}	14.5	12.4
C_{13}	10.6	9.4
C_{33}	39.8	20
Dielectric constant		
ε	10	15.3
Piezoelectric constant $10^{-12}(m/V)$		
d_{31}	–1.7	–1.1
Spontaneous polarization constant		
$P(C/m^2)$	–0.029	–0.032

Appendix B: Pertubation theory

1. Degenerate perturbation theory

Consider an unperturbed system with degenerate eigen states. Sometimes the perturbation Hamiltonian consists of two parts: one which contributes in first order, $H^{(1)}$, and one which contributes in second order, $H^{(2)}$. If these two contributions have the same order of magnitude, then it is better to write the perturbation expansion as [3]

$$H(\lambda) = H^0 + \lambda^2 H^{(1)} + \lambda H^{(2)} \tag{B.1}$$

In this way the first order contribution of $H^{(1)}$ will automatically be paired to the second order contribution of $H^{(2)}$.We write the wave-function as

$$|\psi\rangle = |\psi^{(0)}\rangle + \lambda|\psi^{(1)}\rangle + \lambda^2|\psi^{(2)}\rangle + \ldots \tag{B.2}$$

We equate terms with same power in λ in Schrodinger's equation

$$\begin{aligned}&\left(H^0 + \lambda^2 H^{(1)} + \lambda H^{(2)}\right)\left(|\psi^0\rangle + \lambda|\psi^{(1)}\rangle + \lambda^2|\psi^{(2)}\rangle + \ldots\right) = \\ &\left(E^0 + \lambda E^{(1)} + \lambda^2 H^{(2)} + \ldots\right)\left(|\psi^{(0)}\rangle + \lambda|\psi^{(1)}\rangle + \lambda^2|\psi^{(2)}\rangle + \ldots\right)\end{aligned} \tag{B.3}$$

It follows that

$$H^{(0)}|\psi^{(0)}\rangle = E^{(0)}|\psi^{(0)}\rangle, \tag{B.4}$$

$$H^{(0)}|\psi^{(1)}\rangle + H^{(2)}|\psi^{(0)}\rangle = E^{(0)}|\psi^{(1)}\rangle + E^{(1)}|\psi^{(0)}\rangle, \tag{B.5}$$

$$H^{(0)}|\psi^{(2)}\rangle + H^{(2)}|\psi^{(1)}\rangle + H^{(1)}|\psi^{(0)}\rangle = E^{(0)}|\psi^{(2)}\rangle + E^{(1)}|\psi^{(1)}\rangle + E^{(2)}|\psi^{(0)}\rangle \cdot \tag{B.6}$$

Consider the non-perturbed eigenvalue problem for the degenerate level n, m,… and for the other levels α, β, …

$$H^{(0)}|\psi n\rangle = En|\psi n\rangle, \tag{B.7}$$

$$H^{(0)}|\psi a\rangle = Ea|\psi a\rangle \cdot \tag{B.8}$$

The wave-function components will be written as

$$|\psi^{(0)}\rangle = \sum_n c_n^{(0)}|\psi n\rangle, \tag{B.9}$$

$$\left|\psi^{(1)}\right\rangle = \sum_n c_n^{(1)}|\psi n\rangle + \sum_\alpha c_\alpha^{(1)}|\psi n\rangle \cdot \tag{B.10}$$

In writing (B.10) we have used (B.4) and (B.5). In the limit $\lambda \to 0$ we recover the non-perturbed states. Also

$$E^{(0)} = E_n \ . \tag{B.10}$$

We multiply (B.4) with $\left\langle \psi^{(0)} \right|$. Using (B.51) and the fact that $\left\langle \psi^{(0)} \left| H \right| \psi^{(0)} \right\rangle = 0$ we obtain

$$E^{(1)} = 0 \, . \tag{B.11}$$

We multiply (B.4) with $\left\langle \psi_\beta \right|$ and using (B.5) we obtain

$$E_\beta c_\beta^{(1)} + \left\langle \psi_\beta \left| H^{(2)} \right| \psi^{(0)} \right\rangle = E_n c_\beta^{(1)} . \tag{B.12}$$

Therefore the coefficient $c_\beta^{(0)}$ is

$$c_\beta^{(1)} = \frac{\left\langle \psi_\beta \left| H^{(2)} \right| \psi^{(0)} \right\rangle}{E_n - E_\beta} \cdot \tag{B.13}$$

We multiply (B.5) with $\langle \psi_m |$, and using (B.6) we obtain

$$\left\langle \psi_m \left| H^{(2)} \right| \psi^{(1)} \right\rangle + \left\langle \psi_m \left| H^{(1)} \right| \psi^{(0)} \right\rangle = E^{(2)} c_m^{(0)} \tag{B.14}$$

Using (B.9) and the fact that $\left\langle \psi_m |H| \langle \psi_n | \right\rangle = 0$, the first term of (B.14) reduces to

$$\left\langle \psi_m \left| H^{(2)} \right| \psi^{(1)} \right\rangle = \left\langle \psi_m \left| H^{(2)} \right| \sum_a c_a^{(1)} |\psi_a\rangle \right\rangle \cdot \tag{B.15}$$

Equation (B.14), with the help of (B.15) and (B.13), reduces to

$$\sum_a \frac{\left\langle \psi_a \left| H^{(2)} \right| \psi^{(0)} \right\rangle}{E_n - E_a} \left\langle \psi_m \left| H^{(2)} \right| \psi_a \right\rangle + \left\langle \psi_m \left| H^{(1)} \right| \psi^{(0)} \right\rangle = E^{(2)} c_m^{(0)} \cdot \tag{B.16}$$

By substitution of (B.18) we finally obtain

$$\sum_n \left(\sum_a \frac{\left\langle \psi_m \left| H^{(2)} \right| \psi_a \right\rangle \left\langle \psi_a \left| H^{(2)} \right| \psi_n \right\rangle}{E_n - E_a} + \left\langle \psi_m \left| H^{(1)} \right| \psi_n \right\rangle \right) c_n^{(0)} = E^{(2)} c_m^{(0)} \cdot \tag{B.17}$$

Therefore the coefficients $c_n^{(0)}$ and the energy $E^{(2)}$ are obtained by solving the eigenvalue problem (B.17). In the particular case when $H^{(1)} = 0$ we recover the simpler case of degenerate perturbation theory with second order contributions [3].

2. Löwdin perturbation theory [13, 3]

Consider a Hamiltonian H and a finite set of orthonormalized functions $\psi_n^{(0)}$ which are approximate eigenfunctions of H. Suppose the set of functions $\psi_n^{(0)}$ n s split into two parts, A and B. We will expand the eigenfunctions of H as

$$\psi = \sum_n c_n c_n^{(0)} \cdot \tag{B.18}$$

We substitute (B.18) into the eigenvalue equation

$$H\psi = E\psi \cdot \tag{B.19}$$

We take the scalar product of (B.19) with $\psi_m^{(0)}$ and we obtain

$$\sum\nolimits_n H_{mn} c_n = E c_m, \tag{B.20}$$

$$\sum\nolimits_{n \neq m} H_{mn} c_n = (E - H_{mm}) c_m, \tag{B.21}$$

Where

$$H_{mm} \equiv \left\langle \psi_m^{(0)} \middle| H \middle| \psi_n^{(0)} \right\rangle \cdot \tag{B.22}$$

From (B.21) we formally extract c_m as

$$c_m = \sum_{\alpha \in A, \alpha \neq m} \frac{H_{m\alpha}}{E - H_{mm}} c_\alpha + \sum_{\beta \in B, \beta \neq m} \frac{H_{m\beta}}{E - H_{mm}} c_\beta \tag{B.23}$$

From (B.23) we obtain c_β as

$$c_\beta = \sum_{\alpha \in A} \frac{H_{\beta\alpha}}{E - H_{\beta\beta}} c_\alpha + \sum_{\gamma \in B, \gamma \neq m} \frac{H_{\beta\gamma}}{E - H_{\beta\beta}} c_\gamma \tag{B.24}$$

We substitute (B.24) back into (B.23), and we iterate the process, with the ultimate goal of eliminating all the c_δ 's with $\delta \in B$

$$c_m = \sum_{\alpha \in A, \alpha \neq m} \frac{H_{m\alpha}}{E - H_{mm}} c_\alpha + \sum_{\beta \in B, \beta \neq m} \frac{H_{m\beta}}{E - H_{mm}} \sum_{\alpha \in A} \frac{H_{\beta\alpha}}{E - H_{\beta\beta}} c_\alpha + \ldots \qquad \text{(B.25)}$$

We choose $m \in A$ and we write (B.25) as

$$\sum_{\alpha \in A} U_{m\alpha} c_\alpha = E c_m, \qquad (\mathrm{m} \in \mathrm{A}) \qquad \text{(B.26)}$$

with

$$U_{m\alpha} = H_{m\alpha} + \sum_{\beta \in B, \beta \neq m} \frac{H_{m\beta} H_{\beta\alpha}}{E - H_{\beta\beta}} + \ldots \qquad (\alpha \in A) \qquad \text{(B.27)}$$

We have therefore reduced the eigenvalue problem (B.20) on the full A + B space to the restricted eigenvalue problem (B.26) on the A space. The effect of the B space is taken into account through the 'renormalized' matrix elements (B.27). Equations (B.26) and (B.27) are solved iteratively, until convergence is achieved.

We choose $m \in B$ and we write (B.25) as

$$c_m = \sum_{\alpha \in A} \frac{H_{m\alpha}}{E - H_{mm}} c_\alpha + \ldots \qquad (m \in B) \qquad \text{(B.28)}$$

In this way we have completely determined the coefficients of the eigenfunction expansion (B.18).

Appendix C: Arbitrary Orientated Hamiltonian's direvation

The inverse rotational transformation given in equation (V.3-6) is obtained by finding the inverse of the rotational transformation given in equation (V.1).The A matrix has an inverse only if it is square and its determinant is nonzero, it is derived from this relation [86]:

$$U_{nm}^{-1} = \frac{\text{cofactor of } U_{nm}}{\text{determinant of } U} \qquad \text{or} \qquad U^{-1} = \frac{B^T}{\text{determinant of } U} \tag{C.1}$$

where B is the matrix of cofactors (also called the minor); the cofactor of element U_{mn} is equal to $(-1)^{m+n}$ times the determinant of the sub-matrix obtained from U by removing the mth row and the nth column. Note that when the matrix, representing an operator, has a determinant equal to zero, this operator does not possess an inverse. Note that $U^{-1}U = UU^{-1} = I$ where I is the unit matrix.

$$B_{11} = +\begin{vmatrix} \cos\varphi & 0 \\ \sin\theta\cos\varphi & \cos\theta \end{vmatrix} = \cos\varphi\cos\theta$$

$$B_{12} = -\begin{vmatrix} -\sin\varphi & 0 \\ \sin\theta\cos\varphi & \cos\theta \end{vmatrix} = \sin\varphi\cos\theta$$

$$B_{13} = +\begin{vmatrix} -\sin\varphi & \cos\varphi \\ \sin\theta\cos\varphi & \sin\theta\sin\varphi \end{vmatrix} = -\sin\theta$$

$$B_{21} = -\begin{vmatrix} \cos\varphi\sin\varphi & -\sin\theta \\ \sin\varphi\sin\theta & \cos\theta \end{vmatrix} = -\sin\varphi$$

$$B_{22} = +\begin{vmatrix} \cos\theta\cos\varphi & -\sin\theta \\ \sin\theta\sin\varphi & \cos\theta \end{vmatrix} = \cos\varphi$$

$$B_{23} = -\begin{vmatrix} \cos\theta\cos\varphi & \cos\theta\sin\varphi \\ \sin\theta\cos\varphi & \sin\theta\sin\varphi \end{vmatrix} = 0$$

$$B_{31} = +\begin{vmatrix} \cos\theta\sin\varphi & -\sin\theta \\ \cos\varphi & 0 \end{vmatrix} = \cos\varphi\sin\theta$$

$$B_{32} = -\begin{vmatrix} \cos\theta\cos\varphi & -\sin\theta \\ -\sin\varphi & 0 \end{vmatrix} = \sin\varphi\sin\theta$$

$$B_{33} = +\begin{vmatrix} \cos\theta\cos\varphi & \cos\theta\sin\varphi \\ -\sin\varphi & \cos\varphi \end{vmatrix} = \cos\theta$$

$$B = \begin{pmatrix} \cos\varphi\cos\theta & \sin\varphi\cos\theta & -\sin\theta \\ -\sin\varphi & \cos\varphi & 0 \\ \cos\varphi\sin\theta & \sin\varphi\sin\theta & \cos\theta \end{pmatrix} \tag{C.2}$$

$$B^T = \begin{pmatrix} \cos\varphi\cos\theta & -\sin\varphi & \cos\varphi\sin\theta \\ \sin\varphi\cos\theta & \cos\varphi & \sin\varphi\sin\theta \\ -\sin\theta & 0 & \cos\theta \end{pmatrix} \tag{C.3}$$

$$U^{-1} = \frac{B^T}{\det(U)(=1)} = \begin{pmatrix} \cos\varphi\cos\theta & -\sin\varphi & \cos\varphi\sin\theta \\ \sin\varphi\cos\theta & \cos\varphi & \sin\varphi\sin\theta \\ -\sin\theta & 0 & \cos\theta \end{pmatrix} \tag{C.4}$$

To find the elements of the Hamiltonian in the new coordination we start with repeated factors such as k_z^2 , k_x+ik_y and k_x-ik_y as follow:

$$\begin{pmatrix} k_x \\ k_y \\ k_z \end{pmatrix} = U^{-1} \begin{pmatrix} k_x' \\ k_y' \\ k_z' \end{pmatrix} \tag{C.5}$$

$$\begin{pmatrix} k_x \\ k_y \\ k_z \end{pmatrix} = \begin{pmatrix} \cos\varphi\cos\theta & -\sin\varphi & \cos\varphi\sin\theta \\ \sin\varphi\cos\theta & \cos\varphi & \sin\varphi\sin\theta \\ -\sin\theta & 0 & \cos\theta \end{pmatrix} \begin{pmatrix} k_x' \\ k_y' \\ k_z' \end{pmatrix} \tag{C.6}$$

$$k_x = \cos\varphi\cos\theta k_x' - \sin\varphi k_y' + \cos\varphi\sin\theta k_z'$$

$$k_y = \sin\varphi\cos\theta k_x' + \cos\varphi k_y' + \sin\varphi\sin\theta k_z'$$

$$k_z = -\sin\theta k_x' + \cos\theta k_z'$$

$$\begin{aligned} k_x + ik_y &= \left(\cos\varphi\cos\theta k_x' - \sin\varphi k_y' + \cos\varphi\sin\theta k_z'\right) + i\left(\sin\varphi\cos\theta k_x' + \cos\varphi k_y' + \sin\varphi\sin\theta k_z'\right) \\ &= e^{i\varphi}\left(\cos\theta k_x' + ik_y' + \sin\theta k_z'\right) \end{aligned}$$

$$\begin{aligned} k_x - ik_y &= \left(\cos\varphi\cos\theta k_x' - \sin\varphi k_y' + \cos\varphi\sin\theta k_z'\right) + i\left(\sin\varphi\cos\theta k_x' + \cos\varphi k_y' + \sin\varphi\sin\theta k_z'\right) \\ &= e^{-i\varphi}\left(\cos\theta k_x' - ik_y' + \sin\theta k_z'\right) \end{aligned}$$

$$\begin{aligned} \left(k_x + ik_y\right)\left(k_x - ik_y\right) &= e^{i\varphi}\left(\cos\theta k_x' + ik_y' + \sin\theta k_z'\right)e^{-i\varphi}\left(\cos\theta k_x' - ik_y' + \sin\theta k_z'\right) \\ &= \left(\cos\theta k_x' + \sin\theta k_z'\right)^2 + \left(ik_y'\right)^2 \\ &= \cos^2\theta k_x'^2 + \sin^2\theta k_z'^2 - k_y'^2 \end{aligned}$$

$$\begin{aligned} k_z^2 &= \left(-\sin\theta k_x' + \cos\theta k_z'\right)^2 \\ &= \sin^2\theta k_x'^2 + \cos\theta^2 k_z'^2 - 2\cos\theta\sin\theta k_x' k_z' \end{aligned} \tag{C.7}$$

Appendix D: Fortran program code for CB and VB

```
!%%%%%%%%%%%%%%%%%%%%%%%%%%%%%%%%%%%%%%%%%%%%%%%%%%%%%%%%%%%
!%%% InxGa1-xN/InxGa1-xN/InxGa1-xN  %%%
!%%% VALENCE BAND STRUCTURE        %%%
!%%% BARRIER WIDTH TLB= DIVISI * NB %%%
!%%% WELL WIDTH TLW= DIVISI*(NW+ 1) %%%
!%%%%%%%%%%%%%%%%%%%%%%%%%%%%%%%%%%%%%%%%%%%%%%%%%%%%%%%%%%%
   IMPLICIT REAL*8 (A-H,O-Z)
!
   INTEGER NB,NW,ND,NN,NP,NK
   PARAMETER
(NB=43,NW=17,ND=NB+NW+NB,NN=ND+ND+ND,NP=ND+2,NK=50)
!
         REAL*8 DIVISI,FH(NP),FL(NP),FSO(NP),DEL(NP),DEL1,DEL2(NP)
   REAL*8 A1(NP),A2(NP),A3(NP),A4(NP),A5(NP),A6(NP)
   INTEGER NVB !,KK
!======= VB:EIGENVALUE =====
   OPEN (UNIT=50,FILE='HVADUAS.txt',STATUS='UNKNOWN')
!======= VB STRUCTURE FOR PLOT =====
   OPEN (UNIT=80,FILE='GRPHUAS.txt',STATUS='UNKNOWN')
!
   !WRITE(*,7) ('NVB=')
!7 FORMAT(20F10.5)
!DO 5  KK=1,30
READ (*,*) NVB
         !NVB=7         !I=NN,NN-NVB,-1
!%%%%%% MATERIAL PARAMETERS %%%%%%%%%%
   CALL MATER(DIVISI,A1,A2,A3,A4,A5,A6,FH,FL,FSO,DEL,DEL1,DEL2)
!%%%%% OBTAINING VB EIGENVALUE %%%%%%
!
   CALL
VBEIGEN(NVB,DIVISI,A1,A2,A3,A4,A5,A6,FH,FL,FSO,DEL,DEL1,DEL2)
!
!5       CONTINUE
   STOP
   END
!%%%%%%%%%%%%%%%%%%%%%%%%%%%%%%%%%%%%%%%%%%%%%%%%%%%%%%%%%
!%    MATERIAL PARAMETERS        %%
!%%%%%%%%%%%%%%%%%%%%%%%%%%%%%%%%%%%%%%%%%%%%%%%%%%%%%%%%%
   SUBROUTINE
MATER(DIVISI,A1,A2,A3,A4,A5,A6,FH,FL,FSO,DEL,DEL1,DEL2)
   INTEGER NB,NW,ND,NN,NP,NK
   PARAMETER
(NB=39,NW=30,ND=NB+NW+NB,NN=ND+ND+ND,NP=ND+2,NK=50)
   REAL*8 EV,AUNG
   REAL*8 DIVISI,LL,RATIO,AC1,MO
   INTEGER I1,I2
   REAL*8 BARX,WELLX
   REAL*8 WEG,BEG
```

```
   REAL*8 TLCWELL,TLCBARR,C13,C33,C13B,C33B   !TLCSUB
   REAL*8 AO,EXX,EZZ,AOB,EXXB,EZZB,HBAR
   REAL*8
A1(NP),A2(NP),A3(NP),A4(NP),A5(NP),A6(NP),FH(NP),FL(NP),FSO(NP)
   REAL*8 gan1,inn1,gan2,inn2,gan3,inn3,gan4,inn4,gan5,inn5,gan6,inn6
   REAL*8 AW1,AB1,AW2,AB2,AW3,AB3,AW4,AB4,AW5,AB5,AW6,AB6
   REAL*8 DW1,DB1,DW2,DB2,DW3,DB3,DW4,DB4,QQ
        REAL*8
DEL(NP),DEL1(NP),DEL2(NP),DELW,DEL1W,DEL2W,DELB,DEL1B,DEL2B
   MO=9.1095D-31
        HBAR=1.0546D-34
   EV=1.60219D-19 !Electron-volt energy
   AUNG=1.0D-10
!======= QW STRUCTURE ==============
   DIVISI=2.0*AUNG
   I1=NB !BOUNDARY BETWEEN BARRIER AND WELL
   I2=NB+NW+1 !BOUNDARY BETWEEN OF QW STRUCTURE
   LL=DIVISI*(NB+NW+NB+1)!TOTAL LENGTH OF QW STRUCTURE
   AC1=(ND+1)**2
   RATIO=MO/HBAR*LL/HBAR*LL
!========InxGa1-xN/InxGa1-xN===========
   BARX=0.02
   WELLX=0.15
!=========PARAMETERS===============
        inn1=-9.28
        gan1=-7.24
   AW1=gan1*(1.0-WELLX)+inn1*WELLX
   AB1=gan1*(1.0-BARX)+inn1*BARX
   inn2=-0.60
        gan2=-0.51
        AW2=gan2*(1.0-WELLX)+inn2*WELLX
   AB2=gan2*(1.0-BARX)+inn2*BARX
   inn3=8.68
        gan3=6.73
        AW3=gan3*(1.0-WELLX)+inn3*WELLX
   AB3=gan3*(1.0-BARX)+inn3*BARX
   inn4=-4.34
        gan4=-3.36
        AW4=gan4*(1.0-WELLX)+inn4*WELLX
   AB4=gan4*(1.0-BARX)+inn4*BARX
   inn5=-4.32
        gan5=-3.35
        AW5=gan5*(1.0-WELLX)+inn5*WELLX
   AB5=gan5*(1.0-BARX)+inn5*BARX
   inn6=-6.08
        gan6=-4.72
        AW6=gan6*(1.0-WELLX)+inn6*WELLX
   AB6=gan6*(1.0-BARX)+inn6*BARX

!=====================================
```

```
   WEG=(3.42*(1-WELLX)+1.89*WELLX-3.8*WELLX*(1-WELLX))*EV
   BEG=(3.42*(1-BARX)+1.89*BARX-3.8*BARX*(1-BARX))*EV
!====STRAIN RELATED==================
   TLCWELL=(3.189*(1.0-WELLX)+3.548*WELLX)*AUNG
   TLCBARR=(3.189*(1.0-BARX)+3.548*BARX)*AUNG
   !IF(TLCWELL.GT.TLCBARR)THEN
   TLCSUB=TLCBARR
   !ELSE
        !TLCSUB=TLCBARR
   !ENDIF
!
   C13=(94*(1.0-WELLX)+114*WELLX)
   C33=(200*(1.0-WELLX)+381*WELLX)
   C13B=(94*(1.0-BARX)+114*BARX)
   C33B=(200*(1.0-BARX)+381*BARX)
   AO=(TLCSUB-TLCWELL)/TLCWELL    !3.189*AUNG
   EXX=AO
   EZZ=(-2.0)*C13/C33*EXX
   AOB=(TLCSUB-TLCBARR)/TLCBARR            ! 3.189*AUNG
   EXXB=AOB
   EZZB=(-2.0)*C13B/C33B*EXXB
!  Deformation potentials
        DW1=-0.89*EV
        DW2=4.27*EV
        DW3=5.18*EV
        DW4=-2.59*EV
        DB1=-0.89*EV
        DB2=4.27*EV
        DB3=5.18*EV
        DB4=-2.59*EV
!
   QQ=0.7 !BAND OFFSET IN CONDUCTION BAND
        DELW=(0.0047*(SQRT(2.0))*(1.0-
WELLX)+0.00033*(SQRT(2.0))*WELLX)*EV
        DEL1W=(0.019*(1.0-WELLX)+0.041*WELLX)*EV
        DEL2W=(0.0047*(1.0-WELLX)+0.00033*WELLX)*EV
        DELB=(0.0047*(SQRT(2.0))*(1.0-BARX)+0.00033*(SQRT(2.0))*BARX)*EV
        DEL1B=(0.019*(1.0-BARX)+0.041*BARX)*EV
        DEL2B=(0.0047*(1.0-BARX)+0.00033*BARX)*EV
        !DEL=0.024*(SQRT(2.0))*EV
   !DEL1=0.03*EV
   !DEL2=0.024*EV
        !AW6=gan6*(1.0-WELLX)+inn6*WELLX
   !AB6=gan6*(1.0-BARX)+inn6*BARX

!===LUTTINGER PARAMETERS RELATED
   DO 45 I=1,NP,1
     IF((I.GT.(I1+1)).AND.(I.LT.(I2+1)))THEN
       A1(I)=AW1
       A2(I)=AW2
```

```
    A3(I)=AW3
    A4(I)=AW4
    A5(I)=AW5
    A6(I)=AW6
            FH(I)=RATIO*(DW2*(EXX+EXX)+DW1*EZZ)/AC1
            FL(I)=RATIO*(DW4*(EXX+EXX)+DW3*EZZ)/AC1
            FSO(I)=0
            DEL(I)=RATIO*DELW/AC1
            DEL1(I)=RATIO*DEL1W/AC1
            DEL2(I)=RATIO*DEL2W/AC1
   ELSE
    A1(I)=AB1
    A2(I)=AB2
    A3(I)=AB3
    A4(I)=AB4
    A5(I)=AB5
    A6(I)=AB6
            FH(I)=RATIO*(DB2*(EXXB+EXXB)+DB1*EZZB)/AC1
            FL(I)=RATIO*(DB4*(EXXB+EXXB)+DB3*EZZB)/AC1
            FSO(I)=RATIO*(1.0-QQ)*(BEG-WEG)/AC1
            DEL(I)=RATIO*DELB/AC1
            DEL1(I)=RATIO*DEL1B/AC1
            DEL2(I)=RATIO*DEL2B/AC1
   ENDIF
45  CONTINUE
!
  RETURN
  END
!%%%%%%%%%%%%%%%%%%%%%%%%%%%%%%%%%%%%%%%%%%%
!% DEFINE UPPER & LOWER HAMILTONIAN  %%
!%%%%%%%%%%%%%%%%%%%%%%%%%%%%%%%%%%%%%%%%%%%
  SUBROUTINE
VBMAT(KP,DIVISI,A1,A2,A3,A4,A5,A6,FH,FL,FSO,HUPMAT,DEL,DEL1,DEL2)
  INTEGER NB,NW,ND,NN,NP,NK
  PARAMETER
(NB=39,NW=30,ND=NB+NW+NB,NN=ND+ND+ND,NP=ND+2,NK=50)
  REAL*8 KP,HUPMAT(NN,NN),DIVISI,HBAR,MO
  REAL*8
A1(NP),A2(NP),A3(NP),A4(NP),A5(NP),A6(NP),FH(NP),FL(NP),FSO(NP)
  REAL*8 B11(ND,ND),B12(ND,ND),B13(ND,ND),B21(ND,ND),AC1
      REAL*8
UNIM(ND,ND),B22(ND,ND),B23(ND,ND),B31(ND,ND),B32(ND,ND),B33(ND,ND)
  REAL*8 B11V1(NP),B11V2(NP),B11V3(NP),B12V1(NP),B13V1(NP)
  REAL*8 B21V1(NP),B22V1(NP),B22V2(NP),B22V3(NP),B23V1(NP),B23V2(NP)
  REAL*8 B31V1(NP),B32V1(NP),B32V2(NP),B33V1(NP),B33V2(NP),B33V3(NP)
  REAL*8 B(NN,NN),LL
      REAL*8                          DEL(NP),DEL1(NP),DEL2(NP)
!,DELW,DEL1W,DEL2W,DELB,DEL1B,DEL2B
  INTEGER I,J,I1,I2
!
```

```
   MO=9.1095D-31
   HBAR=1.0546D-34
         I1=NB
   I2=NB+NW+1
   EV=1.60219D-19 !Electron-volt energy
   AUNG=1.0D-10
         DIVISI=2.0*AUNG
   LL=DIVISI*(NB+NW+NB+1)
         !
         !DEL=0.024*(SQRT(2.0))*EV
   !DEL1=0.03*EV
   !DEL2=0.024*EV
         !
   AC1=(ND+1)**2
   RATIO=MO/HBAR*LL/HBAR*LL
   DO 305 I=1,ND,1
   DO 307 J=1,ND,1
   UNIM(I,J)=0.0
307 CONTINUE
305 CONTINUE
       DO 315 I=1,ND,1
       UNIM(I,I)=UNIM(I,I)+1.0
315 CONTINUE
!=====DEFINE MATRIX================
   DO 320 I=1,NP,1
      B11V1(I)=0.5*(A1(I)+A3(I))
      B11V2(I)=0.5*(A2(I)+A4(I))*((KP*LL)**2)
      !
      B22V1(I)=0.5*(A1(I)+A3(I))
      B22V2(I)=0.5*(A2(I)+A4(I))*((KP*LL)**2)
      !
      B33V1(I)=0.5*A1(I)
      B33V2(I)=0.5*A2(I)*((KP*LL)**2)
      !
      B21V1(I)=0.5*A5(I)*((KP*LL)**2)
      !
      B12V1(I)=0.5*A5(I)*((KP*LL)**2)
      B13V1(I)=0.5*A6(I)*(KP*LL)


      B23V1(I)=0.5*A6(I)*(KP*LL)
      B31V1(I)=0.5*A6(I)*(KP*LL)
      B32V1(I)=0.5*A6(I)*(KP*LL)

320 CONTINUE
   DO 325 I=1,NP,1
    IF ((I.EQ.(I1+1)) .OR. (I.EQ.(I2+1))) THEN
     B33V2(I)=(B33V2(I-1)+B33V2(I+1))/2.0
     B33V1(I)=(B33V1(I-1)+B33V1(I+1))/2.0
     B32V1(I)=(B32V1(I-1)+B32V1(I+1))/2.0
```

```
      B31V1(I)=(B31V1(I-1)+B31V1(I+1))/2.0
      B23V1(I)=(B23V1(I-1)+B23V1(I+1))/2.0
      B22V2(I)=(B22V2(I-1)+B22V2(I+1))/2.0
      B22V1(I)=(B22V1(I-1)+B22V1(I+1))/2.0
      B21V1(I)=(B21V1(I-1)+B21V1(I+1))/2.0
      B13V1(I)=(B13V1(I-1)+B13V1(I+1))/2.0
      B12V1(I)=(B12V1(I-1)+B12V1(I+1))/2.0
      B11V2(I)=(B11V2(I-1)+B11V2(I+1))/2.0
      B11V1(I)=(B11V1(I-1)+B11V1(I+1))/2.0
   ENDIF
325 CONTINUE
!
   DO 335 I=1,ND,1
    DO 337 J=1,ND,1
      B11(I,J)=0.0
      B12(I,J)=0.0
      B13(I,J)=0.0
      B21(I,J)=0.0
      B22(I,J)=0.0
      B23(I,J)=0.0
      B31(I,J)=0.0
      B32(I,J)=0.0
      B33(I,J)=0.0
337 CONTINUE
335 CONTINUE
!
   DO 340 I=1,ND,1
      B11(I,I)=B11(I,I)-B11V1(I+1)-(B11V1(I)+B11V1(I+2))/2.0
      B22(I,I)=B22(I,I)-B22V1(I+1)-(B22V1(I)+B22V1(I+2))/2.0
      B33(I,I)=B33(I,I)-B33V1(I+1)-(B33V1(I)+B33V1(I+2))/2.0

340 CONTINUE
!
   DO 350 I=1,ND-1,1
      B11(I,I+1)=B11(I,I+1)+(B11V1(I+1)+B11V1(I+2))/2.0
      B11(I+1,I)=B11(I+1,I)+(B11V1(I+2)+B11V1(I+1))/2.0
                B13(I,I+1)=B13(I,I+1)-(B13V1(I+1)+B13V1(I+2))/2.0
      B13(I+1,I)=B13(I+1,I)+(B13V1(I+2)+B13V1(I+1))/2.0
                B22(I,I+1)=B22(I,I+1)+(B22V1(I+1)+B22V1(I+2))/2.0
      B22(I+1,I)=B22(I+1,I)+(B22V1(I+2)+B22V1(I+1))/2.0
                B23(I,I+1)=B23(I,I+1)-(B23V1(I+1)+B23V1(I+2))/2.0
      B23(I+1,I)=B23(I+1,I)+(B23V1(I+2)+B23V1(I+1))/2.0
      B31(I,I+1)=B31(I+1,I)+(B31V1(I+2)+B31V1(I+1))/2.0
      B31(I+1,I)=B31(I,I+1)-(B31V1(I+1)+B31V1(I+2))/2.0
                B32(I,I+1)=B32(I,I+1)+(B32V1(I+1)+B32V1(I+2))/2.0
      B32(I+1,I)=B32(I+1,I)-(B32V1(I+2)+B32V1(I+1))/2.0
                B33(I,I+1)=B33(I,I+1)+(B33V1(I+1)+B33V1(I+2))/2.0
      B33(I+1,I)=B33(I+1,I)+(B33V1(I+2)+B33V1(I+1))/2.0
350 CONTINUE
!
```

```
          DO 365 I=1,ND,1
     DO 367 J=1,ND,1
                    B11(I,J)=B11(I,J)*AC1
       B13(I,J)=B13(I,J)*SQRT(AC1)/2
       B22(I,J)=B22(I,J)*AC1
       B23(I,J)=B23(I,J)*SQRT(AC1)/2
       B31(I,J)=B31(I,J)*SQRT(AC1)/2
       B32(I,J)=B32(I,J)*SQRT(AC1)/2
       B33(I,J)=B33(I,J)*AC1
367  CONTINUE
365 CONTINUE
!
    N2=ND+ND
    DO 375 I=1,NN,1
     DO 377 J=1,NN,1
       B(I,J)=0.0
377  CONTINUE
375 CONTINUE
!
    DO 380 I=1,ND,1
     DO 383 J=1,ND,1 !here where start filling the matrix
                    B(I,J)=B(I,J)+B11(I,J)+B11V2(I+1)*UNIM(I,J)-
FSO(I+1)*UNIM(I,J)*AC1+(DEL1(I+1)+DEL2(I+1)+FH(I+1)+FL(I+1))*UNIM(I,J)*
AC1
       B(I+ND,J+ND)=B(I+ND,J+ND)+B22(I,J)+B22V2(I+1)*UNIM(I,J)-
FSO(I+1)*UNIM(I,J)*AC1+(DEL1(I+1)-
DEL2(I+1))*UNIM(I,J)*AC1+(FH(I+1)+FL(I+1))*UNIM(I,J)*AC1
       B(I+N2,J+N2)=B(I+N2,J+N2)+B33(I,J)+B33V2(I+1)*UNIM(I,J)-
FSO(I+1)*UNIM(I,J)*AC1+FH(I+1)*UNIM(I,J)*AC1
       B(I+ND,J)=B(I+ND,J)+B21V1(I+1)*UNIM(I,J)
       B(I+N2,J)=B(I+N2,J)+B31(I,J)
       B(I+N2,J+ND)=B(I+N2,J+ND)+B32(I,J)+DEL(I+1)*UNIM(I,J)*AC1
                    B(I,J+ND)=B(I,J+ND)+ B12V1(I+1)*UNIM(I,J)
                    B(I,J+N2)=B(I,J+N2)+B13(I,J)
                    B(I+ND,J+N2)=B(I+ND,J+N2)+B23(I,J)+DEL(I+1)*UNIM(I,J)*AC1
383  CONTINUE
380 CONTINUE
!
    DO 404 I=1,NN,1
     DO 408 J=1,NN,1
       HUPMAT(I,J)=-B(I,J)/AC1
408  CONTINUE
404 CONTINUE
    RETURN
    END
!%%%%%%%%%%%%%%%%%%%%%%%%%%%%%%%%%%%%%%%%%%%%
!% EIGENVLAUE ANDEIGENVECTOR FOR VB  %%
!%%%%%%%%%%%%%%%%%%%%%%%%%%%%%%%%%%%%%%%%%%%%
    SUBROUTINE
VBEIGEN(NVB,DIVISI,A1,A2,A3,A4,A5,A6,FH,FL,FSO,DEL,DEL1,DEL2)
```

```
   INTEGER NB,NW,ND,NN,NP,NK
   PARAMETER
(NB=39,NW=30,ND=NB+NW+NB,NN=ND+ND+ND,NP=ND+2,NK=50)
   REAL*8 DIVISI,B(NN,NN),HBAR,MO
   REAL*8
A1(NP),A2(NP),A3(NP),A4(NP),A5(NP),A6(NP),FH(NP),FL(NP),FSO(NP)
   INTEGER NVB
   INTEGER II,I,J,NLAST
   REAL*8 KPINT,KP,NORM,AUNG,EV,RATIO,AC1,LL
   REAL*8 EVALN(NN),EN(NN),ASKN(NN),HEVEC(NN,NN)
   REAL*8 HUPMAT(NN,NN)
         REAL*8                                          DEL(NP),DEL1(NP),DEL2(NP)
!,DELW,DEL1W,DEL2W,DELB,DEL1B,DEL2B
!
   AUNG=1.0D-10
   HBAR=1.0546D-34
   MO=9.1095D-31
   EV=1.60219D-19 !Electron-volt energy
   NLAST=120
   KPINT=0.001/AUNG
!
         DIVISI=2.0*AUNG
   LL=DIVISI*(NB+NW+NB+1)
   RATIO=MO/HBAR*LL/HBAR*LL
   AC1=(ND+1)**2
!
   DO 1000 II=1,NLAST !START
      KP=KPINT*(II-1)
!%%%%%%%% DEFINE MATRIX %%%%%%%%%
   CALL
VBMAT(KP,DIVISI,A1,A2,A3,A4,A5,A6,FH,FL,FSO,HUPMAT,DEL,DEL1,DEL2)
!
   DO 402 I=1,NN,1
    DO 404 J=1,NN,1
      B(I,J)=HUPMAT(I,J)
404  CONTINUE
402 CONTINUE
!
   DO 653 I=1,NN,1
      EN(I)=0.0
      EVALN(I)=0.0
      ASKN(I)=0.0
653 CONTINUE
!
   DO 4021 I=1,NN,1
    WRITE(*,724)I,(B(I,J),J=1,NN,1) !I=NN,NN-NVB+1,-1
724  FORMAT(620F10.5)
4021 CONTINUE

         CALL TRED2(B,NN,NN,EVALN,EN)
```

```
    CALL TQLI(EVALN,EN,NN,NN,B)
    CALL EIGSRT(EVALN,B,NN,NN)
!=NORMALIZATION OF EIGENVECTOR=====
    DO 712 I=1,NN,1
       NORM=0.0
     DO 715 J=1,NN,1
       NORM=NORM+B(J,I)*B(J,I)
715  CONTINUE
    DO 717 J=1,NN,1
       HEVEC(J,I)=B(J,I)/SQRT(NORM)
717 CONTINUE
712 CONTINUE
!
     DO 720 I=1,NN,1
       ASKN(I)=EVALN(I)/RATIO*AC1/EV !EV UNIT
720  CONTINUE

!=SAVING EIGENVALUES======
    WRITE(*,727)KP*AUNG,(-ASKN(I),I=1,NVB+1,1) !I=NN,NN-NVB+1,-1
727 FORMAT(620F10.5)

    WRITE (80,757)KP*AUNG,(-ASKN(I),I=1,NVB+1,1)
757 FORMAT (620F10.5)
          IF (II.EQ.1) THEN
                   DO 242 I=1,NN,1
    WRITE(50,248)(HEVEC(I,J),J=1,NVB+1,1)
248 FORMAT(900F10.5)
242 CONTINUE
          ENDIF
1000 CONTINUE
!
    RETURN
    END

!%%%%%%%%%%%%%%%%%%%%%%%%%%%%%%%%%%%%%%%%%
!% SUBROUTINES FOR EIGEN:VALUES %%%
!%%%%%%%%%%%%%%%%%%%%%%%%%%%%%%%%%%%%%%%%%
! (C)COPR.1986-92 NUMERICAL RECIPES SOFTWARE 00.
    SUBROUTINE TQLI(D,E,N,NP,Z)
    INTEGER N,NP
    REAL*8 D(NP),E(NP),Z(NP,NP)
    INTEGER I,ITER,K,L,M
    REAL*8 B,C,DD,F,G,P,R,S,PYTHAG
    DO 11 I=2,N
       E(I-1)=E(I)
11  CONTINUE
       E(N)=0.
    DO 15 L=1,N
       ITER=0
1   DO 12 M=L,N-1
```

```
      DD=ABS(D(M))+ABS(D(M+1))
     IF (ABS(E(M))+DD.EQ.DD) GOTO 2
12  CONTINUE
      M=N
2    IF(M.NE.L)THEN
      IF(ITER.EQ.300) PAUSE' TOO MANY ITERATIONS IN TALI '
         ITER=ITER+1
         G=(D(L+1)-D(L))/(2.*E(L))
         R=PYTHAG(G,1.0D0)
         G=D(M)-D(L)+E(L)/(G+SIGN(R,G))
         S=1.
         C=1.
         P=0.
   DO 14 I=M-1,L,-1
      F=S*E(I)
      B=C*E(I)
      R=PYTHAG(F,G)
      E(I+1)=R
    IF(R.EQ.0.)THEN
      D(I+1)=D(I+1)-P
      E(M)=0.
   GOTO 1
   ENDIF
      S=F/R
      C=G/R
      G=D(I+1)-P
      R=(D(I)-G)*S+2.*C*B
      P=S*R
      D(I+1)=G+P
      G=C*R-B
! OMIT LINES FROM HERE ...
   DO 13 K=1,N
      F=Z(K,I+1)
      Z(K,I+1)=S*Z(K,I)+C*F
      Z(K,I)=C*Z(K,I)-S*F
13 CONTINUE
! ... TO HERE WHEN FINDING ONLY EIGENVALUES.
14 CONTINUE
      D(L)=D(L)-P
      E(L)=G
      E(M)=0.
   GOTO 1
   ENDIF
15 CONTINUE
   RETURN
   END
!
   SUBROUTINE TRED2(A,N,NP,D,E)
   INTEGER N,NP
   REAL*8 A(NP,NP),D(NP),E(NP)
```

```
      INTEGER I,J,K,L
      REAL*8 F,G,H,HH,SCALE
      DO 18 I=N,2,-1
         L=I-1
         H=0.
      SCALE=0.
      IF(L.GT.1)THEN
      DO 11 K=1,L
      SCALE=SCALE+ABS(A(I,K))
11 CONTINUE
      IF (SCALE.EQ.0.) THEN
         E(I)=A(I,L)
      ELSE
      DO 12 K=1,L
      A(I,K)=A(I,K)/SCALE
      H=H+A(I,K)**2
12 CONTINUE
      F=A(I,L)
      G=-SIGN(SQRT(H),F)
      E(I)=SCALE*G
      H=H-F*G
      A(I,L)=F-G
      F=0.
      DO 15 J=1,L
! OMIT FOLLOWING LINE IF FINDING ONLY EIGENVALUES
         A(J,I)=A(I,J)/H
         G=0.
      DO 13 K=1,J
      G=G+A(J,K)*A(I,K)
13 CONTINUE
      DO 14 K=J+1,L
         G=G+A(K,J)*A(I,K)
14 CONTINUE
         E(J)=G/H
         F=F+E(J)*A(I,J)
15 CONTINUE
         HH=F/(H+H)
      DO 17 J=1,L
      F=A(I,J)
      G=E(J)-HH*F
      E(J)=G
      DO 16 K=1,J
      A(J,K)=A(J,K)-F*E(K)-G*A(I,K)
16 CONTINUE
17 CONTINUE
      ENDIF
      ELSE
         E(I)=A(I,L)
      ENDIF
      D(I)=H
```

```
18 CONTINUE
! OMIT FOLLOWING LINE IF FINDING ONLY EIGENVALUES.
   D(1)=0.
   E(1)=0.
   DO 24 I=1,N
! DELETE LINES FROM HERE ...
   L=I-1
   IF(D(I).NE.0.)THEN
   DO 22 J=1,L
      G=0.
   DO 19 K=1,L
      G=G+A(I,K)*A(K,J)
19 CONTINUE
   DO 21 K=1,L
      A(K,J)=A(K,J)-G*A(K,I)
21 CONTINUE
22 CONTINUE
   ENDIF
!   ... TO HERE WHEN FINDING ONLY ETGENVALUES.
   D(I)=A(I,I)
! ALSO DELETE LINES FROM HERE ...
   A(I,I)=1.
   DO 23 J=1,L
      A(I,J)=0.
      A(J,I)=0.
23  CONTINUE
! ... TO HERE WHEN FINDING ONLY EIGENVALUES.
24  CONTINUE
   RETURN
   END
! (C) COPR. 1986 - 92 NUMERICAL RECIPES SOFTWARE 00.
   FUNCTION PYTHAG(A,B)
   REAL*8 A,B,PYTHAG
   REAL*8 ABSA,ABSB
   ABSA=ABS(A)
   ABSB=ABS(B)
   IF(ABSA.GT.ABSB)THEN
    PYTHAG=ABSA*SQRT(1.+(ABSB/ABSA)**2)
   ELSE
   IF(ABSB.EQ.0.)THEN
   PYTHAG=0.
   ELSE
   PYTHAG=ABSB*SQRT(1.+(ABSA/ABSB)**2)
   ENDIF
   ENDIF
   RETURN
   END
! (C) COPR. 1986 - 92 NUMERICAL RECIPES SOFTWARE 00.
   SUBROUTINE EIGSRT(D,V,N,NP)
   INTEGER N,NP
```

```
   REAL*8 D(NP),V(NP,NP)
   INTEGER I,J,K
   REAL*8 P
   DO 13 I=1,N-1
      K=I
      P=D(I)
   DO 11 J=I+1,N
    IF(D(J).GE.P)THEN
      K=J
      P=D(J)
   ENDIF
11  CONTINUE
   IF(K.NE.I)THEN
      D(K)=D(I)
      D(I)=P
   DO 12 J=1,N
      P=V(J,I)
      V(J,I)=V(J,K)
      V(J,K)=P
12  CONTINUE
   ENDIF
13 CONTINUE
   RETURN
   END
```

References:

[1] J. Bardeen “An improved calculation of the energies of metallic Li and Na”, J. Chem. Phys. 6, 367-371 (1933).

[2] F. Seitz, the Modem Theory of Solids McGraw Hill, New York, 1940, p. 352.

[3] S. L. Chuang, “Physics of Optoelectronic Devices”, Wiley, New York, 1995.

[4] J. M. Luttinger and W. Kohn, “Motion of electrons and holes in perturbed periodic fields” Phys. Rev. 97, 869-883 (1955).

[5] E. 0. Kane, “Band structure of indium antimonite," J. Phys. Chem. Solids, 1, 249-261 (1957).

[6] E. O. Kane, "The k-p method," Chapter 3, in R. K. Willardson and A. C. Beer, Eds., Semi-conductors and Semi-metals, Vol. 1, Academic, New York, 1966.

[7] C. Galeriu, PhD Thesis , k.p Theory Of Semiconductor Nanostructures, Worcester Polytechnic Institute, Germany.

[8] G.E. Pikus, Sov. Phys. JETP 14(4), 898 (1962)

[9] L. C. L.Y. Voon · M. Willatzen,‘ The k·p Method: Electronic Properties of Semiconductors’, Springer-Verlag Berlin Heidelberg 2009 p 46.

[10] S. L. Chuang and C. S. Chang, k.p method for strained Wurtzite semiconductors, Phys. Rev. B, vol. 54, pp. 2491– 2504, 1996.

[11] J. Wu, W. Walukiewicz, K.M. Yu, J.W.A. III, E.E. Haller, H. Lu, W.J. Schaff, Y. Saito, Y. Nanishi, Appl. Phys. Lett. 80(21)

[12] P. Rinke,M.Winkelnkemper, A. Qteish, D. Bimberg, J. Neugebauer, M. Scheffler, Phys. Rev. B: Condens. Matter Mater. Phys. 77(7), 075202 (2008).

[13] P. Löwdin, J. Phys. Chem. 19 1396 (1951).

[14] G. L. Bir and G. E. Pikus, Symmetry and Strain-Induced Effects in Semiconductor Wiley, New York, (1974).

[15] M. Suzuki, T. Uenoyama, and A. Yanase, Phys. Rev. B 52, 8132 (1995).

[16] S. Kamiyama, K. Ohnaka, M. Suzuki, and T. Uenoyama, Jpn. J. Appl. Phys. 34, L821 (1995).

[17] A. E. H. Love, A Treatise on the Mathematical Theory of Elasticity Dover, New York, (1944), pp. 151–160.

[18] M. Kumagai, S. L. Chuang, and H. Ando, Analytical solutions of the blockdiagonalized hamiltonian for strained Wurtzite semiconductors, Phys. Rev. B, vol. 57, pp. 15303–15314, (1998).

[19] D. Ahn and S. H. Park "Engineering Quantum Mechanics", John Wiley & Sons, Inc, (2011), New Jersey.

[20] http://en.wikipedia.org/wiki/Wurtzite_crystal_structure

[21] H. Hebal and H. Abid , 'Strain effects on electronic properties of ZnO-based structures, to be published .

[22] J. Piperk ,' Semiconductor OptoElectronic Devices Introduction to Physics and Simulation', (2003) , Elsevier Science,(USA) p 30.

[23] J. Wrzesinski, D. Frohlich, Phys. Rev. B 56, 13087 (1997)

[24] R. Dingle, W. Wiegmann, C.H. Henry, Phys. Rev. Lett. 33(14), 827 (1974).

[25] G. Wannier, Phys. Rev. 52, 191 (1937)

[26] G. Bastard, J.K. Furdyna, J. Mycielski, Phys. Rev. B 24(10), 4356(1975)

[27] T. Ando, A.B. Fowler, F. Stern, Rev. Mod. Phys. 54(2), 437 (1982).

[28] G. Bastard, Wave Mechanics Applied to Semiconductor Heterostructures (Les Editions dePhysique, Les Ulis, 1988)

[29] M. Altarelli, Phys. Rev. B 28(2), 842 (1983)

[30] G. Bastard, Phys. Rev. B 24, 5693 (1981)

[31] M.G. Burt, Semicond. Sci. Technol. 2, 460 (1987)

[32] M.G. Burt, Semicond. Sci. Technol. 2, 701 (1987)

[33] B.A. Foreman, Phys. Rev. B 48(7), 4964 (1993)

[34] Ch. Hamaguchi, Basic Semiconductor Physics, Springer Heidelberg Dordrecht London New York, (2010).

[35] G. Fishman, Semi-conducteurs :les bases de la theorie k.p, Editions de l'Ecole Polytechnique, (2010) 91128 Palaiseau Cedex.

[36] S. H. Park and S. L. Chuang 1999 *Phys. Rev. B* **59** 4725– 4737.

[37] A. Bykhovski, B. Gelmont and S. Shur 1993 *Appl. Phys.* Lett. **63** 2243.

[38] S. H. Park and S. L. Chuang 2000 *J. Appl. Phys.* **87** 353.

[39] P. Harrison, Quantum Wells, Wires and Dots, (2005) *John Wiley & Sons Ltd UK* .

[40] G. E. W. Bauer and T. Ando, Phys. Rev. B 38, 6015 (1988).

[41] http://aestimo.ndct.org, https://bitbucket.org/sblisesivdin/aestimo/src.

[42] H. Haken, *Light,* Vol. 1, *Waves* , *Photons, Atoms,* p. 204, Chapter 7, NorthHolland,Amsterdam, (1986).

[43] H. Hebal, H. Abid, Superlattices and Microstructures 75 (2014) 866–878.

[44] S. L. Chuang (1996) *IEEE J. Quantum Electron.* **32** 1791–1800.

[45] W. G. Scheibenzuber, GaN-Based Laser Diodes, Phd Thesis, University of Freiburg, Germany, Springer Verlag Berlin Heidelberg (2012).

[46] M. Lundstrom, Fundamentals of carrier transport, 2ed edition, Cambridge University Press (2000).

[47] N. Ashcroft, N. Mermin, solid state physics,Hartcourt Inc, (1976)

[48] A. Simunek, gilat-raubenheimermethod for k - space integration, *Comp. Phys. Commu.*20 (1980) 349—352.

[49] G. Gilat and L.J. Raubenheimer, *Phys. Rev.* 144 (1966) 390.

[50] L.J. Raubenheimer and G. Gilat, *Phys. Rev.* 157.586 (1967).

[51] H. Hellmann, *Einführung in die Quantenchemie*. Leipzig, Deuticke, 1937.

[52] H. Hebal, H. Abid,,Density of states for ZnO and GaN wurtzite semiconductors in quantum well structure, to be published.

[53] W. W. Chow, S. W. Koch and M. III. Sergent 1994 *Semiconductor-Laser Physics.*

[54] S. H. Park and S. L. Chuang and D. Ahn 2000 *Semicond. Sci.Technol.* **15** 203.

[55] D. Ahn 1994 *Phys. Rev. B* **50** 8310.

[56] S. H. Park, S. L. Chuang, J. Minch and D. Ahn,Semicond. Sci. Technol. 15 (2000) 203–208.

[57] http://python.org

[58] D.S. Seljebotn, "Fast Numerical Computations with Cython," Proc. 8th Python in Science Conf., SciPy Community, 2009

[59] D. C. Look 2001 *Mater. Sci. Eng.* B **80** 383.

[60] J.C. Sun, J.Z. Zhao, H.W. Liang, J.M. Bian, L.Z. Hu, H.Q. Zhang, X.P. Liang, W.F. Liu, G.T. Du 2007 *Appl. Phys. Lett.* **90** 121128 .

[61] D. M. Bagnall, Y. F. Chen, Z. Zhu, T. Yao, M. Y. Shen, and T. Gata, H 1998 *Appl. Phys. Lett.* **73** 1038 .

[62] T. Makino, Y. Segawa, M. Kawasaki, A. Ohtomo, R. Shiroki, K. Tamura,T. Yasuda, and H. Koinuma 2001 *Appl. Phys. Lett.* **78** 1237.

[63] D. W. Ma, Z. Z. Ye, and L. L. Chen 2004 *Phys. Status Solidi A* **201** 2929.

[64] O. Vigil, L. Vaillant, F. Cruz, G. Santana, A. Morales-Acevedo, and G.Contreras-Puente, 2000 *Thin Solid Films* 361–362 **53** .

[65] S. L. Chuang and C. S. Chang 1996 *Phys. Rev. B* **54** 2491–2504 .

[66] S. H. Park and D. Ahn 2006 *Optical and Quantum Electronics* **38** 935–952 .

[67] S. H. Park, D. Ahn , S. L. Chuang 2007 *IEEE J. Quantum Electron.***43** 1175–1182.

[68] S. H. Park and S. L. Chuang 2002 *Semicond. Sci. Technol.***17** 686–691.

[69] D. Ahn and S. H. Park 2012 *Semicond. Sci. Technol.* **27** 9.

[70] J. M. Hinckley and J. Singh 1990 *Phys. Rev. B* **42** 3546.

[71] J. F. Nye 1989 *Physical Properties of* Crystals (Oxford: Clarendon) Chapter 2.

[72] S. L. Chuang and C. S. Chang 1996 *Phys. Rev. B* **54** 2491–2504 .

[73] S. H. Park 2000 *Appl. Phys. Lett.* **77** 4095.

[74] S. H. Park and D. Ahn 2006 *J. Opt. Quantum Electron.* **38** 935–952.

[75] J. Davis and C. Jagadish **2012** GaN *and ZnO-based Materials and Devices* ed S.J. Pearton and C. Jagadish (Springer :Verlag Berlin Heidelberg) Chapter 14.

[76] T. Makino, K. Tamura, C.H. Chia, Y. Segawa, M. Kawasaki, A. Ohtomo, H. Koinuma 2002 *Appl. Phys. Lett.* **81** 2355.

[77] H. Matsui and H. Tabata 2009 *Appl. Phys. Lett.* **94** 161907.

[78] J.M. Chauveau, B. Vinter, M. Laugt, M. Teisseire, P. Vennegues, C. Deparis, J. Zuniga-Perez, C. Morhain and J. Korean 2008 *Phys. Soc.* **53** 2934–2938.

[79] Ü. Özgür, Ya. I. Alivov, C. Liu, A. Teke, M. A. Reshchikov, S. Doğan,V. Avrutin, S.-J. Cho, and H. Morkoçd 2005 *J. Appl. Phys.* **98** 041301.

[80] S. H. Park and J.I. Shim 2013 *J. Appl. Phys.* **102** 221109.

[81] T. Yao and S. K. Hong 2009 *Oxide and Nitride Semiconductors* (Springer :Berlin Heidelberg) p 188.

[82] I. Vurgaftman and J. R. Meyer 2003 *J. Appl. Phys.* **94** 3675–3696.

[83] S. H. Park, Y. T. Lee and J. Park 2009 *J. Opt. Quantum Electron.* **41** 779–785.

[84] S. Seki, T. Yamanaka, W. Lui, and K. Yokoyama 1994 *J. Appl. Phys.* **75** 1299–1303.

[85] S. Seki, T. Yamanaka and W. Lui 1994 *IEEE J. Quantum Electron.* **30**.

[86] N. Zettili, "Quantum Mechanics Concepts and Applications", (2009) John Wiley & Sons *UK*, p 109.

Crystal orientation effects on electronic and optical properties of wurtzite CdZnO/ZnO quantum well lasers

Abstract:

The object of this work is to investigate crystal orientation‘s effects on electronic optical properties of wurtzite CdZnO/ZnO quantum wells (QWs) with piezoelectric (PZ) and spontaneous (SP) polarization using the multiband effective-mass theory and the non-Markovian gain model with many-body effects. In this research, we address the electronic and the optical properties of wurtzite CdZnO grown on ZnO substrate, the valence -band structures for the QW structure are calculated based on the k.p method .The results will be confronted with those of WZ GaN/InGaN QW structures and also similar studies.

Keywords:

Optical gain,Comparative study,II-VI semiconductors,III-V semiconductors,Zinc oxides,Binary compounds,Quantum wells,Carrier density,Optical properties,Crystal orientation ,Semiconductor lasers

ملخص :

الهدف من هذا العمل هو التحقق من تأثير اتجاه الكريستال على الالكترونية و الضوئية لتركيب البئر الكمي الذي اساسه الورتزيت CdZnO/ZnO ذي الخاصية كهربيضغطية والاستقطاب العفوي باستعمال الدراسة لمتعددة الطبقات ذات الكتلة التخيلية و الموديل الغير-مركوفي لالربح الضوئي مع ادماج خاصية تاثير متعدد الجسيمات. في هذا البحث, ندرس الخصائص الالكترونية و الضوئية للورتزيت CdZnO المشكل فوق القعدة ل ZnO , تشكيل طبقة التكافؤ لتركيب البئر الكمي قد تم حسابه باعتماد دراسة طريقة ك.ب .النتائج المتحصل عليها غي هذا البحث سيتم مقارنتها بنضيرتها الخاص ب الورتزيت GaN/InGaN في البئر الكمي وكذألك الدراسات المشابهة.

كلمات مفتاحية:

الربح الضوئي, دراسة مقارنة, II-VI انصاف نواقل, III-V انصاف نواقل, اكسيد الزنك, العناصر الثنائية, البئر الكمي, كثافة الحوامل, الخصائص الضوئية, اتجاه الكريستال, ليزر انصاف النواقل.